

## CHAPTER 9

# External Incompressible Viscous Flow

### Part A Boundary Layers

- 9.1 The Boundary-Layer Concept
- 9.2 Laminar Flat-Plate Boundary Layer: Exact Solution (on the Web)
- 9.3 Momentum Integral Equation
- 9.4 Use of the Momentum Integral Equation for Flow with Zero Pressure Gradient

### 9.5 Pressure Gradients in Boundary-Layer Flow

### Part B Fluid Flow About Immersed Bodies

- 9.6 Drag
- 9.7 Lift
- 9.8 Summary and Useful Equations

## Case Study

### The Blended Wing-Body Aircraft

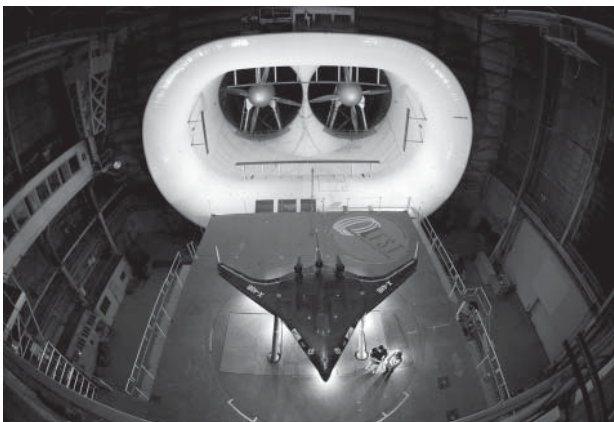
Boeing Phantom Works has partnered with NASA and the U.S. Air Force Research Laboratory to study an advanced-concept, fuel-efficient, blended wing-body (BWB). It is called a blended wing-body because it looks more like a modified triangular-shaped wing than traditional aircraft, which essentially consist of a tube and wing with a tail. The concept of a BWB actually goes back to the 1940s, but developments in composite materials and fly-by-wire controls are making it more feasible. Researchers have tested a 6.3-m wingspan (8.5 percent scale) prototype of the X-48B, a BWB aircraft that could have military and commercial applications. The next step is for NASA to flight-test a scale-model variant called X-48C. The X-48C will be used to examine

how engines mounted to the rear and above the body help to shield the ground from engine noise on takeoff and approach. It also features tail fins for additional noise shielding and for flight control.

The big difference between BWB aircraft and the traditional tube-and-wing aircraft, apart from the fact that the tube is absorbed into the wing shape, is that it does not have a tail. Traditional aircraft need a tail for stability and control; the BWB uses a number of different multiple-control surfaces and possibly tail fins to control the vehicle. There will be a number of advantages to the BWB if it proves feasible. Because the entire structure generates lift, less power is needed for takeoff. Studies have also shown that BWB designs can fit into the 80-m envelope that is the current standard for airplane maneuver at airports. A BWB could carry up to 1000 people, making such a future U.S. product a challenge to Airbus's A380 and future stretched versions.

Apart from possible fuel savings of up to 30 percent due to improved streamlining, the interior of a commercial BWB airplane would be radically different from that of current airplanes. Passengers would enter a room like a movie theater rather than a cramped half-cylinder, there would be no windows (video screens would be connected to external cameras instead), and passengers would be seated in the large movie theater-like room (because seating is not only in the central core but also well out into the blended wings).

In this chapter we will study how lift for the BWB is created by the flow of air over the surfaces. We will also learn how aerodynamic drag on the BWB occurs. Lift and the drag both depend on the nature of the flow pattern and the shape of the airfoil. The material in this chapter will give you insight into the mechanisms of flow over surfaces.



Boeing/Bob Ferguson

The X-48B prototype in the full-scale NASA tunnel.

External flows are flows over bodies immersed in an unbounded fluid. The flow over a sphere (Fig. 2.14b) and the flow over a streamlined body (Fig. 2.16) are examples of external flows, which were discussed qualitatively in Chapter 2. More interesting examples are the flow fields around such objects as airfoils (Fig. 9.1), automobiles, and airplanes. Our objective in this chapter is to quantify the behavior of viscous, incompressible fluids in external flow.

A number of phenomena that occur in external flow over a body are illustrated in the sketch of viscous flow at high Reynolds number over an airfoil (Fig. 9.1). The freestream flow divides at the stagnation point and flows around the body. Fluid at the surface takes on the velocity of the body as a result of the no-slip condition. Boundary layers form on both the upper and lower surfaces of the body. (The boundary-layer thickness on both surfaces in Fig. 9.1 is exaggerated greatly for clarity.) The flow in the boundary layers initially is laminar. Transition to turbulent flow occurs at some distance from the stagnation point, depending on freestream conditions, surface roughness, and pressure gradient. The transition points are indicated by “T” in the figure. The turbulent boundary layer following transition grows more rapidly than the laminar layer. A slight displacement of the streamlines of the external flow is caused by the thickening boundary layers on the surface. In a region of increasing pressure (an *adverse pressure gradient*—so-called because it opposes the fluid motion, tending to decelerate the fluid particles), flow separation may occur. Separation points are indicated by “S” in the figure. Fluid that was in the boundary layers on the body surface forms the viscous wake behind the separation points.

This chapter has two parts. Part A is a review of boundary-layer flows. Here we discuss in a little more detail the ideas introduced in Chapter 2 and then apply the fluid mechanics concepts we have learned to analyze the boundary layer for flow along a flat plate—the simplest possible boundary layer, because the pressure field is constant. We will be interested in seeing how the boundary-layer thickness grows, what the surface friction will be, and so on. We will explore a classic analytical solution for a laminar boundary layer, and see that we need to resort to approximate methods when the boundary layer is turbulent (and we will also be able to use these approximate methods for laminar boundary layers, to avoid using the somewhat difficult analytical method). This will conclude our introduction to boundary layers, except we will briefly discuss the effect of pressure gradients (present for *all* body shapes except flat plates) on boundary-layer behavior.

In Part B we will discuss the force on a submerged body, such as the airfoil of Fig. 9.1. We will see that this force results from both shear and pressure forces acting on the body surface and that both of these are profoundly affected by the fact that we have a boundary layer, especially when this causes flow separation and a wake. Traditionally the force a body experiences is decomposed into the component parallel to the flow, the *drag*, and the component perpendicular to the flow, the *lift*. Because most bodies do have a point of separation and a wake, it is difficult to use analysis to determine the force components, so we will present approximate analyses and experimental data for various interesting body shapes.

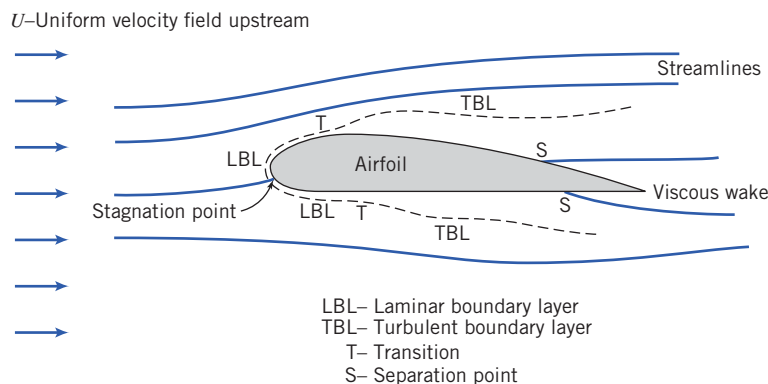
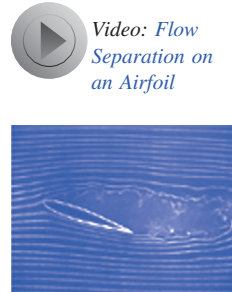


Fig. 9.1 Details of viscous flow around an airfoil.

## Part A BOUNDARY LAYERS

### 9.1 The Boundary-Layer Concept

The concept of a boundary layer was first introduced by Ludwig Prandtl [1], a German aerodynamicist, in 1904.

Prior to Prandtl's historic breakthrough, the science of fluid mechanics had been developing in two rather different directions. *Theoretical hydrodynamics* evolved from Euler's equation of motion for a nonviscous fluid (Eq. 6.1, published by Leonhard Euler in 1755). Since the results of hydrodynamics contradicted many experimental observations (especially, as we saw in Chapter 6, that under the assumption of inviscid flow no bodies experience drag!), practicing engineers developed their own empirical art of *hydraulics*. This was based on experimental data and differed significantly from the purely mathematical approach of theoretical hydrodynamics.

Although the complete equations describing the motion of a viscous fluid (the Navier–Stokes equations, Eq. 5.26, developed by Navier, 1827, and independently by Stokes, 1845) were known prior to Prandtl, the mathematical difficulties in solving these equations (except for a few simple cases) prohibited a theoretical treatment of viscous flows. Prandtl showed [1] that many viscous flows can be analyzed by dividing the flow into two regions, one close to solid boundaries, the other covering the rest of the flow. Only in the thin region adjacent to a solid boundary (the boundary layer) is the effect of viscosity important. In the region outside of the boundary layer, the effect of viscosity is negligible and the fluid may be treated as inviscid.

The boundary-layer concept provided the link that had been missing between theory and practice (for one thing, it introduced the theoretical possibility of drag!). Furthermore, the boundary-layer concept permitted the solution of viscous flow problems that would have been impossible through application of the Navier–Stokes equations to the complete flow field.<sup>1</sup> Thus the introduction of the boundary-layer concept marked the beginning of the modern era of fluid mechanics.

The development of a boundary layer on a solid surface was discussed in Section 2.6. In the boundary layer both viscous and inertia forces are important. Consequently, it is not surprising that the Reynolds number (which represents the ratio of inertia to viscous forces) is significant in characterizing boundary-layer flows. The characteristic length used in the Reynolds number is either the length in the flow direction over which the boundary layer has developed or some measure of the boundary-layer thickness.

As is true for flow in a duct, flow in a boundary layer may be laminar or turbulent. There is no unique value of Reynolds number at which transition from laminar to turbulent flow occurs in a boundary layer. Among the factors that affect boundary-layer transition are pressure gradient, surface roughness, heat transfer, body forces, and freestream disturbances. Detailed consideration of these effects is beyond the scope of this book.

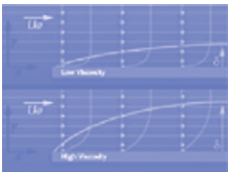
In many real flow situations, a boundary layer develops over a long, essentially flat surface. Examples include flow over ship and submarine hulls, aircraft wings, and atmospheric motions over flat terrain. Since the basic features of all these flows are illustrated in the simpler case of flow over a flat plate, we consider this first. The simplicity of the flow over an infinite flat plate is that the velocity  $U$  outside the boundary layer is constant, and therefore, because this region is steady, inviscid, and incompressible, the pressure will also be constant. This constant pressure is the pressure felt by the boundary layer—obviously the simplest pressure field possible. This is a *zero pressure gradient flow*.

A qualitative picture of the boundary-layer growth over a flat plate is shown in Fig. 9.2. The boundary layer is laminar for a short distance downstream from the leading edge; transition occurs over a region of the plate rather than at a single line across the plate. The transition region extends downstream to the location where the boundary-layer flow becomes completely turbulent.

For incompressible flow over a smooth flat plate (zero pressure gradient), in the absence of heat transfer, transition from laminar to turbulent flow in the boundary layer can be delayed to a Reynolds number,  $Re_x = \rho Ux/\mu$ , greater than one million if external disturbances are minimized. (The length  $x$  is



Video: Effect of Viscosity on Boundary Layer Growth



<sup>1</sup> Today, Computational Fluid Dynamics (CFD) programs are commonly used to solve the Navier–Stokes equations.

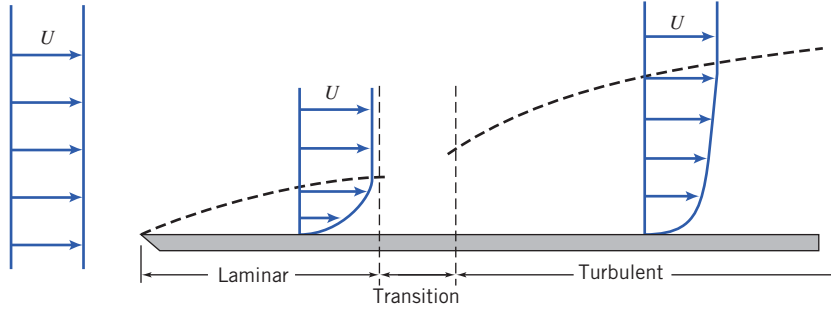


**Fig. 9.2** Boundary layer on a flat plate (vertical thickness exaggerated greatly).

measured from the leading edge.) For calculation purposes, under typical flow conditions, transition usually is considered to occur at a length Reynolds number of 500,000. For air at standard conditions, with freestream velocity  $U = 30$  m/s, this corresponds to  $x \approx 0.24$  m. In the qualitative picture of Fig. 9.2, we have shown the turbulent boundary layer growing faster than the laminar layer. In later sections of this chapter we shall show that this is indeed true.

The boundary layer is the region adjacent to a solid surface in which viscous stresses are present, as opposed to the free stream where viscous stresses are negligible. These stresses are present because we have shearing of the fluid layers, i.e., a velocity gradient, in the boundary layer. As indicated in Fig. 9.2, both laminar and turbulent layers have such gradients, but the difficulty is that the gradients only asymptotically approach zero as we reach the edge of the boundary layer. Hence, the location of the edge, i.e., of the boundary-layer thickness, is not very obvious—we cannot simply define it as where the boundary-layer velocity  $u$  equals the freestream velocity  $U$ . Because of this, several boundary-layer definitions have been developed: the disturbance thickness  $\delta$ , the displacement thickness  $\delta^*$ , and the momentum thickness  $\theta$ . (Each of these increases as we move down the plate, in a manner we have yet to determine.)

The most straightforward definition is the disturbance thickness,  $\delta$ . This is usually defined as the distance from the surface at which the velocity is within 1 percent of the free stream,  $u \approx 0.99 U$  (as shown in Fig. 9.3b). The other two definitions are based on the notion that the boundary layer retards the fluid, so that the mass flux and momentum flux are both less than they would be in the absence of the boundary layer. We imagine that the flow remains at uniform velocity  $U$ , but the surface of the plate is moved upward to reduce either the mass or momentum flux by the same amount that the boundary layer actually does. The *displacement thickness*,  $\delta^*$ , is the distance the plate would be moved so that the loss of mass flux (due to reduction in uniform flow area) is equivalent to the loss the boundary layer causes. The mass flux if we had no boundary layer would be  $\int_0^\infty \rho U dy w$ , where  $w$  is the width of the plate perpendicular to the flow. The actual flow mass flux is  $\int_0^\infty \rho u dy w$ . Hence, the loss due to the boundary layer is  $\int_0^\infty \rho(U - u) dy w$ . If we imagine keeping the velocity at a constant  $U$ , and instead move the plate up a distance  $\delta^*$  (as shown in Fig. 9.3a), the loss of mass flux would be  $\rho U \delta^* w$ . Setting these losses equal to one another gives

$$\rho U \delta^* w = \int_0^\infty \rho(U - u) dy w$$

For incompressible flow,  $\rho = \text{constant}$ , and

$$\delta^* = \int_0^\infty \left(1 - \frac{u}{U}\right) dy \approx \int_0^\delta \left(1 - \frac{u}{U}\right) dy \quad (9.1)$$

Since  $u \approx U$  at  $y = \delta$ , the integrand is essentially zero for  $y \geq \delta$ . Application of the displacement-thickness concept is illustrated in Example 9.1.

The *momentum thickness*,  $\theta$ , is the distance the plate would be moved so that the loss of momentum flux is equivalent to the loss the boundary layer actually causes. The momentum flux if we had no boundary layer would be  $\int_0^\infty \rho u U dy w$  (the actual mass flux is  $\int_0^\infty \rho u dy w$ , and the momentum per unit mass flux of the uniform flow is  $U$  itself). The actual momentum flux of the boundary layer is  $\int_0^\infty \rho u^2 dy w$ . Hence, the loss of momentum in the boundary layer is  $\int_0^\infty \rho u(U - u) dy w$ . If we imagine keeping

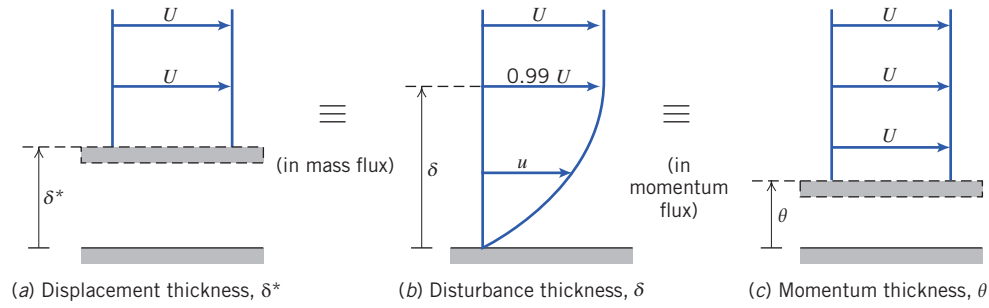


Fig. 9.3 Boundary-layer thickness definitions.

the velocity at a constant  $U$ , and instead move the plate up a distance  $\theta$  (as shown in Fig. 9.3c), the loss of momentum flux would be  $\int_0^\theta \rho U U dy w = \rho U^2 \theta w$ . Setting these losses equal to one another gives

$$\rho U^2 \theta = \int_0^\infty \rho u (U - u) dy$$

and

$$\theta = \int_0^\infty \frac{u}{U} \left(1 - \frac{u}{U}\right) dy \approx \int_0^\delta \frac{u}{U} \left(1 - \frac{u}{U}\right) dy \quad (9.2)$$

Again, the integrand is essentially zero for  $y \geq \delta$ .

The displacement and momentum thicknesses,  $\delta^*$  and  $\theta$ , are *integral thicknesses*, because their definitions, Eqs. 9.1 and 9.2, are in terms of integrals across the boundary layer. Because they are defined in terms of integrals for which the integrand vanishes in the freestream, they are appreciably easier to evaluate accurately from experimental data than the boundary-layer disturbance thickness,  $\delta$ . This fact, coupled with their physical significance, accounts for their common use in specifying boundary-layer thickness.

We have seen that the velocity profile in the boundary layer merges into the local freestream velocity asymptotically. Little error is introduced if the slight difference between velocities at the edge of the boundary layer is ignored for an approximate analysis. Simplifying assumptions usually made for engineering analyses of boundary-layer development are:

- 1  $u \rightarrow U$  at  $y = \delta$
- 2  $\partial u / \partial y \rightarrow 0$  at  $y = \delta$
- 3  $v \ll U$  within the boundary layer

Results of the analyses developed in the following two sections show that the boundary layer is very thin compared with its development length along the surface. Therefore it is also reasonable to assume:

- 4 Pressure variation across the thin boundary layer is negligible. The freestream pressure distribution is *impressed* on the boundary layer.

### Example 9.1 BOUNDARY LAYER IN CHANNEL FLOW

A laboratory wind tunnel has a test section that is 305 mm square. Boundary-layer velocity profiles are measured at two cross sections and displacement thicknesses are evaluated from the measured profiles. At section ①, where the freestream speed is  $U_1 = 26 \text{ m/s}$ , the displacement thickness is  $\delta_1^* = 1.5 \text{ mm}$ . At section ②, located downstream from section ①,  $\delta_2^* = 2.1 \text{ mm}$ . Calculate the change in static pressure between sections ① and ②. Express the result as a fraction of the freestream dynamic pressure at section ①. Assume standard atmosphere conditions.



**Given:** Flow of standard air in laboratory wind tunnel. Test section is  $L = 305$  mm square. Displacement thicknesses are  $\delta_1^* = 1.5$  mm and  $\delta_2^* = 2.1$  mm. Freestream speed is  $U_1 = 26$  m/s.

**Find:** Change in static pressure between sections ① and ②. (Express as a fraction of freestream dynamic pressure at section ①.)

**Solution:** The idea here is that at each location the boundary-layer displacement thickness effectively reduces the area of uniform flow, as indicated in the following figures: Location ② has a smaller effective flow area than location ① (because  $\delta_2^* > \delta_1^*$ ). Hence, from mass conservation the uniform velocity at location ② will be higher. Finally, from the Bernoulli equation the pressure at location ② will be lower than that at location ①.

Apply the continuity and Bernoulli equations to freestream flow outside the boundary-layer displacement thickness, where viscous effects are negligible.

**Governing equations:**

$$= 0(1)$$

$$\frac{\partial}{\partial t} \int_{CV} \rho dV + \int_{CS} \rho \vec{V} \cdot d\vec{A} = 0 \quad (4.12)$$

$$\frac{p_1}{\rho} + \frac{V_1^2}{2} + g z_1 = \frac{p_2}{\rho} + \frac{V_2^2}{2} + g z_2 \quad (4.24)$$

**Assumptions:**

- 1 Steady flow.
- 2 Incompressible flow.
- 3 Flow uniform at each section outside  $\delta^*$ .
- 4 Flow along a streamline between sections ① and ②.
- 5 No frictional effects in freestream.
- 6 Negligible elevation changes.

From the Bernoulli equation we obtain

$$p_1 - p_2 = \frac{1}{2} \rho (V_2^2 - V_1^2) = \frac{1}{2} \rho (U_2^2 - U_1^2) = \frac{1}{2} \rho U_1^2 \left[ \left( \frac{U_2}{U_1} \right)^2 - 1 \right]$$

or

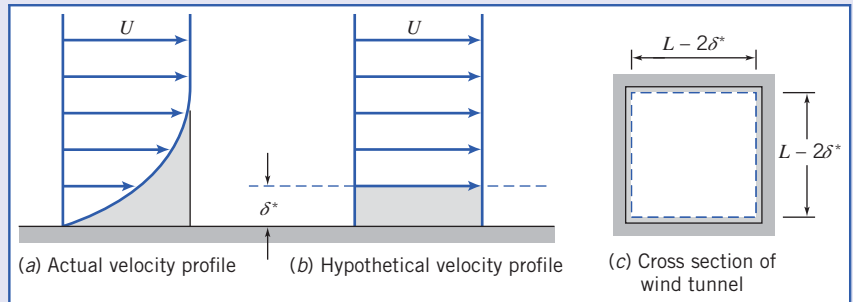
$$\frac{p_1 - p_2}{\frac{1}{2} \rho U_1^2} = \left( \frac{U_2}{U_1} \right)^2 - 1$$

From continuity,  $V_1 A_1 = U_1 A_1 = V_2 A_2 = U_2 A_2$ , so  $U_2/U_1 = A_1/A_2$ , where  $A = (L - 2\delta^*)^2$  is the effective flow area. Substituting gives

$$\frac{p_1 - p_2}{\frac{1}{2} \rho U_1^2} = \left( \frac{A_1}{A_2} \right)^2 - 1 = \left[ \frac{(L - 2\delta_1^*)^2}{(L - 2\delta_2^*)^2} \right]^2 - 1$$

$$\frac{p_1 - p_2}{\frac{1}{2} \rho U_1^2} = \left[ \frac{305 - 2(1.5)}{305 - 2(2.1)} \right]^4 - 1 = 0.0161 \quad \text{or}$$

$$\frac{p_1 - p_2}{\frac{1}{2} \rho U_1^2} = 1.61 \text{ percent} \leftarrow \frac{p_1 - p_2}{\frac{1}{2} \rho U_1^2}$$



**Notes:**

- This problem illustrates a basic application of the displacement-thickness concept. It is somewhat unusual in that, because the flow is confined, the reduction in flow area caused by the boundary layer leads to the result that the pressure in the inviscid flow region drops (if only slightly). In most applications the pressure distribution is determined from the inviscid flow and then applied to the boundary layer.
- We saw a similar phenomenon in Section 8.1, where we discovered that the centerline velocity at the entrance of a pipe increases due to the boundary layer “squeezing” the effective flow area.

## 9.2 Laminar Flat-Plate Boundary Layer: Exact Solution (on the Web)

### 9.3 Momentum Integral Equation

Blasius' exact solution, discussed in Section 9.2 (on the web), analyzed a laminar boundary layer on a flat plate. Even this simplest case (i.e., constant freestream velocity  $U$  and pressure  $p$ , laminar flow) involved a rather subtle mathematical transformation of two differential equations. The solution was based on the insight that the laminar boundary-layer velocity profile is self-similar—only its scale changes as we move along the plate. Numerical integration was necessary to obtain results for the boundary-layer thickness  $\delta(x)$ , velocity profile  $u/U$  versus  $y/\delta$ , and wall shear stress  $\tau_w(x)$ .

We would like to obtain a method for analyzing the general case—that is, for laminar *and* turbulent boundary layers, for which the freestream velocity  $U(x)$  and pressure  $p(x)$  are known functions of position along the surface  $x$ , such as on the curved surface of an airfoil or on the flat but divergent surfaces of a flow diffuser. The approach is one in which we will again apply the basic equations to a control volume. The derivation, from the mass conservation (or continuity) equation and the momentum equation, will take several pages.

Consider incompressible, steady, two-dimensional flow over a solid surface. The boundary-layer thickness,  $\delta$ , grows in some manner with increasing distance,  $x$ . For our analysis we choose a differential control volume, of length  $dx$ , width  $w$ , and height  $\delta(x)$ , as shown in Fig. 9.4. The freestream velocity is  $U(x)$ .

We wish to determine the boundary-layer thickness,  $\delta$ , as a function of  $x$ . There will be mass flow across surfaces  $ab$  and  $cd$  of differential control volume  $abcd$ . What about surface  $bc$ ? Surface  $bc$  is *not* a streamline (see Example W9.1, on the web); it is the imaginary boundary that separates the viscous boundary layer and the inviscid freestream flow. Thus there will be mass flow across surface  $bc$ . Since control surface  $ad$  is adjacent to a solid boundary, there will not be flow across  $ad$ . Before considering the forces acting on the control volume and the momentum fluxes through the control surface, let us apply the continuity equation to determine the mass flux through each portion of the control surface.

#### a. Continuity Equation

Basic equation:

$$\frac{\partial}{\partial t} \int_{CV} \rho \, dV + \int_{CS} \rho \, \vec{V} \cdot d\vec{A} = 0 \quad (4.12)$$

Assumptions:

- 1 Steady flow.
- 2 Two-dimensional flow.

Then

$$\int_{CS} \rho \, \vec{V} \cdot d\vec{A} = 0$$

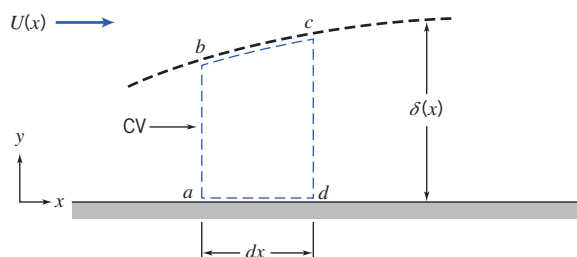


**Fig. 9.4** Differential control volume in a boundary layer.

Hence

$$\dot{m}_{ab} + \dot{m}_{bc} + \dot{m}_{cd} = 0$$

or

$$\dot{m}_{bc} = -\dot{m}_{ab} - \dot{m}_{cd}$$

Now let us evaluate these terms for the differential control volume of width  $w$ :

Surface	Mass Flux
$ab$	Surface $ab$ is located at $x$ . Since the flow is two-dimensional (no variation with $z$ ), the mass flux through $ab$ is $\dot{m}_{ab} = - \left\{ \int_0^\delta \rho u \, dy \right\} w$
$cd$	Surface $cd$ is located at $x + dx$ . Expanding the $\dot{m}$ in a Taylor series about location $x$ , we obtain $\dot{m}_{x+dx} = \dot{m}_x + \left. \frac{\partial \dot{m}}{\partial x} \right _x dx$ and hence $\dot{m}_{cd} = \left\{ \int_0^\delta \rho u \, dy + \frac{\partial}{\partial x} \left[ \int_0^\delta \rho u \, dy \right] dx \right\} w$
$bc$	Thus for surface $bc$ we obtain, from the continuity equation and the above results, $\dot{m}_{bc} = - \left\{ \frac{\partial}{\partial x} \left[ \int_0^\delta \rho u \, dy \right] dx \right\} w$

(Note that the velocity  $u$  and boundary-layer thickness  $\delta$  both depend on  $x$ .)

Now let us consider the momentum fluxes and forces associated with control volume  $abcd$ . These are related by the momentum equation.

### b. Momentum Equation

Apply the  $x$  component of the momentum equation to control volume  $abcd$ :

Basic equation:

$$F_{S_x} + F_{B_x} = \frac{\partial}{\partial t} \int_{CV} u \rho \, dV + \int_{CS} u \rho \, \vec{V} \cdot d\vec{A} \quad (4.18a)$$

Assumptions:

$$3 \quad F_{B_x} = 0$$

Then

$$F_{S_x} = \text{mf}_{ab} + \text{mf}_{bc} + \text{mf}_{cd}$$

where  $\text{mf}$  represents the  $x$  component of momentum flux.

To apply this equation to differential control volume  $abcd$ , we must obtain expressions for the  $x$  momentum flux through the control surface and also the surface forces acting on the control volume in the  $x$  direction. Let us consider the momentum flux first and again consider each segment of the control surface.



Surface	Momentum Flux (mf)
<i>ab</i>	Surface <i>ab</i> is located at $x$ . Since the flow is two-dimensional, the $x$ momentum flux through <i>ab</i> is $\text{mf}_{ab} = - \left\{ \int_0^\delta u \rho u dy \right\}_w$
<i>cd</i>	Surface <i>cd</i> is located at $x + dx$ . Expanding the $x$ momentum flux (mf) in a Taylor series about location $x$ , we obtain $\text{mf}_{x+dx} = \text{mf}_x + \left. \frac{\partial \text{mf}}{\partial x} \right]_x dx$ or $\text{mf}_{cd} = \left\{ \int_0^\delta u \rho u dy + \frac{\partial}{\partial x} \left[ \int_0^\delta u \rho u dy \right] dx \right\}_w$
<i>bc</i>	Since the mass crossing surface <i>bc</i> has velocity component $U$ in the $x$ direction, the $x$ momentum flux across <i>bc</i> is given by $\text{mf}_{bc} = U \dot{m}_{bc}$ $\text{mf}_{bc} = -U \left\{ \frac{\partial}{\partial x} \left[ \int_0^\delta \rho u dy \right] dx \right\}_w$

From the above, we can evaluate the net  $x$  momentum flux through the control surface as

$$\begin{aligned} \int_{CS} u \rho \vec{V} \cdot d\vec{A} = & - \left\{ \int_0^\delta u \rho u dy \right\}_w + \left\{ \int_0^\delta u \rho u dy \right\}_w \\ & + \left\{ \frac{\partial}{\partial x} \left[ \int_0^\delta u \rho u dy \right] dx \right\}_w - U \left\{ \frac{\partial}{\partial x} \left[ \int_0^\delta \rho u dy \right] dx \right\}_w \end{aligned}$$

Collecting terms, we find that

$$\int_{CS} u \rho \vec{V} \cdot d\vec{A} = \left\{ \frac{\partial}{\partial x} \left[ \int_0^\delta u \rho u dy \right] dx - U \frac{\partial}{\partial x} \left[ \int_0^\delta \rho u dy \right] dx \right\}_w$$

Now that we have a suitable expression for the  $x$  momentum flux through the control surface, let us consider the surface forces acting on the control volume in the  $x$  direction. (For convenience the differential control volume has been redrawn in Fig. 9.5.) Note that surfaces *ab*, *bc*, and *cd* all experience normal forces (i.e., pressure) that generate force in the  $x$  direction. In addition, a shear force acts on surface *ad*. Since, by definition of the boundary layer, the velocity gradient goes to zero at the edge of the boundary layer, the shear force acting along surface *bc* is negligible.

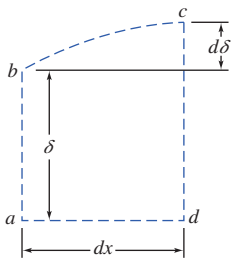


**Fig. 9.5** Differential control volume.

Surface	Force
<i>ab</i>	If the pressure at $x$ is $p$ , then the force acting on surface <i>ab</i> is given by $F_{ab} = p w \delta$ <p>[The boundary layer is very thin; its thickness has been greatly exaggerated in all the sketches we have made. Because it is thin, pressure variations in the <math>y</math> direction may be neglected, and we assume that within the boundary layer, <math>p = p(x)</math> only.]</p>
<i>cd</i>	Expanding in a Taylor series, the pressure at $x + dx$ is given by

$$p_{x+dx} = p + \left. \frac{dp}{dx} \right]_x dx$$

**Table** (Continued)

Surface	Force
	The force on surface $cd$ is then given by
	$F_{cd} = - \left( p + \frac{dp}{dx} \right)_x dx w (\delta + d\delta)$
$bc$	The average pressure acting over surface $bc$ is
	$p + \frac{1}{2} \frac{dp}{dx} dx$
	Then the $x$ component of the normal force acting over $bc$ is given by
	$F_{bc} = \left( p + \frac{1}{2} \frac{dp}{dx} \right)_x dx w d\delta$
$ad$	The average shear force acting on $ad$ is given by
	$F_{ad} = - \left( \tau_w + \frac{1}{2} d\tau_w \right) w dx$

Summing these  $x$  components, we obtain the total force acting in the  $x$  direction on the control volume,

$$F_{S_x} = \left\{ -\frac{dp}{dx} \delta dx - \frac{1}{2} \frac{dp}{dx} dx d\delta - \tau_w dx - \frac{1}{2} d\tau_w dx \right\} w$$

where we note that  $dx d\delta \ll \delta dx$  and  $d\tau_w \ll \tau_w$ , and so neglect the second and fourth terms.

Substituting the expressions, for  $\int_{CS} u \rho \vec{V} \cdot d\vec{A}$  and  $F_{S_x}$  into the  $x$  momentum equation (Eq. 4.18a), we obtain

$$\left\{ -\frac{dp}{dx} \delta dx - \tau_w dx \right\} w = \left\{ \frac{\partial}{\partial x} \left[ \int_0^\delta u \rho u dy \right] dx - U \frac{\partial}{\partial x} \left[ \int_0^\delta \rho u dy \right] dx \right\} w$$

Dividing this equation by  $w dx$  gives

$$-\delta \frac{dp}{dx} - \tau_w = \frac{\partial}{\partial x} \int_0^\delta u \rho u dy - U \frac{\partial}{\partial x} \int_0^\delta \rho u dy \quad (9.16)$$

Equation 9.16 is a “momentum integral” equation that gives a relation between the  $x$  components of the forces acting in a boundary layer and the  $x$  momentum flux.

The pressure gradient,  $dp/dx$ , can be determined by applying the Bernoulli equation to the inviscid flow outside the boundary layer:  $dp/dx = -\rho U dU/dx$ . If we recognize that  $\delta = \int_0^\delta dy$ , then Eq. 9.16 can be written as

$$\tau_w = -\frac{\partial}{\partial x} \int_0^\delta u \rho u dy + U \frac{\partial}{\partial x} \int_0^\delta \rho u dy + \frac{dU}{dx} \int_0^\delta \rho U dy$$

Since

$$U \frac{\partial}{\partial x} \int_0^\delta \rho u dy = \frac{\partial}{\partial x} \int_0^\delta \rho u U dy - \frac{dU}{dx} \int_0^\delta \rho u dy$$

we have

$$\tau_w = \frac{\partial}{\partial x} \int_0^\delta \rho u (U - u) dy + \frac{dU}{dx} \int_0^\delta \rho (U - u) dy$$

and

$$\tau_w = \frac{\partial}{\partial x} U^2 \int_0^\delta \rho \frac{u}{U} \left(1 - \frac{u}{U}\right) dy + U \frac{dU}{dx} \int_0^\delta \rho \left(1 - \frac{u}{U}\right) dy$$

Using the definitions of displacement thickness,  $\delta^*$  (Eq. 9.1), and momentum thickness,  $\theta$  (Eq. 9.2), we obtain

$$\frac{\tau_w}{\rho} = \frac{d}{dx} (U^2 \theta) + \delta^* U \frac{dU}{dx} \quad (9.17)$$

Equation 9.17 is the *momentum integral equation*. This equation will yield an ordinary differential equation for boundary-layer thickness  $\delta$  as a function of  $x$ . Where does  $\delta$  appear in Eq. 9.17? It appears in the upper limits of the integrals that define  $\delta^*$  and  $\theta$ ! All we need to do is provide a suitable expression for the velocity profile  $u/U$  and somehow relate the wall stress  $\tau_w$  to other variables—not necessarily easy tasks! Once the boundary-layer thickness is determined, expressions for the momentum thickness, displacement thickness, and wall shear stress can then be obtained.

Equation 9.17 was obtained by applying the basic equations (continuity and  $x$  momentum) to a differential control volume. Reviewing the assumptions we made in the derivation, we see that the equation is restricted to steady, incompressible, two-dimensional flow with no body forces parallel to the surface.

We have not made any specific assumption relating the wall shear stress,  $\tau_w$ , to the velocity field. Thus Eq. 9.17 is valid for either a laminar or turbulent boundary-layer flow. In order to use this equation to estimate the boundary-layer thickness as a function of  $x$ , we must first:

- 1 Obtain a first approximation to the freestream velocity distribution,  $U(x)$ . This is determined from inviscid flow theory (the velocity that would exist in the absence of a boundary layer) and depends on body shape.
- 2 Assume a reasonable velocity-profile shape inside the boundary layer.
- 3 Derive an expression for  $\tau_w$  using the results obtained from item 2.

To illustrate the application of Eq. 9.17 to boundary-layer flows, we consider first the case of flow with zero pressure gradient over a flat plate (Section 9.4). The results we obtain for a laminar boundary layer can then be compared to the exact Blasius results. The effects of pressure gradients in boundary-layer flow are then discussed in Section 9.5.

## 9.4 Use of the Momentum Integral Equation for Flow with Zero Pressure Gradient

For the special case of a flat plate (zero pressure gradient), the freestream pressure  $p$  and velocity  $U$  are both constant, so for item 1 we have  $U(x) = U = \text{constant}$ .

The momentum integral equation then reduces to

$$\tau_w = \rho U^2 \frac{d\theta}{dx} = \rho U^2 \frac{d}{dx} \int_0^\delta \frac{u}{U} \left(1 - \frac{u}{U}\right) dy \quad (9.18)$$

The velocity distribution,  $u/U$ , in the boundary layer is assumed to be similar for all values of  $x$  and normally is specified as a function of  $y/\delta$ . (Note that  $u/U$  is dimensionless and  $\delta$  is a function of  $x$  only.) Consequently, it is convenient to change the variable of integration from  $y$  to  $y/\delta$ . Defining

$$\eta = \frac{y}{\delta}$$

we get

$$dy = \delta d\eta$$

and the momentum integral equation for zero pressure gradient is written

$$\tau_w = \rho U^2 \frac{d\theta}{dx} = \rho U^2 \frac{d\delta}{dx} \int_0^1 \frac{u}{U} \left(1 - \frac{u}{U}\right) d\eta \quad (9.19)$$

We wish to solve this equation for the boundary-layer thickness as a function of  $x$ . To do this, we must satisfy the remaining items:

2 Assume a velocity distribution in the boundary layer—a functional relationship of the form

$$\frac{u}{U} = f\left(\frac{y}{\delta}\right)$$

(a) The assumed velocity distribution should satisfy the following approximate physical boundary conditions:

$$\begin{aligned} \text{at } y = 0, \quad u &= 0 \\ \text{at } y = \delta, \quad u &= U \\ \text{at } y = \delta, \quad \frac{\partial u}{\partial y} &= 0 \end{aligned}$$

(b) Note that once we have assumed a velocity distribution, from the definition of the momentum thickness (Eq. 9.2), the numerical value of the integral in Eq. 9.19 is simply

$$\int_0^1 \frac{u}{U} \left(1 - \frac{u}{U}\right) d\eta = \frac{\theta}{\delta} = \text{constant} = \beta$$

and the momentum integral equation becomes

$$\tau_w = \rho U^2 \frac{d\delta}{dx} \beta$$

3 Obtain an expression for  $\tau_w$  in terms of  $\delta$ . This will then permit us to solve for  $\delta(x)$ , as illustrated below.

## Laminar Flow

For laminar flow over a flat plate, a reasonable assumption for the velocity profile is a polynomial in  $y$ :

$$u = a + by + cy^2$$

The physical boundary conditions are:

$$\begin{aligned} \text{at } y = 0, \quad u &= 0 \\ \text{at } y = \delta, \quad u &= U \\ \text{at } y = \delta, \quad \frac{\partial u}{\partial y} &= 0 \end{aligned}$$

Evaluating constants  $a$ ,  $b$ , and  $c$  gives

$$\frac{u}{U} = 2\left(\frac{y}{\delta}\right) - \left(\frac{y}{\delta}\right)^2 = 2\eta - \eta^2 \quad (9.20)$$

Equation 9.20 satisfies item 2. For item 3, we recall that the wall shear stress is given by

$$\tau_w = \mu \left. \frac{\partial u}{\partial y} \right|_{y=0}$$

Substituting the assumed velocity profile, Eq. 9.20, into this expression for  $\tau_w$  gives

$$\tau_w = \mu \left. \frac{\partial u}{\partial y} \right|_{y=0} = \mu \left. \frac{U \partial(u/U)}{\delta \partial(y/\delta)} \right|_{y/\delta=0} = \frac{\mu U}{\delta} \left. \frac{d(u/U)}{d\eta} \right|_{\eta=0}$$

or

$$\tau_w = \frac{\mu U}{\delta} \frac{d}{d\eta} (2\eta - \eta^2) \Big|_{\eta=0} = \frac{\mu U}{\delta} (2 - 2\eta) \Big|_{\eta=0} = \frac{2\mu U}{\delta}$$

Note that this shows that the wall stress  $\tau_w$  is a function of  $x$ , since the boundary-layer thickness  $\delta = \delta(x)$ . Now that we have completed items **1**, **2**, and **3**, we can return to the momentum integral equation

$$\tau_w = \rho U^2 \frac{d\delta}{dx} \int_0^1 \frac{u}{U} \left(1 - \frac{u}{U}\right) d\eta \quad (9.19)$$

Substituting for  $\tau_w$  and  $u/U$ , we obtain

$$\frac{2\mu U}{\delta} = \rho U^2 \frac{d\delta}{dx} \int_0^1 (2\eta - \eta^2)(1 - 2\eta + \eta^2) d\eta$$

or

$$\frac{2\mu U}{\delta \rho U^2} = \frac{d\delta}{dx} \int_0^1 (2\eta - 5\eta^2 + 4\eta^3 - \eta^4) d\eta$$

Integrating and substituting limits yield

$$\frac{2\mu}{\delta \rho U} = \frac{2}{15} \frac{d\delta}{dx} \quad \text{or} \quad \delta d\delta = \frac{15\mu}{\rho U} dx$$

which is a differential equation for  $\delta$ . Integrating again gives

$$\frac{\delta^2}{2} = \frac{15\mu}{\rho U} x + c$$

If we assume that  $\delta = 0$  at  $x = 0$ , then  $c = 0$ , and thus

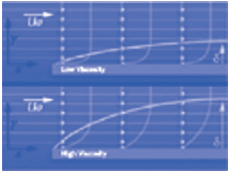
$$\delta = \sqrt{\frac{30\mu x}{\rho U}}$$

Note that this shows that the laminar boundary-layer thickness  $\delta$  grows as  $\sqrt{x}$ ; it has a parabolic shape. Traditionally this is expressed in dimensionless form:



Video: Examples  
of Boundary  
Layer Growth

$$\frac{\delta}{x} = \sqrt{\frac{30\mu}{\rho U x}} = \frac{5.48}{\sqrt{Re_x}} \quad (9.21)$$



Equation 9.21 shows that the ratio of laminar boundary-layer thickness to distance along a flat plate varies inversely with the square root of length Reynolds number. It has the same form as the exact solution derived from the complete differential equations of motion by H. Blasius in 1908. Remarkably, Eq. 9.21 is only in error (the constant is too large) by about 10 percent compared with the exact solution (Section 9.2 on the web). Table 9.2 summarizes corresponding results calculated using other approximate velocity profiles and lists results obtained from the exact solution. The only thing that changes in the analysis when we choose a different velocity profile is the value of  $\beta$  in  $\tau_w = \rho U^2 (d\delta/dx)\beta$ . The shapes of the approximate profiles may be compared readily by plotting  $u/U$  versus  $y/\delta$ .

Once we know the boundary-layer thickness, all details of the flow may be determined. The wall shear stress, or “skin friction,” coefficient is defined as

$$C_f \equiv \frac{\tau_w}{\frac{1}{2}\rho U^2} \quad (9.22)$$

Substituting from the velocity profile and Eq. 9.21 gives

$$C_f = \frac{\tau_w}{\frac{1}{2}\rho U^2} = \frac{2\mu(U/\delta)}{\frac{1}{2}\rho U^2} = \frac{4\mu}{\rho U \delta} = 4 \frac{\mu}{\rho U x} \frac{x}{\delta} = 4 \frac{1}{Re_x} \frac{\sqrt{Re_x}}{5.48}$$

**Table 9.2**

Results of the Calculation of Laminar Boundary-Layer Flow over a Flat Plate at Zero Incidence Based on Approximate Velocity Profiles

Velocity Distribution $\frac{u}{U} = f\left(\frac{y}{\delta}\right) = f(\eta)$	$\beta \equiv \frac{\theta}{\delta}$	$\frac{\delta^*}{\delta}$	$H \equiv \frac{\delta^*}{\theta}$	Constant $a$ in $\frac{\delta}{x} = \frac{a}{\sqrt{Re_x}}$	Constant $b$ in $C_f = \frac{b}{\sqrt{Re_x}}$
$f(\eta) = \eta$	$\frac{1}{6}$	$\frac{1}{2}$	3.00	3.46	0.577
$f(\eta) = 2\eta - \eta^2$	$\frac{2}{15}$	$\frac{1}{3}$	2.50	5.48	0.730
$f(\eta) = \frac{3}{2}\eta - \frac{1}{2}\eta^3$	$\frac{39}{280}$	$\frac{3}{8}$	2.69	4.64	0.647
$f(\eta) = 2\eta - 2\eta^3 + \eta^4$	$\frac{37}{315}$	$\frac{3}{10}$	2.55	5.84	0.685
$f(\eta) = \sin\left(\frac{\pi}{2}\eta\right)$	$\frac{4-\pi}{2\pi}$	$\frac{\pi-2}{\pi}$	2.66	4.80	0.654
Exact	0.133	0.344	2.59	5.00	0.664

Finally,

$$C_f = \frac{0.730}{\sqrt{Re_x}} \quad (9.23)$$

Once the variation of  $\tau_w$  is known, the viscous drag on the surface can be evaluated by integrating over the area of the flat plate, as illustrated in Example 9.2.

Equation 9.21 can be used to calculate the thickness of the laminar boundary layer at transition. At  $Re_x = 5 \times 10^5$ , with  $U = 30$  m/s, for example,  $x = 0.24$  m for air at standard conditions. Thus

$$\frac{\delta}{x} = \frac{5.48}{\sqrt{Re_x}} = \frac{5.48}{\sqrt{5 \times 10^5}} = 0.00775$$

and the boundary-layer thickness is

$$\delta = 0.00775x = 0.00775(0.24 \text{ m}) = 1.86 \text{ mm}$$

The boundary-layer thickness at transition is less than 1 percent of the development length,  $x$ . These calculations confirm that viscous effects are confined to a very thin layer near the surface of a body.

The results in Table 9.2 indicate that reasonable results may be obtained with a variety of approximate velocity profiles.

### Example 9.2 LAMINAR BOUNDARY LAYER ON A FLAT PLATE: APPROXIMATE SOLUTION USING SINUSOIDAL VELOCITY PROFILE

Consider two-dimensional laminar boundary-layer flow along a flat plate. Assume that the velocity profile in the boundary layer is sinusoidal,

$$\frac{u}{U} = \sin\left(\frac{\pi y}{2\delta}\right)$$

Find expressions for:

- The rate of growth of  $\delta$  as a function of  $x$ .
- The displacement thickness,  $\delta^*$ , as a function of  $x$ .
- The total friction force on a plate of length  $L$  and width  $b$ .

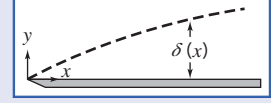


**Given:** Two-dimensional, laminar boundary-layer flow along a flat plate. The boundary-layer velocity profile is

$$\frac{u}{U} = \sin\left(\frac{\pi y}{2\delta}\right) \quad \text{for } 0 \leq y \leq \delta$$

and

$$\frac{u}{U} = 1 \quad \text{for } y > \delta$$



- Find:** (a)  $\delta(x)$ .  
 (b)  $\delta^*$ .  
 (c) Total friction force on a plate of length  $L$  and width  $b$ .

**Solution:** For flat plate flow,  $U = \text{constant}$ ,  $dp/dx = 0$ , and

$$\tau_w = \rho U^2 \frac{d\theta}{dx} = \rho U^2 \frac{d\delta}{dx} \int_0^1 \frac{u}{U} \left(1 - \frac{u}{U}\right) d\eta \quad (9.19)$$

**Assumptions:**

- 1 Steady flow.
- 2 Incompressible flow.

Substituting  $\frac{u}{U} = \sin\frac{\pi}{2}\eta$  into Eq. 9.19, we obtain

$$\begin{aligned} \tau_w &= \rho U^2 \frac{d\delta}{dx} \int_0^1 \sin\frac{\pi}{2}\eta \left(1 - \sin\frac{\pi}{2}\eta\right) d\eta = \rho U^2 \frac{d\delta}{dx} \int_0^1 \left(\sin\frac{\pi}{2}\eta - \sin^2\frac{\pi}{2}\eta\right) d\eta \\ &= \rho U^2 \frac{d\delta}{dx} \frac{2}{\pi} \left[-\cos\frac{\pi}{2}\eta - \frac{1}{2}\frac{\pi}{2}\eta + \frac{1}{4}\sin\pi\eta\right]_0^1 = \rho U^2 \frac{d\delta}{dx} \frac{2}{\pi} \left[0 + 1 - \frac{\pi}{4} + 0 + 0 - 0\right] \\ \tau_w &= 0.137 \rho U^2 \frac{d\delta}{dx} = \beta \rho U^2 \frac{d\delta}{dx}; \quad \beta = 0.137 \end{aligned}$$

Now

$$\tau_w = \mu \left. \frac{\partial u}{\partial y} \right|_{y=0} = \mu \frac{U}{\delta} \left. \frac{\partial(u/U)}{\partial(y/\delta)} \right|_{y=0} = \mu \frac{U}{\delta} \frac{\pi}{2} \cos\frac{\pi}{2}\eta \Big|_{\eta=0} = \frac{\pi\mu U}{2\delta}$$

Therefore,

$$\tau_w = \frac{\pi\mu U}{2\delta} = 0.137 \rho U^2 \frac{d\delta}{dx}$$

Separating variables gives

$$\delta d\delta = 11.5 \frac{\mu}{\rho U} dx$$

Integrating, we obtain

$$\frac{\delta^2}{2} = 11.5 \frac{\mu}{\rho U} x + c$$

But  $c = 0$ , since  $\delta = 0$  at  $x = 0$ , so

$$\delta = \sqrt{23.0 \frac{x\mu}{\rho U}}$$

or

$$\frac{\delta}{x} = 4.80 \sqrt{\frac{\mu}{\rho U x}} = \frac{4.80}{\sqrt{Re_x}} \leftarrow \delta(x)$$

The displacement thickness,  $\delta^*$ , is given by

$$\begin{aligned}\delta^* &= \delta \int_0^1 \left(1 - \frac{u}{U}\right) d\eta \\ &= \delta \int_0^1 \left(1 - \sin \frac{\pi}{2} \eta\right) d\eta = \delta \left[ \eta + \frac{2}{\pi} \cos \frac{\pi}{2} \eta \right]_0^1 \\ \delta^* &= \delta \left[ 1 - 0 + 0 - \frac{2}{\pi} \right] = \delta \left[ 1 - \frac{2}{\pi} \right]\end{aligned}$$

Since, from part (a),

$$\frac{\delta}{x} = \frac{4.80}{\sqrt{Re_x}}$$

then

$$\frac{\delta^*}{x} = \left(1 - \frac{2}{\pi}\right) \frac{4.80}{\sqrt{Re_x}} = \frac{1.74}{\sqrt{Re_x}} \leftarrow \delta^*(x)$$

The total friction force on one side of the plate is given by

$$F = \int_{A_p} \tau_w dA$$

Since  $dA = b dx$  and  $0 \leq x \leq L$ , then

$$\begin{aligned}F &= \int_0^L \tau_w b dx = \int_0^L \rho U^2 \frac{d\theta}{dx} b dx = \rho U^2 b \int_0^{\theta_L} d\theta = \rho U^2 b \theta_L \\ \theta_L &= \int_0^{\delta_L} \frac{u}{U} \left(1 - \frac{u}{U}\right) dy = \delta_L \int_0^1 \frac{u}{U} \left(1 - \frac{u}{U}\right) d\eta = \beta \delta_L\end{aligned}$$

From part (a),  $\beta = 0.137$  and  $\delta_L = \frac{4.80L}{\sqrt{Re_L}}$ , so

$$F = \frac{0.658 \rho U^2 b L}{\sqrt{Re_L}} \leftarrow F$$

This problem illustrates application of the momentum integral equation to the laminar boundary layer on a flat plate.



The Excel workbook for this problem plots the growth of  $\delta$  and  $\delta^*$  in the boundary layer, and the exact solution (Eq. 9.13 on the web). It also shows wall shear stress distributions for the sinusoidal velocity profile and the exact solution.

## Turbulent Flow

For the flat plate, we still have for item **1** that  $U = \text{constant}$ . As for the laminar boundary layer, we need to satisfy item **2** (an approximation for the turbulent velocity profile) and item **3** (an expression for  $\tau_w$ ) in order to solve Eq. 9.19 for  $\delta(x)$ :

$$\tau_w = \rho U^2 \frac{d\delta}{dx} \int_0^1 \frac{u}{U} \left(1 - \frac{u}{U}\right) d\eta \quad (9.19)$$

Details of the turbulent velocity profile for boundary layers at zero pressure gradient are very similar to those for turbulent flow in pipes and channels. Data for turbulent boundary layers plot on the universal velocity profile using coordinates of  $\bar{u}/u_*$  versus  $yu_*/\nu$ , as shown in Fig. 8.9. However, this profile is rather complex mathematically for easy use with the momentum integral equation. The momentum integral equation is approximate; hence, an acceptable velocity profile for turbulent boundary layers on smooth flat plates is the empirical power-law profile. An exponent of  $\frac{1}{7}$  is typically used to model the turbulent velocity profile. Thus

$$\frac{u}{U} = \left(\frac{y}{\delta}\right)^{1/7} = \eta^{1/7} \quad (9.24)$$

However, this profile does not hold in the immediate vicinity of the wall, since at the wall it predicts  $du/dy = \infty$ . Consequently, we cannot use this profile in the definition of  $\tau_w$  to obtain an expression for  $\tau_w$  in terms of  $\delta$  as we did for laminar boundary-layer flow. For turbulent boundary-layer flow we adapt the expression developed for pipe flow,

$$\tau_w = 0.0332 \rho \bar{V}^2 \left[ \frac{\nu}{R \bar{V}} \right]^{0.25} \quad (8.39)$$

For a  $\frac{1}{7}$ -power profile in a pipe, Eq. 8.24 gives  $\bar{V}/U = 0.817$ . Substituting  $\bar{V} = 0.817U$  and  $R = \delta$  into Eq. 8.39, we obtain

$$\tau_w = 0.0233 \rho U^2 \left( \frac{\nu}{U \delta} \right)^{1/4} \quad (9.25)$$

Substituting for  $\tau_w$  and  $u/U$  into Eq. 9.19 and integrating, we obtain

$$0.0233 \left( \frac{\nu}{U \delta} \right)^{1/4} = \frac{d\delta}{dx} \int_0^1 \eta^{1/7} (1 - \eta^{1/7}) d\eta = \frac{7}{72} \frac{d\delta}{dx}$$

Thus we obtain a differential equation for  $\delta$ :

$$\delta^{1/4} d\delta = 0.240 \left( \frac{\nu}{U} \right)^{1/4} dx$$

Integrating gives

$$\frac{4}{5} \delta^{5/4} = 0.240 \left( \frac{\nu}{U} \right)^{1/4} x + c$$

If we assume that  $\delta \simeq 0$  at  $x = 0$  (this is equivalent to assuming turbulent flow from the leading edge), then  $c = 0$  and

$$\delta = 0.382 \left( \frac{\nu}{U} \right)^{1/5} x^{4/5}$$

Note that this shows that the turbulent boundary-layer thickness  $\delta$  grows as  $x^{4/5}$ ; it grows almost linearly (recall that  $\delta$  grows more slowly, as  $\sqrt{x}$ , for the laminar boundary layer). Traditionally this is expressed in dimensionless form:

$$\frac{\delta}{x} = 0.382 \left( \frac{\nu}{U x} \right)^{1/5} = \frac{0.382}{Re_x^{1/5}} \quad (9.26)$$

Using Eq. 9.25, we obtain the skin friction coefficient in terms of  $\delta$ :

$$C_f = \frac{\tau_w}{\frac{1}{2} \rho U^2} = 0.0466 \left( \frac{\nu}{U \delta} \right)^{1/4}$$

Substituting for  $\delta$ , we obtain

$$C_f = \frac{\tau_w}{\frac{1}{2} \rho U^2} = \frac{0.0594}{Re_x^{1/5}} \quad (9.27)$$

Experiments show that Eq. 9.27 predicts turbulent skin friction on a flat plate very well for  $5 \times 10^5 < Re_x < 10^7$ . This agreement is remarkable in view of the approximate nature of our analysis.

Application of the momentum integral equation for turbulent boundary-layer flow is illustrated in Example 9.3.

### Example 9.3 TURBULENT BOUNDARY LAYER ON A FLAT PLATE: APPROXIMATE SOLUTION USING $\frac{1}{7}$ -POWER VELOCITY PROFILE

Water flows at  $U = 1$  m/s past a flat plate with  $L = 1$  m in the flow direction. The boundary layer is tripped so it becomes turbulent at the leading edge. Evaluate the disturbance thickness,  $\delta$ , displacement thickness,  $\delta^*$ , and wall shear stress,  $\tau_w$ , at  $x = L$ . Compare with laminar flow maintained to the same position. Assume a  $\frac{1}{7}$ -power turbulent velocity profile.

**Given:** Flat-plate boundary-layer flow; turbulent flow from the leading edge. Assume  $\frac{1}{7}$ -power velocity profile.

- Find:** (a) Disturbance thickness,  $\delta_L$ .  
 (b) Displacement thickness,  $\delta_L^*$ .  
 (c) Wall shear stress,  $\tau_w(L)$ .  
 (d) Comparison with results for laminar flow from the leading edge.

**Solution:** Apply results from the momentum integral equation.

**Governing equations:**

$$\frac{\delta}{x} = \frac{0.382}{Re_x^{1/5}} \quad (9.26)$$

$$\delta^* = \int_0^\infty \left(1 - \frac{u}{U}\right) dy \quad (9.1)$$

$$C_f = \frac{\tau_w}{\frac{1}{2}\rho U^2} = \frac{0.0594}{Re_x^{1/5}} \quad (9.27)$$

At  $x = L$ , with  $\nu = 1.00 \times 10^{-6} \text{ m}^2/\text{s}$  for water ( $T = 20^\circ\text{C}$ ),

$$Re_L = \frac{UL}{\nu} = 1 \frac{\text{m}}{\text{s}} \times 1 \text{ m} \times \frac{\text{s}}{10^{-6} \text{ m}^2} = 10^6$$

From Eq. 9.26,

$$\delta_L = \frac{0.382}{Re_L^{1/5}} L = \frac{0.382}{(10^6)^{1/5}} \times 1 \text{ m} = 0.0241 \text{ m} \quad \text{or} \quad \delta_L = 24.1 \text{ mm} \quad \delta_L$$

Using Eq. 9.1, with  $u/U = (y/\delta)^{1/7} = \eta^{1/7}$ , we obtain

$$\begin{aligned} \delta_L^* &= \int_0^\infty \left(1 - \frac{u}{U}\right) dy = \delta_L \int_0^1 \left(\frac{u}{U}\right) d\left(\frac{y}{\delta}\right) = \delta_L \int_0^1 (1 - \eta^{1/7}) d\eta = \delta_L \left[ \eta - \frac{7}{8} \eta^{8/7} \right]_0^1 \\ \delta_L^* &= \frac{\delta_L}{8} = \frac{24.1 \text{ mm}}{8} = 3.01 \text{ mm} \quad \delta_L^* \end{aligned}$$

From Eq. 9.27,

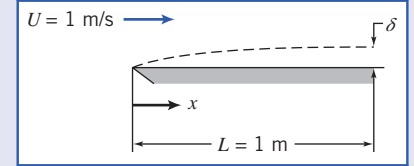
$$\begin{aligned} C_f &= \frac{0.0594}{(10^6)^{1/5}} = 0.00375 \\ \tau_w &= C_f \frac{1}{2} \rho U^2 = 0.00375 \times \frac{1}{2} \times 999 \frac{\text{kg}}{\text{m}^3} \times (1)^2 \frac{\text{m}^2}{\text{s}^2} \times \frac{\text{N} \cdot \text{s}^2}{\text{kg} \cdot \text{m}} \\ \tau_w &= 1.87 \text{ N/m}^2 \quad \tau_w(L) \end{aligned}$$

For laminar flow, use Blasius solution values. From Eq. 9.13 (on the web),

$$\delta_L = \frac{5.0}{\sqrt{Re_L}} L = \frac{5.0}{(10^6)^{1/2}} \times 1 \text{ m} = 0.005 \text{ m} \quad \text{or} \quad 5.00 \text{ mm}$$

From Example W9.1,  $\delta^*/\delta = 0.344$ , so

$$\delta^* = 0.344 \quad \delta = 0.344 \times 5.0 \text{ mm} = 1.72 \text{ mm}$$



From Eq. 9.15,  $C_f = \frac{0.664}{\sqrt{Re_x}}$ , so

$$\tau_w = C_f \frac{1}{2} \rho U^2 = \frac{0.664}{\sqrt{10^6}} \times \frac{1}{2} \times 999 \frac{\text{kg}}{\text{m}^3} \times (1)^2 \frac{\text{m}^2}{\text{s}^2} \times \frac{\text{N} \cdot \text{s}^2}{\text{kg} \cdot \text{m}} = 0.332 \text{ N/m}^2$$

Comparing values at  $x = L$ , we obtain

$$\begin{aligned} \text{Disturbance thickness, } \frac{\delta_{\text{turbulent}}}{\delta_{\text{laminar}}} &= \frac{24.1 \text{ mm}}{5.00 \text{ mm}} = 4.82 \\ \text{Displacement thickness, } \frac{\delta_{\text{turbulent}}^*}{\delta_{\text{laminar}}^*} &= \frac{3.01 \text{ mm}}{1.72 \text{ mm}} = 1.75 \\ \text{Wall shear stress, } \frac{\tau_{w, \text{turbulent}}}{\tau_{w, \text{laminar}}} &= \frac{1.87 \text{ N/m}^2}{0.332 \text{ N/m}^2} = 5.63 \end{aligned}$$

This problem illustrates application of the momentum integral equation to the turbulent boundary layer on a flat plate. Compared to a laminar boundary layer, it is clear that the turbulent boundary layer grows much more rapidly—because the turbulent wall stress is significantly greater than the laminar wall stress.



The Excel workbook for this example plots the  $\frac{1}{7}$ -power-law turbulent boundary layer (Eq. 9.26) and the laminar boundary layer (Eq. 9.13 on the web). It also shows the wall stress distributions for both cases.

## Summary of Results for Boundary-Layer Flow with Zero Pressure Gradient

Use of the momentum integral equation is an approximate technique to predict boundary-layer development; the equation predicts trends correctly. Parameters of the laminar boundary layer vary as  $Re_x^{-1/2}$ ; those for the turbulent boundary layer vary as  $Re_x^{-1/5}$ . Thus the turbulent boundary layer develops more rapidly than the laminar boundary layer.

Laminar and turbulent boundary layers were compared in Example 9.3. Wall shear stress is much higher in the turbulent boundary layer than in the laminar layer. This is the primary reason for the more rapid development of turbulent boundary layers.

The agreement we have obtained with experimental results shows that use of the momentum integral equation is an effective approximate method that gives us considerable insight into the general behavior of boundary layers.

## 9.5 Pressure Gradients in Boundary-Layer Flow

The boundary layer (laminar or turbulent) with a uniform flow along an infinite flat plate is the easiest one to study because the pressure gradient is zero—the fluid particles in the boundary layer are slowed only by shear stresses, leading to boundary-layer growth. We now consider the effects caused by a pressure gradient, which will be present for all bodies except, as we have seen, a flat plate.

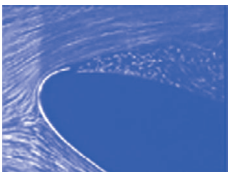
A *favorable pressure gradient* is one in which the pressure decreases in the flow direction (i.e.,  $\partial p / \partial x < 0$ ); it is called favorable because it tends to overcome the slowing of fluid particles caused by friction in the boundary layer. This pressure gradient arises when the freestream velocity  $U$  is increasing with  $x$ , for example, in the converging flow field in a nozzle. On the other hand, an *adverse pressure gradient* is one in which pressure increases in the flow direction (i.e.,  $\partial p / \partial x > 0$ ); it is called adverse because it will cause fluid particles in the boundary layer to slow down at a greater rate than that due to boundary-layer friction alone. If the adverse pressure gradient is severe enough, the fluid particles in the boundary layer will actually be brought to rest. When this occurs, the particles will be forced away from the body surface (a phenomenon called *flow separation*) as they make room for following particles, ultimately leading to a *wake* in which flow is turbulent. Examples of this are when the walls of a diffuser diverge too rapidly and when an airfoil has too large an angle of attack; both of these are generally very undesirable!

This description, of the adverse pressure gradient and friction in the boundary layer together forcing flow separation, certainly makes intuitive sense; the question arises whether we can more formally see when this occurs. For example, can we have flow separation and a wake for uniform flow over a flat plate, for which  $\partial p / \partial x = 0$ ? We can gain insight into this question by considering when the velocity in the boundary layer will become zero. Consider the velocity  $u$  in the boundary layer at an infinitesimal distance  $\Delta y$  above the plate. This will be

$$u_{y=\Delta y} = u_0 + \left( \frac{\partial u}{\partial y} \right)_{y=0} \Delta y = \left( \frac{\partial u}{\partial y} \right)_{y=0} \Delta y$$



Video: Flow Separation: Airfoil



where  $u_0 = 0$  is the velocity at the surface of the plate. It is clear that  $u_{y=\Delta y}$  will be zero (i.e., separation will occur) only when  $\partial u / \partial y|_{y=0} = 0$ . Hence, we can use this as our litmus test for flow separation. We recall that the velocity gradient near the surface in a laminar boundary layer, and in the viscous sublayer of a turbulent boundary layer, was related to the wall shear stress by

$$\tau_w = \mu \left. \frac{\partial u}{\partial y} \right|_{y=0}$$

Further, we learned in the previous section that the wall shear stress for the flat plate is given by

$$\frac{\tau_w(x)}{\rho U^2} = \frac{\text{constant}}{\sqrt{Re_x}}$$

for a laminar boundary layer and

$$\frac{\tau_w(x)}{\rho U^2} = \frac{\text{constant}}{Re_x^{1/5}}$$

for a turbulent boundary layer. We see that for the flow over a flat plate, the wall stress is always  $\tau_w > 0$ . Hence,  $\partial u / \partial y|_{y=0} > 0$  always; and therefore, finally,  $u_{y=\Delta y} > 0$  always. We conclude that for uniform flow over a flat plate the flow *never* separates, and we never develop a wake region, whether the boundary layer is laminar or turbulent, regardless of plate length.

We conclude that flow will not separate for flow over a flat plate, when  $\partial p / \partial x = 0$ . Clearly, for flows in which  $\partial p / \partial x < 0$  (whenever the freestream velocity is increasing), we can be sure that there will be no flow separation; for flows in which  $\partial p / \partial x > 0$  (i.e., adverse pressure gradients) we *could* have flow separation. We should not conclude that an adverse pressure gradient *always* leads to flow separation and a wake; we have only concluded that it is a necessary condition for flow separation to occur.

To illustrate these results consider the variable cross-sectional flow shown in Fig. 9.6. Outside the boundary layer the velocity field is one in which the flow accelerates (Region 1), has a constant velocity region (Region 2), and then a deceleration region (Region 3). Corresponding to these, the pressure gradient is favorable, zero, and adverse, respectively, as shown. Note that the straight wall is not a simple flat plate—it has these various pressure gradients because the flow above the wall is not a uniform flow. From our discussions above, we conclude that separation cannot occur in Region 1 or 2 but can occur in Region 3. Could we avoid flow separation in a device like this? Intuitively, we can see that if we make the divergent section less severe, we may be able to eliminate flow separation. In other words, we may eliminate flow separation if we make the adverse pressure gradient  $\partial p / \partial x$  small enough. The final question remaining is how small the adverse pressure gradient needs to be to accomplish this. This, and a more rigorous proof that we must have  $\partial p / \partial x > 0$  for a chance of flow separation, is beyond the scope of this text [3]. We conclude that flow separation is possible, but not guaranteed, when we have an adverse pressure gradient.

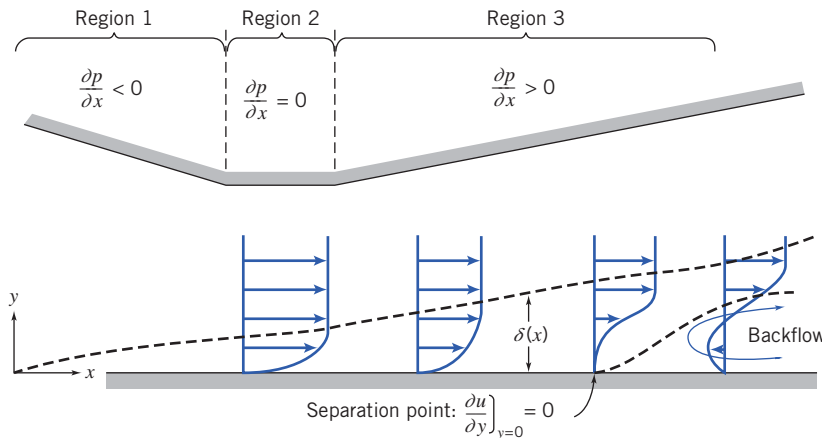


**Fig. 9.6** Boundary-layer flow with pressure gradient (boundary-layer thickness exaggerated for clarity).



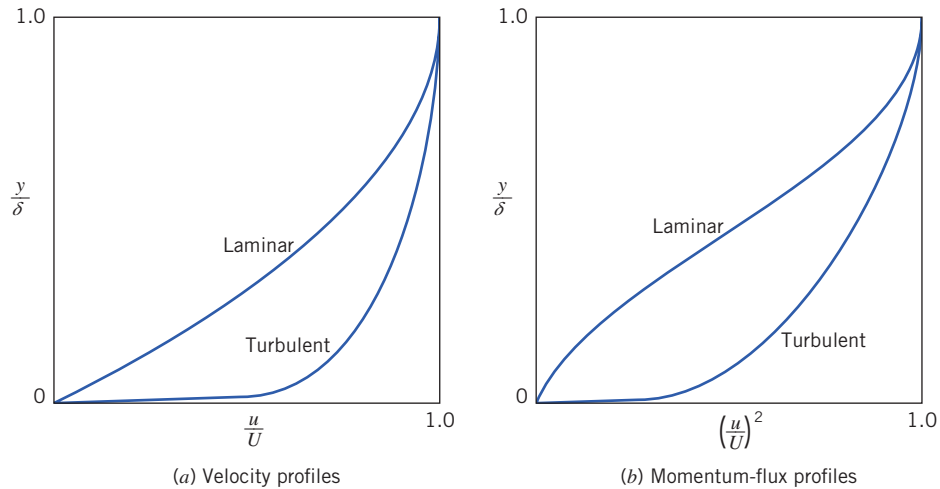


**Fig. 9.7** Nondimensional profiles for flat plate boundary-layer flow.

The nondimensional velocity profiles for laminar and turbulent boundary-layer flow over a flat plate are shown in Fig. 9.7a. The turbulent profile is much fuller (more blunt) than the laminar profile. At the same freestream speed, the momentum flux within the turbulent boundary layer is greater than within the laminar layer (Fig. 9.7b). Separation occurs when the momentum of fluid layers near the surface is reduced to zero by the combined action of pressure and viscous forces. As shown in Fig. 9.7b, the momentum of the fluid near the surface is significantly greater for the turbulent profile. Consequently, the turbulent layer is better able to resist separation in an adverse pressure gradient. We shall discuss some consequences of this behavior in Section 9.6.

Adverse pressure gradients cause significant changes in velocity profiles for both laminar and turbulent boundary-layer flows. Approximate solutions for nonzero pressure gradient flow may be obtained from the momentum integral equation

$$\frac{\tau_w}{\rho} = \frac{d}{dx}(U^2\theta) + \delta^*U \frac{dU}{dx} \quad (9.17)$$

Expanding the first term, we can write

$$\frac{\tau_w}{\rho} = U^2 \frac{d\theta}{dx} + (\delta^* + 2\theta)U \frac{dU}{dx}$$

or

$$\frac{\tau_w}{\rho U^2} = \frac{C_f}{2} = \frac{d\theta}{dx} + (H + 2)\frac{\theta}{U} \frac{dU}{dx} \quad (9.28)$$

where  $H = \delta^*/\theta$  is a velocity-profile “shape factor.” The shape factor increases in an adverse pressure gradient. For turbulent boundary-layer flow,  $H$  increases from 1.3 for a zero pressure gradient to approximately 2.5 at separation. For laminar flow with zero pressure gradient,  $H = 2.6$ ; at separation  $H = 3.5$ .

The freestream velocity distribution,  $U(x)$ , must be known before Eq. 9.28 can be applied. Since  $dp/dx = -\rho U dU/dx$ , specifying  $U(x)$  is equivalent to specifying the pressure gradient. We can obtain a first approximation for  $U(x)$  from ideal flow theory for an inviscid flow under the same conditions. As pointed out in Chapter 6, for frictionless irrotational flow (potential flow), the stream function,  $\psi$ , and the velocity potential,  $\phi$ , satisfy Laplace’s equation. These can be used to determine  $U(x)$  over the body surface.

Much effort has been devoted to calculation of velocity distributions over bodies of known shape (the “direct” problem) and to the determination of body shapes to produce a desired pressure distribution (the “inverse” problem). Smith and co-workers [6] have developed calculation methods that use singularities distributed over the body surface to solve the direct problem for two-dimensional or axisymmetric body shapes. A type of finite-element method that uses singularities defined on discrete surface panels (the “panel” method [7]) recently has gained increased popularity for application to

three-dimensional flows. Recall also that in Section 5.5 we briefly reviewed some basic ideas of CFD (Computational Fluid Dynamics).

Once the velocity distribution,  $U(x)$ , is known, Eq. 9.28 can be integrated to determine  $\theta(x)$ , if  $H$  and  $C_f$  can be correlated with  $\theta$ . A detailed discussion of various calculation methods for flows with nonzero pressure gradient is beyond the scope of this book. Numerous solutions for laminar flows are given in Kraus [8]. Calculation methods for turbulent boundary-layer flow based on the momentum integral equation are reviewed in Rotta [9].

Because of the importance of turbulent boundary layers in engineering flow situations, the state of the art of calculation schemes is advancing rapidly. Numerous calculation schemes have been proposed [10, 11]; most such schemes for turbulent flow use models to predict turbulent shear stress and then solve the boundary-layer equations numerically [12, 13]. Continuing improvement in size and speed of computers is beginning to make possible the solution of the full Navier–Stokes equations using numerical methods [14, 15].

## Part B FLUID FLOW ABOUT IMMERSED BODIES

Whenever there is relative motion between a solid body and the viscous fluid surrounding it, the body will experience a net force  $\vec{F}$ . The magnitude of this force depends on many factors—certainly the relative velocity  $\vec{V}$ , but also the body shape and size, and the fluid properties ( $\rho$ ,  $\mu$ , etc.). As the fluid flows around the body, it will generate surface stresses on each element of the surface, and it is these that lead to the net force. The surface stresses are composed of tangential stresses due to viscous action and normal stresses due to the local pressure. We might be tempted to think that we can analytically derive the net force by integrating these over the body surface. The first step might be: Given the shape of the body (and assuming that the Reynolds number is high enough that we can use inviscid flow theory), compute the pressure distribution. Then integrate the pressure over the body surface to obtain the contribution of pressure forces to the net force  $\vec{F}$ . As we discussed in Chapter 6, this step was developed very early in the history of fluid mechanics; it led to the result that no bodies experience drag! The second step might be: Use this pressure distribution to find the surface viscous stress  $\tau_w$  (at least in principle, using, for example, Eq. 9.17). Then integrate the viscous stress over the body surface to obtain its contribution to the net force  $\vec{F}$ . This procedure sounds conceptually straightforward, but in practice is quite difficult except for the simplest body shapes. In addition, even if possible, it leads to erroneous results in most cases because it takes no account of a very important consequence of the existence of boundary layers—flow separation. This causes a wake, which not only creates a low-pressure region usually leading to large drag on the body but also radically changes the overall flow field and hence the inviscid flow region and pressure distribution on the body.

For these reasons we must usually resort to experimental or CFD methods to determine the net force for most body shapes. Traditionally the net force  $\vec{F}$  is resolved into the drag force,  $F_D$ , defined as the component of the force parallel to the direction of motion, and the lift force,  $F_L$  (if it exists for a body), defined as the component of the force perpendicular to the direction of motion. In Sections 9.6 and 9.7 we will examine these forces for a number of different body shapes.

### 9.6 Drag

Drag is the component of force on a body acting parallel to the direction of relative motion. In discussing the need for experimental results in fluid mechanics (Chapter 7), we considered the problem of determining the drag force,  $F_D$ , on a smooth sphere of diameter  $d$ , moving through a viscous, incompressible fluid with speed  $V$ ; the fluid density and viscosity were  $\rho$  and  $\mu$ , respectively. The drag force,  $F_D$ , was written in the functional form

$$F_D = f_1(d, V, \mu, \rho)$$

Application of the Buckingham Pi theorem resulted in two dimensionless  $\Pi$  parameters that were written in functional form as

$$\frac{F_D}{\rho V^2 d^2} = f_2\left(\frac{\rho V d}{\mu}\right)$$



Video: *Flow about a Sports Car*



Note that  $d^2$  is proportional to the cross-sectional area ( $A = \pi d^2/4$ ) and therefore we could write

$$\frac{F_D}{\rho V^2 A} = f_3 \left( \frac{\rho V d}{\mu} \right) = f_3(Re) \quad (9.29)$$

Although Eq. 9.29 was obtained for a sphere, the form of the equation is valid for incompressible flow over *any* body; the characteristic length used in the Reynolds number depends on the body shape.

The *drag coefficient*,  $C_D$ , is defined as

$$C_D \equiv \frac{F_D}{\frac{1}{2} \rho V^2 A} \quad (9.30)$$

The number  $\frac{1}{2}$  has been inserted (as was done in the defining equation for the friction factor) to form the familiar dynamic pressure. Then Eq. 9.29 can be written as

$$C_D = f(Re) \quad (9.31)$$

We have not considered compressibility or free-surface effects in this discussion of the drag force. Had these been included, we would have obtained the functional form

$$C_D = f(Re, Fr, M)$$

At this point we shall consider the drag force on several bodies for which Eq. 9.31 is valid. The total drag force is the sum of friction drag and pressure drag. However, the drag coefficient is a function only of the Reynolds number.

We now consider the drag force and drag coefficient for a number of bodies, starting with the simplest: a flat plate parallel to the flow (which has only friction drag); a flat plate normal to the flow (which has only pressure drag); and cylinders and spheres (the simplest 2D and 3D bodies, which have both friction and pressure drag). We will also briefly discuss streamlining.

### Pure Friction Drag: Flow over a Flat Plate Parallel to the Flow

This flow situation was considered in detail in Section 9.4. Since the pressure gradient is zero (and in any event the pressure forces are perpendicular to the plate and therefore do not contribute to drag), the total drag is equal to the friction drag. Thus

$$F_D = \int_{\text{plate surface}} \tau_w dA$$

and

$$C_D = \frac{F_D}{\frac{1}{2} \rho V^2 A} = \frac{\int_{PS} \tau_w dA}{\frac{1}{2} \rho V^2 A} \quad (9.32)$$

where  $A$  is the total surface area in contact with the fluid (i.e., the *wetted area*). The drag coefficient for a flat plate parallel to the flow depends on the shear stress distribution along the plate.

For laminar flow over a flat plate, the shear stress coefficient was given by

$$C_f = \frac{\tau_w}{\frac{1}{2} \rho U^2} = \frac{0.664}{\sqrt{Re_x}} \quad (9.15)$$

The drag coefficient for flow with freestream velocity  $V$ , over a flat plate of length  $L$  and width  $b$ , is obtained by substituting for  $\tau_w$  from Eq. 9.15 into Eq. 9.32. Thus

$$\begin{aligned} C_D &= \frac{1}{A} \int_A 0.664 Re_x^{-0.5} dA = \frac{1}{bL} \int_0^L 0.664 \left( \frac{V}{\nu} \right)^{-0.5} x^{-0.5} b dx \\ &= \frac{0.664}{L} \left( \frac{\nu}{V} \right)^{0.5} \left[ \frac{x^{0.5}}{0.5} \right]_0^L = 1.33 \left( \frac{\nu}{VL} \right)^{0.5} \end{aligned}$$

$$C_D = \frac{1.33}{\sqrt{Re_L}} \quad (9.33)$$

Assuming the boundary layer is turbulent from the leading edge, the shear stress coefficient, based on the approximate analysis of Section 9.4, is given by

$$C_f = \frac{\tau_w}{\frac{1}{2}\rho U^2} = \frac{0.0594}{Re_x^{1/5}} \quad (9.27)$$

Substituting for  $\tau_w$  from Eq. 9.27 into Eq. 9.32, we obtain

$$\begin{aligned} C_D &= \frac{1}{A} \int_A 0.0594 Re_x^{-0.2} dA = \frac{1}{bL} \int_0^L 0.0594 \left(\frac{V}{\nu}\right)^{-0.2} x^{-0.2} b dx \\ &= \frac{0.0594}{L} \left(\frac{\nu}{V}\right)^{0.2} \left[\frac{x^{0.8}}{0.8}\right]_0^L = 0.0742 \left(\frac{\nu}{VL}\right)^{0.2} \end{aligned}$$

$$C_D = \frac{0.0742}{Re_L^{1/5}} \quad (9.34)$$

Equation 9.34 is valid for  $5 \times 10^5 < Re_L < 10^7$ .

For  $Re_L < 10^9$  the empirical equation given by Schlichting [3]

$$C_D = \frac{0.455}{(\log Re_L)^{2.58}} \quad (9.35)$$

fits experimental data very well.

For a boundary layer that is initially laminar and undergoes transition at some location on the plate, the turbulent drag coefficient must be adjusted to account for the laminar flow over the initial length. The adjustment is made by subtracting the quantity  $B/Re_L$  from the  $C_D$  determined for completely turbulent flow. The value of  $B$  depends on the Reynolds number at transition;  $B$  is given by

$$B = Re_{tr}(C_{D_{turbulent}} - C_{D_{laminar}}) \quad (9.36)$$

For a transition Reynolds number of  $5 \times 10^5$ , the drag coefficient may be calculated by making the adjustment to Eq. 9.34, in which case

$$C_D = \frac{0.0742}{Re_L^{1/5}} - \frac{1740}{Re_L} \quad (5 \times 10^5 < Re_L < 10^7) \quad (9.37a)$$

or to Eq. 9.35, in which case

$$C_D = \frac{0.455}{(\log Re_L)^{2.58}} - \frac{1610}{Re_L} \quad (5 \times 10^5 < Re_L < 10^9) \quad (9.37b)$$

The variation in drag coefficient for a flat plate parallel to the flow is shown in Fig. 9.8.

In the plot of Fig. 9.8, transition was assumed to occur at  $Re_x = 5 \times 10^5$  for flows in which the boundary layer was initially laminar. The actual Reynolds number at which transition occurs depends on a combination of factors, such as surface roughness and freestream disturbances. Transition tends to occur earlier (at lower Reynolds number) as surface roughness or freestream turbulence is increased. For transition at other than  $Re_x = 5 \times 10^5$ , the constant in the second term of Eqs. 9.37 is modified using Eq. 9.36. Figure 9.8 shows that the drag coefficient is less, for a given length of plate, when laminar flow is maintained over the longest possible distance. However, at large  $Re_L (> 10^7)$  the contribution of the laminar drag is negligible. Example 9.4 illustrates how the skin friction force due to a turbulent boundary layer is calculated.

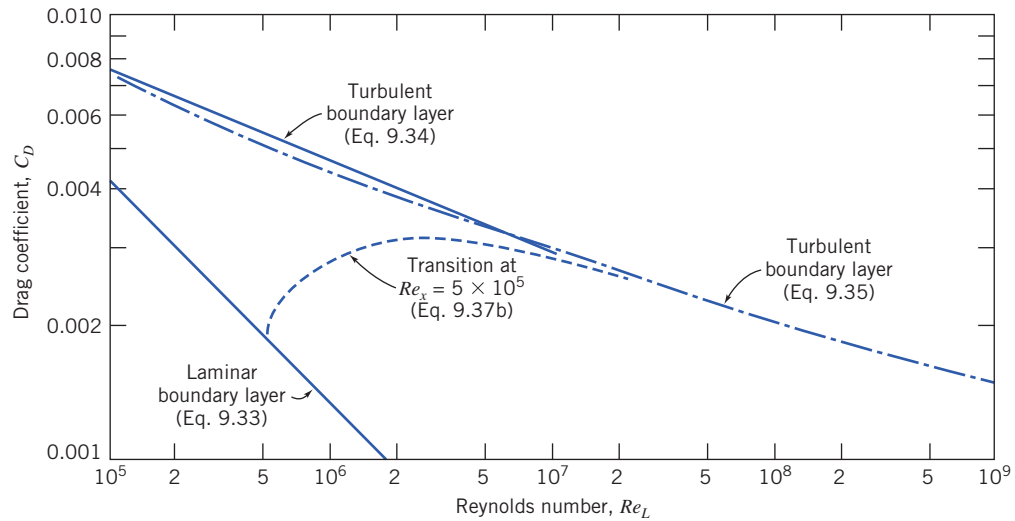


**Fig. 9.8** Variation of drag coefficient with Reynolds number for a smooth flat plate parallel to the flow.

### Example 9.4 SKIN FRICTION DRAG ON A SUPERTANKER

A supertanker is 360 m long and has a beam width of 70 m and a draft of 25 m. Estimate the force and power required to overcome skin friction drag at a cruising speed of 13 kt in seawater at 10°C.

**Given:** Supertanker cruising at  $U = 13$  kt.

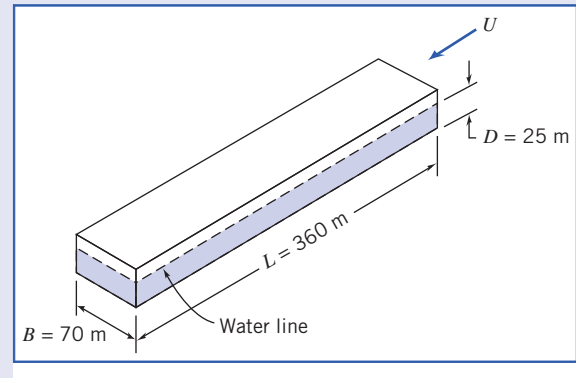
**Find:** (a) Force.  
(b) Power required to overcome skin friction drag.

**Solution:** Model the tanker hull as a flat plate, of length  $L$  and width  $b = B + 2D$ , in contact with water. Estimate skin friction drag from the drag coefficient.

**Governing equations:**

$$C_D = \frac{F_D}{\frac{1}{2}\rho U^2 A} \quad (9.32)$$

$$C_D = \frac{0.455}{(\log Re_L)^{2.58}} - \frac{1610}{Re_L} \quad (9.37b)$$



The ship speed is 13 kt (nautical miles per hour), so

$$U = 13 \frac{\text{nm}}{\text{h}} \times 6076 \frac{\text{ft}}{\text{nm}} \times 0.305 \frac{\text{m}}{\text{ft}} \times \frac{\text{h}}{3600 \text{ s}} = 6.69 \text{ m/s}$$

From Appendix A, at 10°C,  $\nu = 1.37 \times 10^{-6} \text{ m}^2/\text{s}$  for seawater. Then

$$Re_L = \frac{UL}{\nu} = 6.69 \frac{\text{m}}{\text{s}} \times 360 \text{ m} \times \frac{\text{s}}{1.37 \times 10^{-6} \text{ m}^2} = 1.76 \times 10^9$$

Assuming Eq. 9.37b is valid,

$$C_D = \frac{0.455}{(\log 1.76 \times 10^9)^{2.58}} - \frac{1610}{1.76 \times 10^9} = 0.00147$$

and from Eq. 9.32,

$$F_D = C_D A \frac{1}{2} \rho U^2$$

$$= 0.00147 \times (360 \text{ m})(70 + 50) \text{ m} \times \frac{1}{2} \times 1020 \frac{\text{kg}}{\text{m}^3} \times (6.69)^2 \frac{\text{m}^2}{\text{s}^2} \times \frac{\text{N} \cdot \text{s}^2}{\text{kg} \cdot \text{m}}$$

$$F_D = 1.45 \text{ MN} \leftarrow F_D$$

The corresponding power is

$$\mathcal{P} = F_D U = 1.45 \times 10^6 \text{ N} \times 6.69 \frac{\text{m}}{\text{s}} \times \frac{\text{W} \cdot \text{s}}{\text{N} \cdot \text{m}}$$

$$\mathcal{P} = 9.70 \text{ MW} \leftarrow \mathcal{P}$$

This problem illustrates application of drag coefficient equations for a flat plate parallel to the flow.

- The power required (about 13,000 hp) is very large because although the friction stress is small, it acts over a substantial area.
- The boundary layer is turbulent for almost the entire length of the ship (transition occurs at  $x \approx 0.1 \text{ m}$ ).

### Pure Pressure Drag: Flow over a Flat Plate Normal to the Flow

In flow over a flat plate normal to the flow (Fig. 9.9), the wall shear stress is perpendicular to the flow direction and therefore does not contribute to the drag force. The drag is given by

$$F_D = \int_{\text{surface}} p dA$$

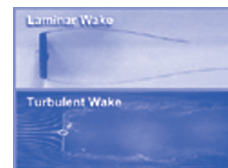
For this geometry the flow separates from the edges of the plate; there is back-flow in the low energy wake of the plate. Although the pressure over the rear surface of the plate is essentially constant, its magnitude cannot be determined analytically. Consequently, we must resort to experiments to determine the drag force.

The drag coefficient for flow over an immersed object usually is based on the *frontal area* (or projected area) of the object. (For airfoils and wings, the *planform area* is used; see Section 9.7.)

The drag coefficient for a finite plate normal to the flow depends on the ratio of plate width to height and on the Reynolds number. For  $Re$  (based on height) greater than about 1000, the drag coefficient is essentially independent of Reynolds number. The variation of  $C_D$  with the ratio of plate width to height ( $b/h$ ) is shown in Fig. 9.10. (The ratio  $b/h$  is defined as the *aspect ratio* of the plate.) For  $b/h = 1.0$ , the drag coefficient is a minimum at  $C_D = 1.18$  this is just slightly higher than for a circular disk ( $C_D = 1.17$ ) at large Reynolds number.

The drag coefficient for all objects with sharp edges is essentially independent of Reynolds number (for  $Re \gtrsim 1000$ ) because the separation points and therefore the size of the wake are fixed by the geometry of the object. Drag coefficients for selected objects are given in Table 9.3.

 Video: *Plate Normal to the Flow*



### Friction and Pressure Drag: Flow over a Sphere and Cylinder

We have looked at two special flow cases in which either friction or pressure drag was the sole form of drag present. In the former case, the drag coefficient was a strong function of Reynolds number, while in the latter case,  $C_D$  was essentially independent of Reynolds number for  $Re \gtrsim 1000$ .

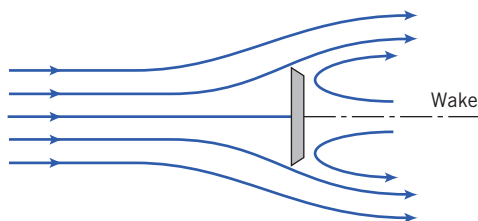


**Fig. 9.9** Flow over a flat plate normal to the flow.



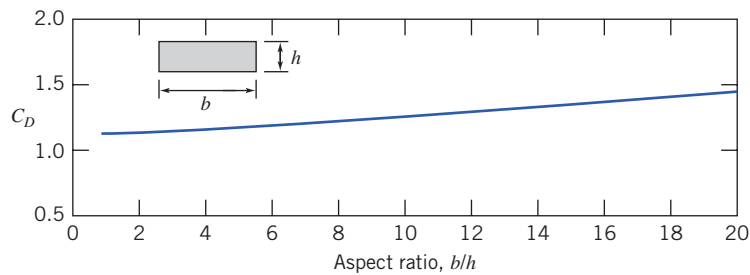
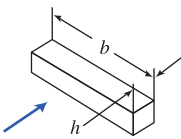




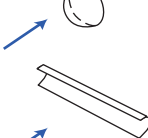
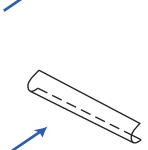


Fig. 9.10 Variation of drag coefficient with aspect ratio for a flat plate of finite width normal to the flow with  $Re_h > 1000$  [16].

Table 9.3  
Drag Coefficient Data for Selected Objects ( $Re \gtrsim 10^3$ )<sup>a</sup>

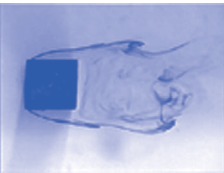
Object	Diagram	$C_D(Re \gtrsim 10^3)$
Square prism		$b/h = \infty$ 2.05 $b/h = 1$ 1.05
Disk		1.17
Ring		$1.20^b$
Hemisphere (open end facing flow)		1.42
Hemisphere (open end facing downstream)		0.38
C-section (open side facing flow)		2.30
C-section (open side facing downstream)		1.20

<sup>a</sup> Data from Hoerner [16].

<sup>b</sup> Based on ring area.



Video: An Object with a High Drag Coefficient



In the case of flow over a sphere, both friction drag and pressure drag contribute to total drag. The drag coefficient for flow over a smooth sphere is shown in Fig. 9.11 as a function of Reynolds number.

At very low Reynolds number,<sup>2</sup>  $Re \leq 1$ , there is no flow separation from a sphere; the wake is laminar and the drag is predominantly friction drag. Stokes has shown analytically, for very low Reynolds number flows where inertia forces may be neglected, that the drag force on a sphere of diameter  $d$ , moving at speed  $V$ , through a fluid of viscosity  $\mu$ , is given by

$$F_D = 3\pi\mu Vd$$

The drag coefficient,  $C_D$ , defined by Eq. 9.30, is then

$$C_D = \frac{24}{Re}$$

As shown in Fig. 9.11, this expression agrees with experimental values at low Reynolds number but begins to deviate significantly from the experimental data for  $Re > 1.0$ .

<sup>2</sup> See Shapiro [17] for a good discussion of drag on spheres and other shapes. See also Fage [18].

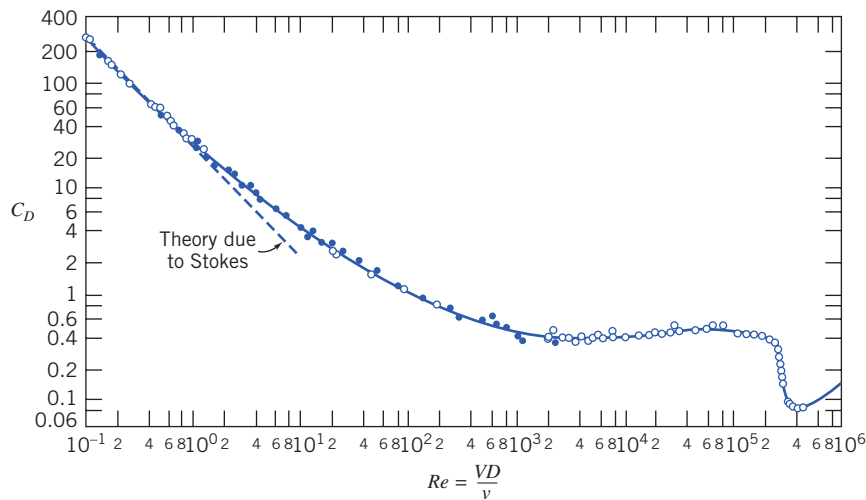


**Fig. 9.11** Drag coefficient of a smooth sphere as a function of Reynolds number (data from References [38], [39], and [3]).

As the Reynolds number is further increased, the drag coefficient drops continuously up to a Reynolds number of about 1000, but not as rapidly as predicted by Stokes' theory. A turbulent wake (not incorporated in Stokes' theory) develops and grows at the rear of the sphere as the separation point moves from the rear of the sphere toward the front; this wake is at a relatively low pressure, leading to a large pressure drag. By the time  $Re \approx 1000$ , about 95% of total drag is due to pressure. For  $10^3 < Re < 3 \times 10^5$  the drag coefficient is approximately constant. In this range the entire rear of the sphere has a low-pressure turbulent wake, as indicated in Fig. 9.12, and most of the drag is caused by the front-rear pressure asymmetry. Note that  $C_D \propto 1/Re$  corresponds to  $F_D \propto V$ , and that  $C_D \sim \text{constant}$  corresponds to  $F_D \propto V^2$ , indicating a quite rapid increase in drag.

 *Video: Examples of Flow around a Sphere*

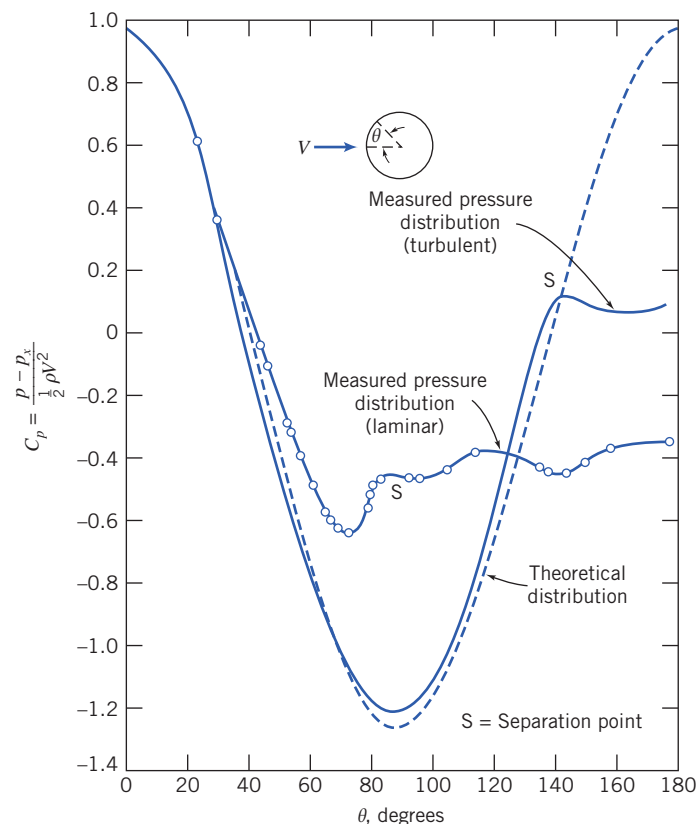


**Fig. 9.12** Pressure distribution around a smooth sphere for laminar and turbulent boundary-layer flow, compared with inviscid flow [18].

For Reynolds numbers larger than about  $3 \times 10^5$ , transition occurs and the boundary layer on the forward portion of the sphere becomes turbulent. The point of separation then moves downstream from the sphere midsection, and the size of the wake decreases. The net pressure force on the sphere is reduced (Fig. 9.12), and the drag coefficient decreases abruptly.

A turbulent boundary layer, since it has more momentum flux than a laminar boundary layer, can better resist an adverse pressure gradient, as discussed in Section 9.5. Consequently, turbulent boundary-layer flow is desirable on a blunt body because it delays separation and thus reduces the pressure drag.

Transition in the boundary layer is affected by roughness of the sphere surface and turbulence in the flow stream. Therefore, the reduction in drag associated with a turbulent boundary layer does not occur at a unique value of Reynolds number. Experiments with smooth spheres in a flow with low turbulence level show that transition may be delayed to a critical Reynolds number,  $Re_D$ , of about  $4 \times 10^5$ . For rough surfaces and/or highly turbulent freestream flow, transition can occur at a critical Reynolds number as low as 50,000.

The drag coefficient of a sphere with turbulent boundary-layer flow is about one-fifth that for laminar flow near the critical Reynolds number. The corresponding reduction in drag force can affect the range of a sphere (e.g., a golf ball) appreciably. The “dimples” on a golf ball are designed to “trip” the boundary layer and, thus, to guarantee turbulent boundary-layer flow and minimum drag. To illustrate this effect graphically, we obtained samples of golf balls without dimples some years ago. One of our students volunteered to hit drives with the smooth balls. In 50 tries with each type of ball, the average distance with the standard balls was 196.51 m; the average with the smooth balls was only 114.25 m.

Adding roughness elements to a sphere also can suppress local oscillations in location of the transition between laminar and turbulent flow in the boundary layer. These oscillations can lead to variations in drag and to random fluctuations in lift (see Section 9.7). In baseball, the “knuckle ball” pitch is intended to behave erratically to confuse the batter. By throwing the ball with almost no spin, the pitcher relies on the seams to cause transition in an unpredictable fashion as the ball moves on its way to the batter. This causes the desired variation in the flight path of the ball.

Figure 9.13 shows the drag coefficient for flow over a smooth cylinder. The variation of  $C_D$  with Reynolds number shows the same characteristics as observed in the flow over a smooth sphere, but the values of  $C_D$  are about twice as high. The use of Fig. 9.13 to determine the drag force on a chimney is shown in Example 9.5, and the use of the drag coefficient data in Table 9.3 to find the drag of a parachute is given in Example 9.6.

Flow about a smooth circular cylinder may develop a regular pattern of alternating vortices downstream. The *vortex trail*<sup>3</sup> causes an oscillatory lift force on the cylinder perpendicular to the stream

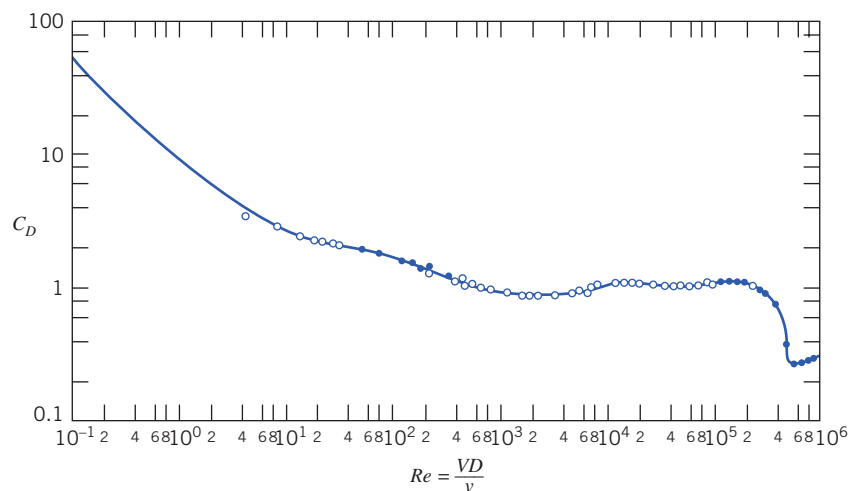


**Fig. 9.13** Drag coefficient for a smooth circular cylinder as a function of Reynolds number (data from References [38], [39], and [3]).

<sup>3</sup> The regular pattern of vortices in the wake of a cylinder sometimes is called a Karman vortex street in honor of the prominent fluid mechanician, Theodore von Kármán, who was first to predict the stable spacing of the vortex trail on theoretical grounds in 1911; see Goldstein [19].

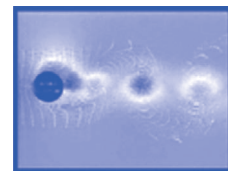
motion. Vortex shedding excites oscillations that cause telegraph wires to “sing” and ropes on flag poles to “slap” annoyingly. Sometimes structural oscillations can reach dangerous magnitudes and cause high stresses; they can be reduced or eliminated by applying roughness elements or fins—either axial or helical (sometimes seen on chimneys or automobile antennas)—that destroy the symmetry of the cylinder and stabilize the flow.

Experimental data show that regular vortex shedding occurs most strongly in the range of Reynolds number from about 60 to 5000. For  $Re > 1000$  the dimensionless frequency of vortex shedding, expressed as a Strouhal number,  $St = fD/V$ , is approximately equal to 0.21 [3].

Roughness affects drag of cylinders and spheres similarly: the critical Reynolds number is reduced by the rough surface, and transition from laminar to turbulent flow in the boundary layers occurs earlier. The drag coefficient is reduced by a factor of about 4 when the boundary layer on the cylinder becomes turbulent.



Video: *Vortex Trail behind a Cylinder*



### Example 9.5 AERODYNAMIC DRAG AND MOMENT ON A CHIMNEY

A cylindrical chimney 1 m in diameter and 25 m tall is exposed to a uniform 50 km/h wind at standard atmospheric conditions. End effects and gusts may be neglected. Estimate the bending moment at the base of the chimney due to wind forces.

**Given:** Cylindrical chimney,  $D = 1$  m,  $L = 25$  m, in uniform flow with

$$V = 50 \text{ km/h} \quad p = 101 \text{ kPa (abs)} \quad T = 15^\circ\text{C}$$

Neglect end effects.

**Find:** Bending moment at bottom of chimney.

**Solution:** The drag coefficient is given by  $C_D = F_D / (\frac{1}{2} \rho V^2 A)$ , and thus  $F_D = C_D A \frac{1}{2} \rho V^2$ . Since the force per unit length is uniform over the entire length, the resultant force,  $F_D$ , will act at the midpoint of the chimney. Hence the moment about the chimney base is

$$M_0 = F_D \frac{L}{2} = C_D A \frac{1}{2} \rho V^2 \frac{L}{2} = C_D A \frac{L}{4} \rho V^2$$

$$V = 50 \frac{\text{km}}{\text{h}} \times 10^3 \frac{\text{m}}{\text{km}} \times \frac{\text{h}}{3600 \text{ s}} = 13.9 \text{ m/s}$$

For air at standard conditions,  $\rho = 1.23 \text{ kg/m}^3$  and  $\mu = 1.79 \times 10^{-5} \text{ kg/(m} \cdot \text{s)}$ . Thus

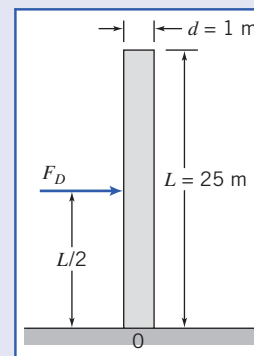
$$Re = \frac{\rho V D}{\mu} = 1.23 \frac{\text{kg}}{\text{m}^3} \times 13.9 \frac{\text{m}}{\text{s}} \times 1 \text{ m} \times \frac{\text{m} \cdot \text{s}}{1.79 \times 10^{-5} \text{ kg}} = 9.55 \times 10^5$$

From Fig. 9.13,  $C_D \approx 0.35$ . For a cylinder,  $A = DL$ , so

$$M_0 = C_D A \frac{L}{4} \rho V^2 = C_D D L \frac{L}{4} \rho V^2 = C_D D \frac{L^2}{4} \rho V^2$$

$$= \frac{1}{4} \times 0.35 \times 1 \text{ m} \times (25)^2 \text{ m}^2 \times 1.23 \frac{\text{kg}}{\text{m}^3} \times (13.9)^2 \frac{\text{m}^2}{\text{s}^2} \times \frac{\text{N} \cdot \text{s}^2}{\text{kg} \cdot \text{m}}$$

$$M_0 = 13.0 \text{ kN} \cdot \text{m} \leftarrow$$



This problem illustrates application of drag-coefficient data to calculate the force and moment on a structure. We modeled the wind as a uniform flow; more realistically, the lower atmosphere is often modeled as a huge turbulent boundary layer, with a power-law velocity profile,  $u \sim y^{1/n}$  ( $y$  is the elevation).

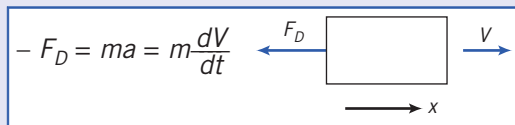
**Example 9.6** DECELERATION OF AN AUTOMOBILE BY A DRAG PARACHUTE

A dragster weighing 7120 N attains a speed of 430 km/h in the quarter mile. Immediately after passing through the timing lights, the driver opens the drag chute, of area  $A = 2.3 \text{ m}^2$ . Air and rolling resistance of the car may be neglected. Find the time required for the machine to decelerate to 160 km/h in standard air.

**Given:** Dragster weighing 7120 N, moving with initial speed  $V_0 = 430 \text{ km/h}$ , is slowed by the drag force on a chute of area  $A = 2.3 \text{ m}^2$ . Neglect air and rolling resistance of the car. Assume standard air.

**Find:** Time required for the machine to decelerate to 160 km/h.

**Solution:** Taking the car as a system and writing Newton's second law in the direction of motion gives



$$V_0 = 430 \text{ km/h}$$

$$V_f = 160 \text{ km/h}$$

$$\rho = 1.227 \text{ kg/m}^3$$

Since  $C_D = \frac{F_D}{\frac{1}{2} \rho V^2 A}$ , then  $F_D = \frac{1}{2} C_D \rho V^2 A$ .

Substituting into Newton's second law gives

$$-\frac{1}{2} C_D \rho V^2 A = m \frac{dV}{dt}$$

Separating variables and integrating, we obtain

$$\begin{aligned} -\frac{1}{2} C_D \rho \frac{A}{m} \int_0^t dt &= \int_{V_0}^{V_f} \frac{dV}{V^2} \\ -\frac{1}{2} C_D \rho \frac{A}{m} t &= -\frac{1}{V} \Big|_{V_0}^{V_f} = -\frac{1}{V_f} + \frac{1}{V_0} = -\frac{(V_0 - V_f)}{V_f V_0} \end{aligned}$$

Finally,

$$t = \frac{(V_0 - V_f)}{V_f V_0} \frac{2m}{C_D \rho A} = \frac{(V_0 - V_f)}{V_f V_0} \frac{2W}{C_D \rho A g}$$

Model the drag chute as a hemisphere (with open end facing flow). From Table 9.3,  $C_D = 1.42$  (assuming  $Re > 10^3$ ). Then, substituting numerical values,

$$\begin{aligned} t &= \frac{(430 - 160) \text{ km/h}}{160 \text{ km/h} \times 430 \text{ km/h}} \times \frac{2 \times 7120 \text{ N}}{1.42 \times 1.227 \text{ kg/m}^3 \times 2.3 \text{ m}^2 \times 9.81 \frac{\text{m}}{\text{s}^2}} \times \frac{\text{km}}{1000 \text{ m}} \\ &\quad \times \frac{3600 \text{ s}}{\text{h}} \times \frac{\text{kg} \cdot \text{m}}{\text{N} \cdot \text{s}^2} \\ t &= 5.12 \text{ s} \end{aligned}$$

Check the assumption on  $Re$ :

$$\begin{aligned} Re &= \frac{DV}{\nu} = \left[ \frac{4A}{\pi} \right]^{1/2} \frac{V}{\nu} \\ &= \left[ \frac{4}{\pi} \times 2.3 \text{ m}^2 \right]^{1/2} \times 160 \frac{\text{km}}{\text{h}} \times \frac{1000 \text{ m}}{\text{km}} \times \frac{\text{h}}{3600 \text{ s}} \times \frac{\text{s}}{1.46 \times 10^{-5} \text{ m}^2} \\ Re &= 5.21 \times 10^6 \end{aligned}$$

Hence the assumption is valid.

This problem illustrates application of drag-coefficient data to calculate the drag on a vehicle parachute.



The Excel workbook for this problem plots the dragster velocity (and distance traveled) as a function of time; it also allows "what-ifs," e.g., we can find the parachute area  $A$  required to slow the dragster to 96 km/h in 5 s.

All experimental data presented in this section are for single objects immersed in an unbounded fluid stream. The objective of wind tunnel tests is to simulate the conditions of an unbounded flow. Limitations on equipment size make this goal unreachable in practice. Frequently it is necessary to apply corrections to measured data to obtain results applicable to unbounded flow conditions.

In numerous realistic flow situations, interactions occur with nearby objects or surfaces. Drag can be reduced significantly when two or more objects, moving in tandem, interact. This phenomenon is well known to bicycle riders and those interested in automobile racing, where “drafting” is a common practice. Drag reductions of 80 percent may be achieved with optimum spacing [20]. Drag also can be increased significantly when spacing is not optimum.

Drag can be affected by neighbors alongside as well. Small particles falling under gravity travel more slowly when they have neighbors than when they are isolated. This phenomenon has important applications to mixing and sedimentation processes.

Experimental data for drag coefficients on objects must be selected and applied carefully. Due regard must be given to the differences between the actual conditions and the more controlled conditions under which measurements were made.

## Streamlining

The extent of the separated flow region behind many of the objects discussed in the previous section can be reduced or eliminated by streamlining, or fairing, the body shape. We have seen that due to the convergent body shape at the rear of any object (after all, every object is of finite length!), the streamlines will diverge, so that the velocity will decrease, and therefore, more importantly (as shown by the Bernoulli equation, applicable in the freestream region) the pressure will increase. Hence, we initially have an adverse pressure gradient at the rear of the body, leading to boundary-layer separation and ultimately to a low-pressure wake leading to large pressure drag. Streamlining is the attempt to reduce the drag on a body. We can reduce the drag on a body by making the rear of the body more tapered (e.g., we can reduce the drag on a sphere by making it “teardrop” shaped), which will reduce the adverse pressure gradient and hence make the turbulent wake smaller. However, as we do so, we are in danger of increasing the skin friction drag simply because we have increased the surface area. In practice, there is an optimum amount of fairing or tapering at which the total drag (the sum of pressure and skin friction drag) is minimized.

The pressure gradient around a “teardrop” shape (a “streamlined” cylinder) is less severe than that around a cylinder of circular section. The trade-off between pressure and friction drag for this case is shown schematically in Fig. 9.14. The pressure drag increases as the thickness is increased, while the friction drag due to the boundary layer flow decreases. The total drag is the sum of the two contributions and is a minimum at some value of thickness. This minimum drag is considerably less than that of a

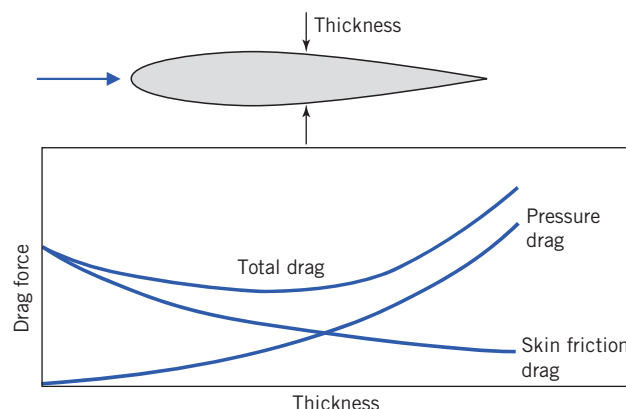


**Fig. 9.14** Drag coefficient on a streamlined airfoil as a function of thickness showing contributions of skin friction and pressure to total drag (adapted from [19]).



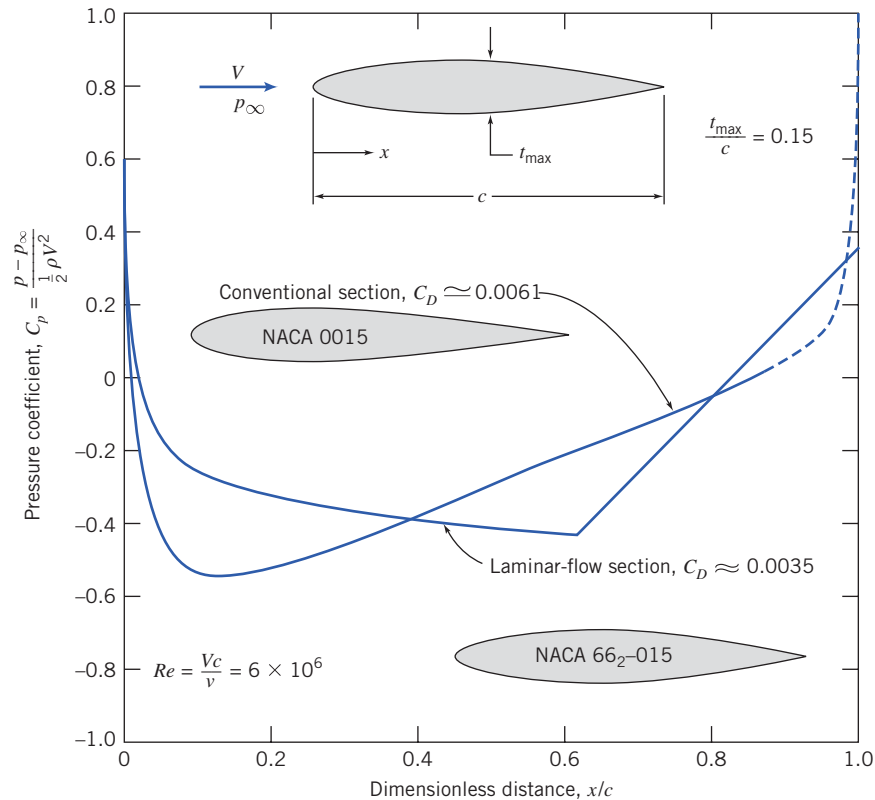


**Fig. 9.15** Theoretical pressure distributions at zero angle of attack for two symmetric airfoil sections of 15 percent thickness ratio. (Data from Abbott and von Doenhoff [21].)

cylinder with a diameter equal to this value of thickness. As a result, streamlining of the structural members on aircraft and automobiles leads to significant savings.

The effect of the airfoil shape on the pressure distribution and drag coefficient<sup>4</sup> is shown in Fig. 9.15 for two symmetric airfoils of infinite span and 15 percent thickness at zero angle of attack. These results were generated by the National Advisory Committee for Aeronautics (NACA), which was founded in 1915 and undertook aeronautical research and development until it was replaced by the National Aeronautics and Space Administration (NASA) in 1958. Transition on the conventional (NACA 0015) airfoil takes place where the pressure gradient becomes adverse, at  $x/c = 0.13$ , near the point of maximum thickness. Thus most of the airfoil surface is covered with a turbulent boundary layer; the drag coefficient is  $C_D \approx 0.0061$ . The point of maximum thickness has been moved aft on the airfoil (NACA 66<sub>2</sub>-015) designed for laminar flow. The boundary layer is maintained in the laminar regime by the favorable pressure gradient to  $x/c = 0.63$ . Thus the bulk of the flow is laminar;  $C_D \approx 0.0035$  for this section, based on planform area. The drag coefficient based on frontal area is  $C_{D_f} = C_D/0.15 = 0.0233$ , or about 40 percent of the optimum for the shapes shown in Fig. 9.14.

Tests in special wind tunnels have shown that laminar flow can be maintained up to length Reynolds numbers as high as 30 million by appropriate profile shaping. Because they have favorable drag characteristics, laminar-flow airfoils are used in the design of most modern subsonic aircraft.

Recent advances have made possible development of low-drag shapes even better than the NACA 60-series shapes. Experiments [21, 22] led to the development of a pressure distribution that prevented separation while maintaining the turbulent boundary layer in a condition that produces negligible skin

<sup>4</sup> Note that drag coefficients for airfoils are based on the *planform* area, i.e.,  $C_D = F_D / \frac{1}{2} \rho V^2 A_p$ , where  $A_p$  is the maximum projected wing area.

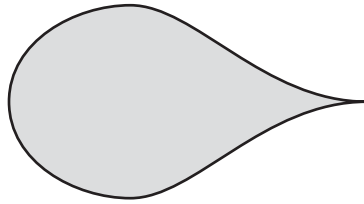


**Fig. 9.16** Nearly optimum shape for low-drag strut [24].

friction. Improved methods for calculating body shapes that produced a desired pressure distribution [23, 24] led to development of nearly optimum shapes for thick struts with low drag. Figure 9.16 shows an example of the results.

Reduction of aerodynamic drag also is important for road vehicle applications. Interest in fuel economy has provided significant incentive to balance efficient aerodynamic performance with attractive design for automobiles. Drag reduction also has become important for buses and trucks.

Practical considerations limit the overall length of road vehicles. Fully streamlined tails are impractical for all but land-speed-record cars. Consequently, it is not possible to achieve results comparable to those for optimum airfoil shapes. However, it is possible to optimize both front and rear contours within given constraints on overall length [25–27].

Much attention has been focused on front contours. Studies on buses have shown that drag reductions up to 25 percent are possible with careful attention to front contour [27]. Thus it is possible to reduce the drag coefficient of a bus from about 0.65 to less than 0.5 with practical designs. Highway tractor-trailer rigs have higher drag coefficients— $C_D$  values from 0.90 to 1.1 have been reported. Commercially available add-on devices offer improvements in drag of up to 15 percent, particularly for windy conditions where yaw angles are nonzero. The typical fuel saving is half the percentage by which aerodynamic drag is reduced.

Front contours and details are important for automobiles. A low nose and smoothly rounded contours are the primary features that promote low drag. Radii of “A-pillar” and windshield header, and blending of accessories to reduce parasite and interference drag have received increased attention. As a result, drag coefficients have been reduced from about 0.55 to 0.30 or less for recent production vehicles. Recent advances in computational methods have led to development of computer-generated optimum shapes. A number of designs have been proposed, with claims of  $C_D$  values below 0.2 for vehicles complete with running gear.

## 9.7 Lift

For most objects in relative motion in a fluid, the most significant fluid force is the drag. However, there are some objects, such as airfoils, for which the lift is significant. Lift is defined as the component of fluid force perpendicular to the fluid motion. For an airfoil, the *lift coefficient*,  $C_L$ , is defined as

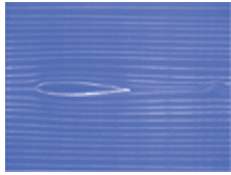
$$C_L \equiv \frac{F_L}{\frac{1}{2} \rho V^2 A_p} \quad (9.38)$$

It is worth noting that the lift coefficient defined above and the drag coefficient (Eq. 9.30) are each defined as the ratio of an actual force (lift or drag) divided by the product of dynamic pressure and area. This denominator can be viewed as the force that would be generated if we imagined bringing to rest the fluid directly approaching the area (recall that the dynamic pressure is the difference between total and static pressures). This gives us a “feel” for the meaning of the coefficients: They indicate the ratio of the actual force to this force. We note also that the coefficient definitions include  $V^2$  in the denominator, so that  $F_L$  (or  $F_D$ ) being proportional to  $V^2$  corresponds to a constant  $C_L$  (or  $C_D$ ), and that  $F_L$  (or  $F_D$ ) increasing with  $V$  at a lower rate than quadratic corresponds to a decrease in  $C_L$  (or  $C_D$ ) with  $V$ .

\*



Video: Flow  
Past an  
Airfoil ( $\alpha = 0^\circ$ )



The lift and drag coefficients for an airfoil are functions of both Reynolds number and angle of attack; the angle of attack,  $\alpha$ , is the angle between the airfoil chord and the freestream velocity vector. The *chord* of an airfoil is the straight line joining the leading edge and the trailing edge. The wing section shape is obtained by combining a *mean line* and a thickness distribution (see Reference [21] for details). When the airfoil has a symmetric section, the mean line and the chord line both are straight lines, and they coincide. An airfoil with a curved mean line is said to be *cambered*.

The area at right angles to the flow changes with angle of attack. Consequently, the planform area,  $A_p$  (the maximum projected area of the wing), is used to define lift and drag coefficients for an airfoil.

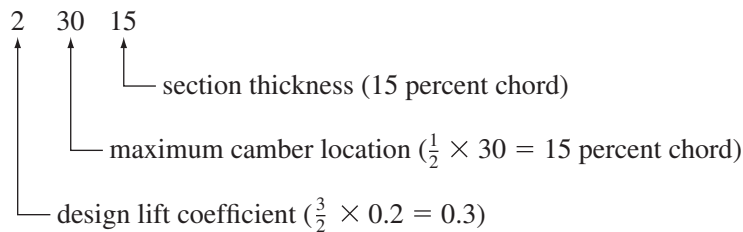
The phenomenon of aerodynamic lift is commonly explained by the velocity increase causing pressure to decrease (the Bernoulli effect) over the top surface of the airfoil and the velocity decrease (causing pressure to increase) along the bottom surface of the airfoil. Because of the pressure differences relative to atmosphere, the upper surface of the airfoil may be called the *suction surface* and the lower surface the *pressure surface*.

As was shown in Example 6.12, lift on a body can also be related to the circulation around the profile: In order for lift to be generated, there must be a net circulation around the profile. One may imagine the circulation to be caused by a vortex “bound” within the profile.

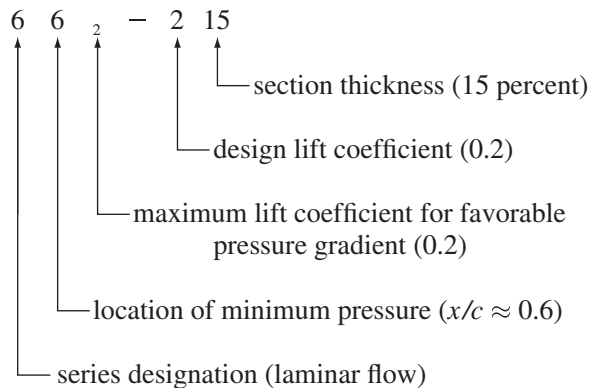
Advances continue in computational methods and computer hardware. However, most airfoil data available in the literature were obtained from wind tunnel tests. Reference [21] contains results from a large number of tests conducted by NACA. Data for some representative NACA profile shapes are described in the following few paragraphs.

Lift and drag coefficient data for typical conventional and laminar-flow profiles are plotted in Fig. 9.17 for a Reynolds number of  $9 \times 10^6$  based on chord length. The section shapes in Fig. 9.17 are designated as follows:

#### Conventional—23015



#### Laminar Flow—66<sub>2</sub>—215



Both sections are cambered to give lift at zero angle of attack. As the angle of attack is increased, the  $\Delta p$  between the upper and lower surfaces increases, causing the lift coefficient to increase smoothly until a maximum is reached. Further increases in angle of attack produce a sudden decrease in  $C_L$ . The airfoil is said to have *stalled* when  $C_L$  drops in this fashion.

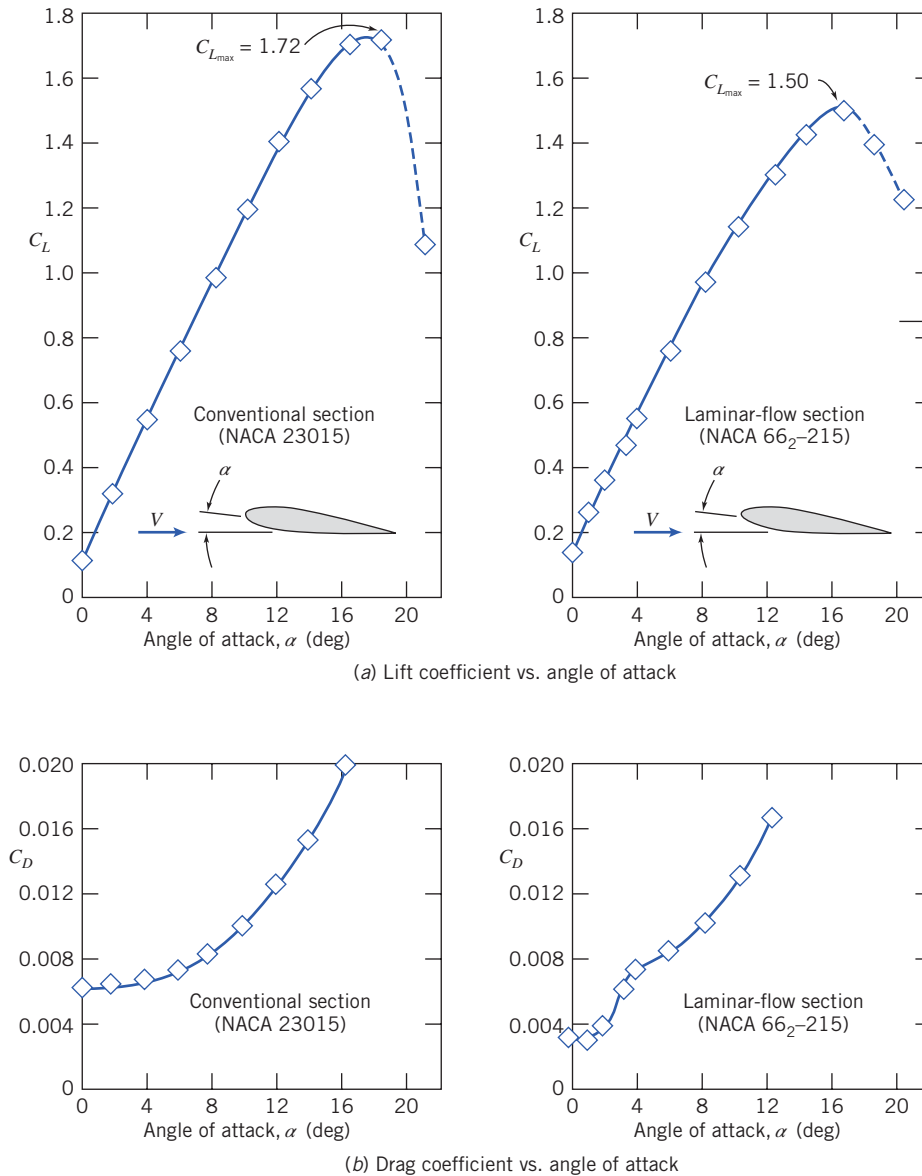


**Fig. 9.17** Lift and drag coefficients versus angle of attack for two airfoil sections of 15 percent thickness ratio at  $Re_c = 9 \times 10^6$ . (Data from Abbott and von Doenhoff [21].)

Airfoil stall results when flow separation occurs over a major portion of the upper surface of the airfoil. As the angle of attack is increased, the stagnation point moves back along the lower surface of the airfoil, as shown schematically for the symmetric laminar-flow section in Fig. 9.18a. Flow on the upper surface then must accelerate sharply to round the nose of the airfoil. The effect of angle of attack on the theoretical upper-surface pressure distribution is shown in Fig. 9.18b. The minimum pressure becomes lower, and its location moves forward on the upper surface. A severe adverse pressure gradient appears following the point of minimum pressure; finally, the adverse pressure gradient causes the flow to separate completely from the upper surface and the airfoil stalls (the uniform pressure in the turbulent wake will be approximately equal to the pressure just before separation, i.e., low).

Movement of the minimum pressure point and accentuation of the adverse pressure gradient are responsible for the sudden increase in  $C_D$  for the laminar-flow section, which is apparent in Fig. 9.17. The sudden rise in  $C_D$  is caused by early transition from laminar to turbulent boundary-layer flow on the upper surface. Aircraft with laminar-flow sections are designed to cruise in the low-drag region.

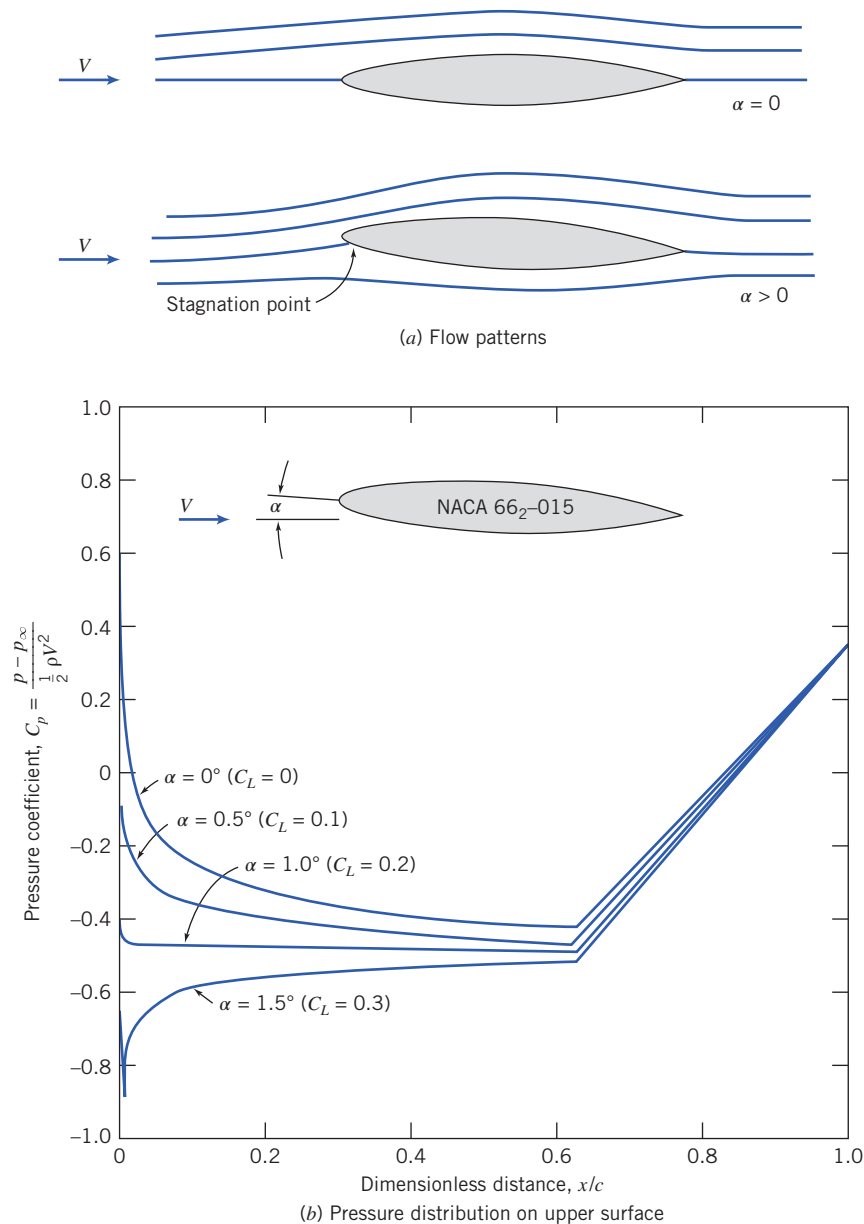


**Fig. 9.18** Effect of angle of attack on flow pattern and theoretical pressure distribution for a symmetric laminar-flow airfoil of 15 percent thickness ratio. (Data from Abbott and von Doenhoff [21].)

Because laminar-flow sections have very sharp leading edges, all of the effects we have described are exaggerated, and they stall at lower angles of attack than conventional sections, as shown in Fig. 9.17. The maximum possible lift coefficient,  $C_{L_{\max}}$ , also is less for laminar-flow sections.

Plots of  $C_L$  versus  $C_D$  (called lift-drag polars) often are used to present airfoil data in compact form. A polar plot is given in Fig. 9.19 for the two sections we have discussed. The lift/drag ratio,  $C_L/C_D$ , is shown at the design lift coefficient for both sections. This ratio is very important in the design of aircraft: The lift coefficient determines the lift of the wing and hence the load that can be carried, and the drag coefficient indicates a large part (in addition to that caused by the fuselage, etc.) of the drag the airplane engines have to work against in order to generate the needed lift; hence, in general, a high  $C_L/C_D$  is the goal, at which the laminar airfoil clearly excels.

Recent improvements in modeling and computational capabilities have made it possible to design airfoil sections that develop high lift while maintaining very low drag [23, 24]. Boundary-layer calculation codes are used with inverse methods for calculating potential flow to develop pressure

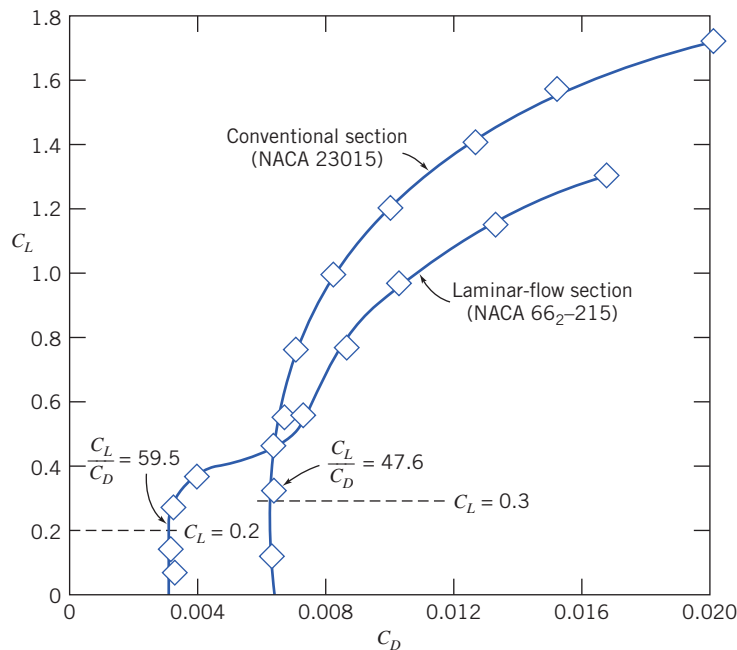


**Fig. 9.19** Lift drag polars for two airfoil sections of 15 percent thickness ratio. (Data from Abbott and von Doenhoff [21].)

distributions and—the resulting body shapes that postpone transition to the most rearward location possible. The turbulent boundary layer following transition is maintained in a state of incipient separation with nearly zero skin friction by appropriate shaping of the pressure distribution.

Such computer-designed airfoils have been used on racing cars to develop very high negative lift (downforce) to improve high-speed stability and cornering performance [23]. Airfoil sections especially designed for operation at low Reynolds number were used for the wings and propeller on the Kremer prize-winning man-powered “Gossamer Condor” [28], which now hangs in the National Air and Space Museum in Washington, D.C.

All real airfoils—*wings*—are of finite span and have less lift and more drag than their airfoil section data would indicate. There are several ways to explain this. If we consider the pressure distribution near the end of the wing, the low pressure on the upper and high pressure on the lower surface cause flow to occur around the wing tip, leading to *trailing vortices* (as shown in Fig. 9.20), and the pressure difference is reduced, leading to less lift. These trailing vortices can also be explained more abstractly, in terms of circulation: We learned in Section 6.5 that circulation around a wing section is present whenever we have lift and that the circulation is solenoidal—that is, it cannot end in the fluid; hence, the circulation extends beyond the wing in the form of trailing vortices. Trailing vortices can be very strong and persistent, possibly being a hazard to other aircraft for 8 to 16 km behind a large airplane—air speeds of greater than 320 km/h have been measured.<sup>5</sup>

 **Video: Wing Tip Vortices**

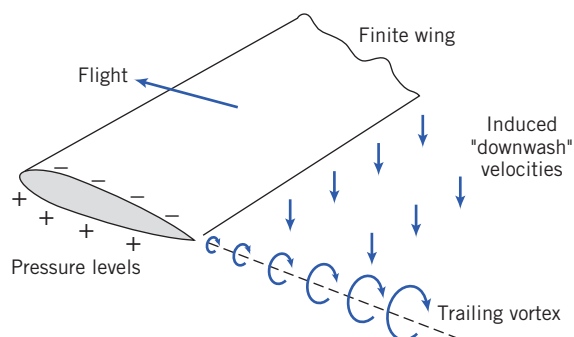
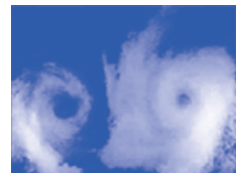


**Fig. 9.20** Schematic representation of the trailing vortex system of a finite wing.

<sup>5</sup> Sforza, P. M., “Aircraft Vortices: Benign or Baleful?” *Space/Aeronautics*, 53, 4, April 1970, pp. 42–49.

Trailing vortices reduce lift because of the loss of pressure difference, as we just mentioned. This reduction and an increase in drag (called *induced drag*) can also be explained in the following way: The “downwash” velocities induced by the vortices mean that the effective angle of attack is reduced—the wing “sees” a flow at approximately the mean of the upstream and downstream directions—explaining why the wing has less lift than its section data would suggest. This also causes the lift force (which is perpendicular to the effective angle of attack) to “lean backward” a little, resulting in some of the lift appearing as drag.

Loss of lift and increase in drag caused by finite-span effects are concentrated near the tip of the wing; hence, it is clear that a short, stubby wing will experience these effects more severely than a very long wing. We should therefore expect the effects to correlate with the wing *aspect ratio*, defined as

$$AR \equiv \frac{b^2}{A_p} \quad (9.39)$$

where  $A_p$  is planform area and  $b$  is wingspan. For a rectangular planform of wingspan  $b$  and chord length  $c$ ,

$$AR = \frac{b^2}{A_p} = \frac{b^2}{bc} = \frac{b}{c}$$

The maximum lift/drag ratio ( $L/D = C_L/C_D$ ) for a modern low-drag section may be as high as 400 for infinite aspect ratio. A high-performance sailplane (glider) with  $AR = 40$  might have  $L/D = 40$ , and a typical light plane ( $AR \approx 12$ ) might have  $L/D \approx 20$  or so. Two examples of rather poor shapes are lifting bodies used for reentry from the upper atmosphere, and water skis, which are *hydrofoils* of low aspect ratio. For both of these shapes,  $L/D$  typically is less than unity.

Variations in aspect ratio are seen in nature. Soaring birds, such as the albatross or California condor, have thin wings of long span. Birds that must maneuver quickly to catch their prey, such as hawks, have wings of relatively short span, but large area, which gives low *wing loading* (ratio of weight to planform area) and thus high maneuverability.

It makes sense that as we try to generate more lift from a finite wing (by, for example, increasing the angle of attack), the trailing vortices and therefore the downwash increase; we also learned that the downwash causes the effective angle of attack to be less than that of the corresponding airfoil section (i.e., when  $AR = \infty$ ), ultimately leading to loss of lift and to induced drag. Hence, we conclude that the effects of the finite aspect ratio can be characterized as a reduction  $\Delta\alpha$  in the effective angle of attack and that this (which is usually undesirable) becomes worse as we generate more lift (i.e., as the lift coefficient  $C_L$  increases) and as the aspect ratio  $AR$  is made smaller. Theory and experiment indicate that

$$\Delta\alpha \approx \frac{C_L}{\pi AR} \quad (9.40)$$

Compared with an airfoil section ( $AR = \infty$ ), the geometric angle of attack of a wing (finite  $AR$ ) must be increased by this amount to get the same lift, as shown in Fig. 9.21. It also means that instead of being

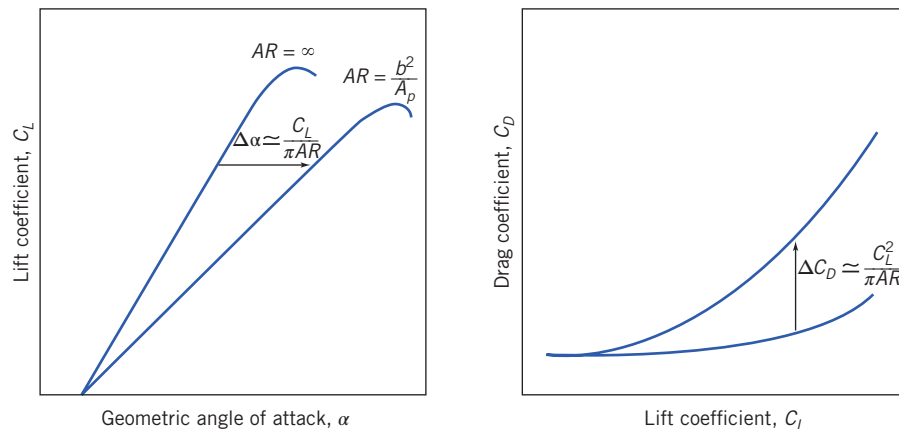


**Fig. 9.21** Effect of finite aspect ratio on lift and drag coefficients for a wing.



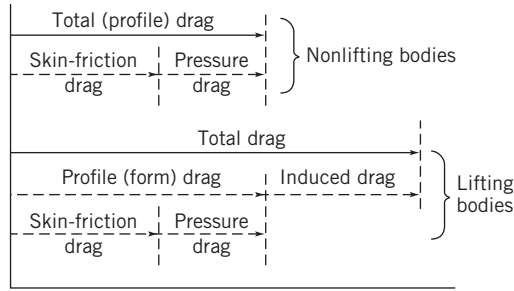


**Fig. 9.22** Drag breakdown on nonlifting and lifting bodies.

perpendicular to the motion, the lift force leans angle  $\Delta\alpha$  backward from the perpendicular—we have an induced drag component of the drag coefficient. From simple geometry

$$\Delta C_D \approx C_L \Delta\alpha \approx \frac{C_L^2}{\pi AR} \quad (9.41)$$

This is also shown in Fig. 9.21.

When written in terms of aspect ratio, the drag of a wing of finite span becomes [21]

$$C_D = C_{D,\infty} + C_{D,i} = C_{D,\infty} + \frac{C_L^2}{\pi AR} \quad (9.42)$$

where  $C_{D,\infty}$  is the section drag coefficient at  $C_L$ ,  $C_{D,i}$  is the induced drag coefficient at  $C_L$  and  $AR$  is the aspect ratio of the finite-span wing.

Drag on airfoils arises from viscous and pressure forces. Viscous drag changes with Reynolds number but only slightly with angle of attack. These relationships and some commonly used terminology are illustrated in Fig. 9.22.

A useful approximation to the drag polar for a complete aircraft may be obtained by adding the induced drag to the drag at zero lift. The drag at any lift coefficient is obtained from

$$C_D = C_{D,0} + C_{D,i} = C_{D,0} + \frac{C_L^2}{\pi AR} \quad (9.43)$$

where  $C_{D,0}$  is the drag coefficient at zero lift and  $AR$  is the aspect ratio. The optimum cruising speed of an aircraft brings in these lift and drag relations, as shown in Example 9.7.

### Example 9.7 OPTIMUM CRUISE PERFORMANCE OF A JET TRANSPORT

Jet engines burn fuel at a rate proportional to thrust delivered. The optimum cruise condition for a jet aircraft is at maximum speed for a given thrust. In steady level flight, thrust and drag are equal. Hence, optimum cruise occurs at the speed when the ratio of drag force to air speed is minimized.

A Boeing 727-200 jet transport has wing planform area  $A_p = 149 \text{ m}^2$  and aspect ratio  $AR = 6.5$ . Stall speed at sea level for this aircraft with flaps up and a gross weight of 667,500 N is 280 km/h. Below  $M = 0.6$ , drag due to compressibility effects is negligible, so Eq. 9.43 may be used to estimate total drag on the aircraft.  $C_{D,0}$  for the aircraft is constant at 0.0182. Assume that sonic speed at sea level is  $c = 1214 \text{ km/h}$ .

Evaluate the performance envelope for this aircraft at sea level by plotting drag force versus speed, between stall and  $M = 0.6$ . Use this graph to estimate optimum cruise speed for the aircraft at sea-level conditions. Comment on stall speed and optimum cruise speed for the aircraft at 9140 m altitude on a standard day.

**Given:** Boeing 727-200 jet transport at sea-level conditions.

$$W = 667,500 \text{ N}, \quad A = 149 \text{ m}^2, \quad AR = 6.5, \quad \text{and} \quad C_{D,0} = 0.0182$$

Stall speed is  $V_{\text{stall}} = 1214 \text{ km/h}$ , and compressibility effects on drag are negligible for  $M \leq 0.6$  (sonic speed at sea level is  $c = 280 \text{ km/h}$ ).

**Find:** (a) Drag force as a function of speed from  $V_{\text{stall}}$  to  $M = 0.6$ ; plot results.  
 (b) Estimate of optimum cruise speed at sea level.  
 (c) Stall speed and optimum cruise speed at 9140 m altitude.

**Solution:** For steady level flight, weight equals lift and thrust equals drag.

**Governing equations:**

$$F_L = C_L A \frac{1}{2} \rho V^2 = W \quad C_D = C_{D,0} + \frac{C_L^2}{\pi AR}$$

$$F_D = C_D A \frac{1}{2} \rho V^2 = T \quad M = \frac{V}{c}$$

At sea level,  $\rho = 1.227 \text{ kg/m}^3$ , and  $c = 1214 \text{ km/h}$ .

Since  $F_L = W$  for level flight at any speed, then

$$C_L = \frac{W}{\frac{1}{2} \rho V^2 A} = \frac{2W}{\rho V^2 A}$$

At stall speed,  $V = 280 \text{ km/h}$ , so

$$C_L = \frac{2 \times 667,500 \text{ N}}{1.227 \frac{\text{kg}}{\text{m}^3} \times (280)^2 (\text{kg/h})^2 \times 149 \text{ m}^2} \times \frac{\text{kg} \cdot \text{m}}{\text{N} \cdot \text{s}^2} \times \left( \frac{3600 \text{ s}}{\text{h}} \right)^2 \times \left( \frac{\text{km}}{1000 \text{ m}} \right)^2$$

$$C_L = \frac{9.46 \times 10^4}{V(\text{km/h})^2} = \frac{9.46 \times 10^4}{(280)^2} = 1.207$$

$$C_D = C_{D,0} + \frac{C_L^2}{\pi AR} = 0.0182 + \frac{(1.207)^2}{\pi(6.5)} = 0.0895$$

Then

$$F_D = W \frac{C_D}{C_L} = 667,500 \left( \frac{0.0895}{1.207} \right) = 49,496 \text{ N}$$

At  $M = 0.6$ ,  $V = Mc = (0.6)1214 \text{ km/h} = 728 \text{ km/h}$ , so  $C_L = 0.177$  and

$$C_D = 0.0182 + \frac{(0.178)^2}{\pi(6.5)} = 0.0198$$

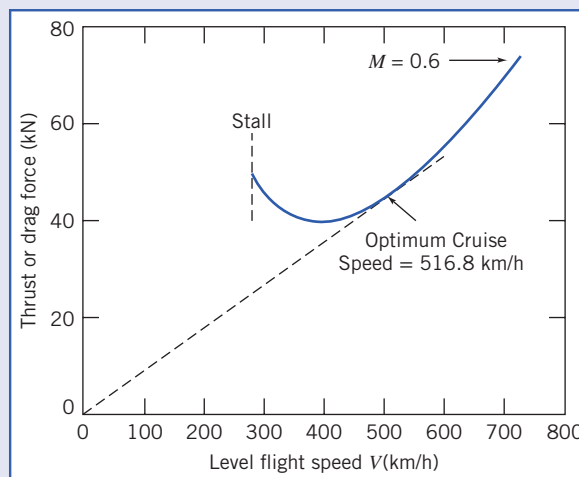
so

$$F_D = 667,500 \text{ N} \left( \frac{0.0198}{0.178} \right) = 74,250 \text{ N}$$

Similar calculations lead to the following table (computed using *Excel*):

$V(\text{km/h})$	280	320	480	640	730
$C_L$	1.207	0.924	0.411	0.231	0.178
$C_D$	0.0895	0.0600	0.0265	0.0208	0.0197
$F_D(\text{N})$	49,510	43,348	43,009	60,150	74,237

These data may be plotted as:



From the plot, the optimum cruise speed at sea level is estimated as 516.8 km/h (and using *Excel* we obtain 518.4 km/h).

At 9140 m altitude, the density is only about 0.375 times sea level density, from Table A.3. The speeds for corresponding forces are calculated from

$$F_L = C_L A \frac{1}{2} \rho V^2 \quad \text{or} \quad V = \sqrt{\frac{2F_L}{C_L \rho A}} \quad \text{or} \quad \frac{V_{30}}{V_{SL}} = \sqrt{\frac{\rho_{SL}}{\rho_{30}}} = \sqrt{\frac{1}{0.375}} = 1.63$$

Thus, speeds increase 63 percent at 9140 m altitude:

$$\begin{aligned} V_{\text{stall}} &\approx 456 \text{ km/h} \\ V_{\text{cruise}} &\approx 845 \text{ km/h} \end{aligned}$$

This problem illustrates that high-altitude flight increases the optimum cruising speed—in general this speed depends on aircraft configuration, gross weight, segment length, and winds aloft.



The *Excel* workbook for this problem plots the drag or thrust and power as functions of speed. It also allows “what-ifs,” e.g., what happens to the optimum speed if altitude is increased, or if the aspect ratio is increased, and so on.

It is possible to increase the *effective* aspect ratio for a wing of given geometric ratio by adding an *endplate* or *winglet* to the wing tip. An endplate may be a simple plate attached at the tip, perpendicular to the wing span, as on the rear-mounted wing of a racing car (see Fig. 9.26). An endplate functions by blocking the flow that tends to migrate from the high-pressure region below the wing tip to the low-pressure region above the tip when the wing is producing lift. When the endplate is added, the strength of the trailing vortex and the induced drag are reduced.

Winglets are short, aerodynamically contoured wings set perpendicular to the wing at the tip. Like the endplate, the winglet reduces the strength of the trailing vortex system and the induced drag. The winglet also produces a small component of force in the flight direction, which has the effect of further reducing the overall drag of the aircraft. The contour and angle of attack of the winglet are adjusted based on wind tunnel tests to provide optimum results.

As we have seen, aircraft can be fitted with low-drag airfoils to give excellent performance at cruise conditions. However, since the maximum lift coefficient is low for thin airfoils, additional effort must be expended to obtain acceptably low landing speeds. In steady-state flight conditions, lift must equal aircraft weight. Thus,

$$W = F_L = C_L \frac{1}{2} \rho V^2 A$$

Minimum flight speed is therefore obtained when  $C_L = C_{L_{\max}}$ . Solving for  $V_{\min}$ ,

$$V_{\min} = \sqrt{\frac{2W}{\rho C_{L_{\max}} A}} \quad (9.44)$$

According to Eq. 9.44, the minimum landing speed can be reduced by increasing either  $C_{L_{\max}}$  or wing area. Two basic techniques are available to control these variables: variable-geometry wing sections (e.g., obtained through the use of flaps) or boundary-layer control techniques.

Flaps are movable portions of a wing trailing edge that may be extended during landing and takeoff to increase effective wing area. The effects on lift and drag of two typical flap configurations are shown in Fig. 9.23, as applied to the NACA 23012 airfoil section. The maximum lift coefficient for this section is increased from 1.52 in the “clean” condition to 3.48 with double-slotted flaps. From Eq. 9.44, the corresponding reduction in landing speed would be 34 percent.

Figure 9.23 shows that section drag is increased substantially by high-lift devices. From Fig. 9.23b, section drag at  $C_{L_{\max}}$  ( $C_D \approx 0.28$ ) with double-slotted flaps is about 5 times as high as section drag at  $C_{L_{\max}}$  ( $C_D \approx 0.055$ ) for the clean airfoil. Induced drag due to lift must be added to section drag to obtain total drag. Because induced drag is proportional to  $C_L^2$  (Eq. 9.41), total drag rises sharply at low aircraft speeds. At speeds near stall, drag may increase enough to exceed the thrust available from the engines. To avoid this dangerous region of unstable operation, the Federal Aviation Administration (FAA) limits operation of commercial aircraft to speeds above 1.2 times stall speed.

Although details are beyond the scope of this book, the basic purpose of all boundary-layer control techniques is to delay separation or reduce drag, by adding momentum to the boundary layer through

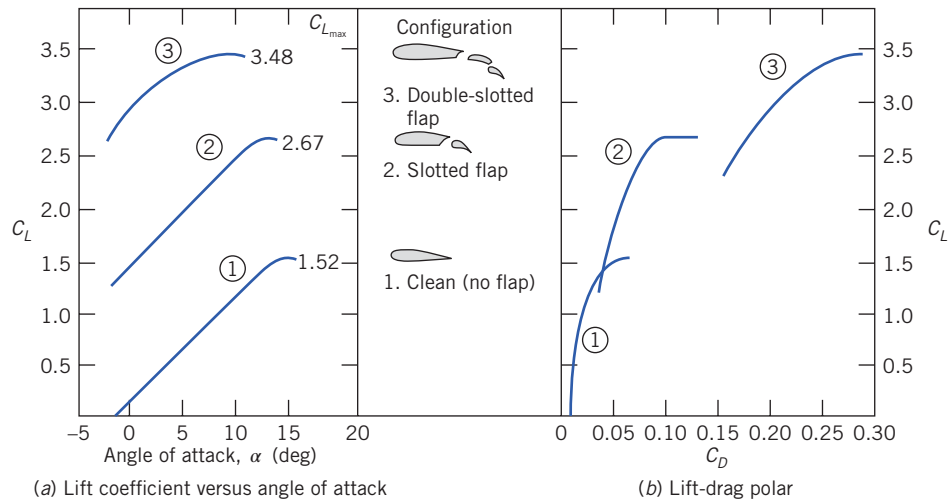
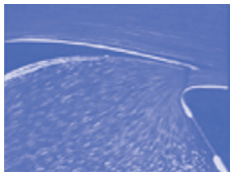


**Fig. 9.23** Effect of flaps on aerodynamic characteristics of NACA 23012 airfoil section. (Data from Abbott and von Doenhoff [21].)



Video: Leading Edge Slats



blowing, or by removing low-momentum boundary-layer fluid by suction. Many examples of practical boundary-layer control systems may be seen on commercial transport aircraft at your local airport. Two typical systems are shown in Fig. 9.24.

Aerodynamic lift is an important consideration in the design of high-speed land vehicles such as racing cars and land-speed-record machines. A road vehicle generates lift by virtue of its shape [29]. A representative centerline pressure distribution measured in the wind tunnel for an automobile is shown in Fig. 9.25. The regions of positive and negative pressure coefficient are labeled with + and −, respectively, and indicate the levels of pressure on the automobile surfaces.

The pressure is low around the nose because of streamline curvature as the flow rounds the nose. The pressure reaches a maximum at the base of the windshield, again as a result of streamline curvature. Low-pressure regions also occur at the windshield header and over the top of the automobile. The air speed across the top is approximately 30 percent higher than the freestream air speed. The same effect occurs around the “A-pillars” at the windshield edges. The drag increase caused by an added object, such as an antenna, spotlight, or mirror at that location, thus would be  $(1.3)^2 \approx 1.7$  times the drag the object would experience in an undisturbed flow field. Thus the *parasite drag* of an added component can be much higher than would be predicted from its drag calculated for free flow.

At high speeds, aerodynamic lift forces can unload tires, causing serious reductions in steering control and reducing stability to a dangerous extent. Lift forces on early racing cars were counteracted somewhat by “spoilers,” at considerable penalty in drag. In 1965 Jim Hall introduced the use of movable inverted airfoils on his Chaparral sports cars to develop aerodynamic downforce and provide aerodynamic braking [31]. Since then the developments in application of aerodynamic devices have been rapid. Aerodynamic design is used to reduce lift on all modern racing cars, as exemplified in Fig. 9.26. Liebeck airfoils [23] are used frequently for high-speed automobiles. Their high lift coefficients and relatively low drag allow downforce equal to or greater than the car weight to be developed at racing speeds. “Ground effect” cars use venturi-shaped ducts under the car and side skirts to seal leakage flows. The net result of these aerodynamic effects is that the downward force (which increases with speed) generates excellent traction without adding significant weight to the vehicle, allowing faster speeds through curves and leading to lower lap times.

Another method of boundary-layer control is use of moving surfaces to reduce skin friction effects on the boundary layer [32]. This method is hard to apply to practical devices, because of geometric and weight complications, but it is very important in recreation. Most golfers, tennis players, soccer players, and baseball pitchers can attest to this! Tennis and soccer players use spin to control the trajectory and bounce of a shot. In golf, a drive can leave the tee at 84 m/s or more, with backspin of 9000 rpm! Spin provides significant aerodynamic lift that substantially increases the carry of a drive. Spin is also largely



Chad Slattery/Stone/Getty Images

**Fig. 9.24** (a) Application of high-lift boundary-layer control devices to reduce landing speed of a jet transport aircraft. The wing of the Boeing 777 is highly mechanized. In the landing configuration, large slotted trailing-edge flaps roll out from under the wing and deflect downward to increase wing area and camber, thus increasing the lift coefficient. Slats at the leading edge of the wing move forward and down, to increase the effective radius of the leading edge and prevent flow separation, and to open a slot that helps keep air flow attached to the wing's upper surface. After touchdown, spoilers (not shown in use) are raised in front of each flap to decrease lift and ensure that the plane remains on the ground, despite use of the lift-augmenting devices. (This photograph was taken during a flight test. Flow cones are attached to the flaps and ailerons to identify regions of separated flow on these surfaces.)



Jeremy Simms/Getty Images, Inc.

**Fig. 9.24** (b) Application of high-lift boundary-layer control devices to reduce takeoff speed of a jet transport aircraft. This is another view of the Boeing 777 wing. In the takeoff configuration, large slotted trailing-edge flaps deflect to increase the lift coefficient. The low-speed aileron near the wingtip also deflects to improve span loading during takeoff. This view also shows the single-slotted outboard flap, the high-speed aileron, and nearest the fuselage, the double-slotted inboard flap.



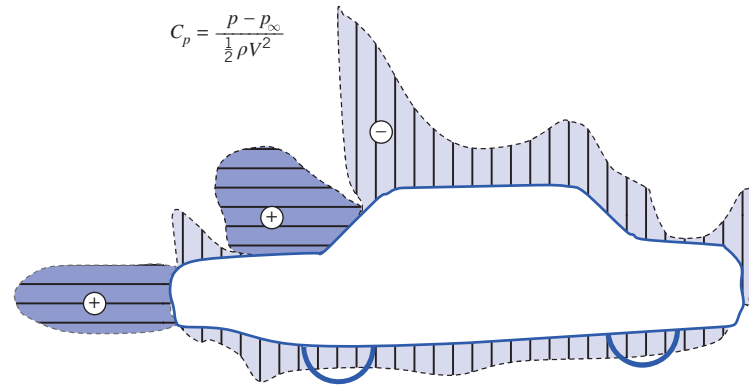
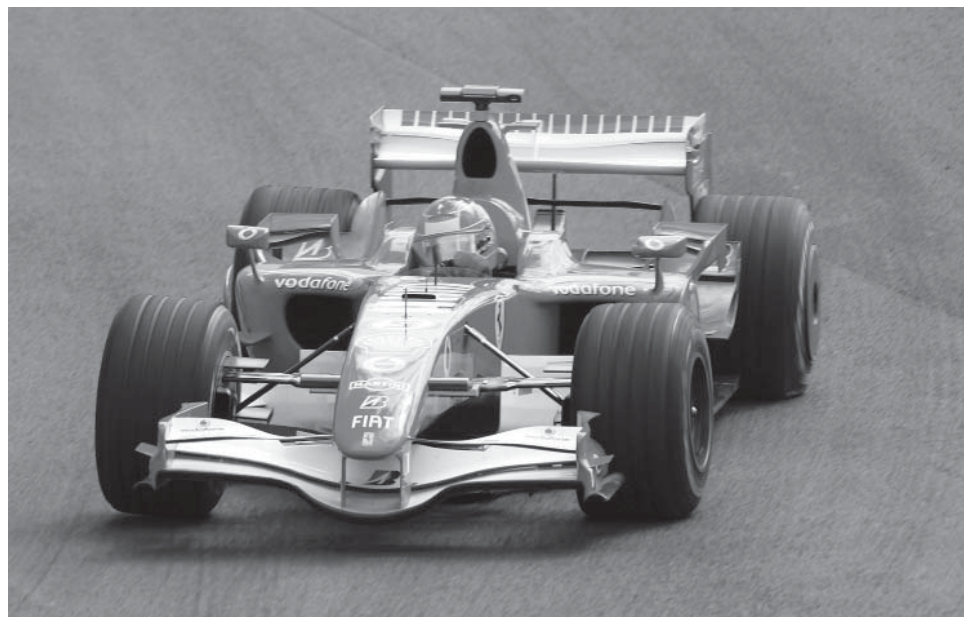


**Fig. 9.25** Pressure distribution along the centerline of an automobile (based on data from Reference [30]).



Gero Breloer/picture-alliance/dpa/AP Images

**Fig. 9.26** Contemporary racing car showing aerodynamic features. The car's front and rear wings are designed to provide significant downforce at speed to improve traction. Also visible are fairings to direct hot air from the radiators around the rear tires, and at the front of the car, cool air toward the brakes. Not shown are other aerodynamic features such as the fuselage bottom, which is designed to route the air flow carefully, using diffusers, to develop the most negative pressure, and to cause this negative pressure to act over the largest possible area under the car, to develop additional downforce.

responsible for hooking and slicing when shots are not hit squarely. The baseball pitcher uses spin to throw a curve ball.

Flow about a spinning sphere is shown in Fig. 9.27a. Spin alters the pressure distribution and also affects the location of boundary-layer separation. Separation is delayed on the upper surface of the sphere in Fig. 9.27a, and it occurs earlier on the lower surface. Thus pressure (because of the Bernoulli effect) is reduced on the upper surface and increased on the lower surface; the wake is deflected downward as shown. Pressure forces cause a lift in the direction shown; spin in the opposite direction would produce negative lift—a downward force. The force is directed perpendicular to both  $V$  and the spin axis.

Lift and drag data for spinning smooth spheres are presented in Fig. 9.27b. The most important parameter is the *spin ratio*,  $\omega D/2V$ , the ratio of surface speed to freestream flow speed; Reynolds number plays a secondary role. At low spin ratio, lift is negative in terms of the directions shown in Fig. 9.27a. Only above  $\omega D/2V \approx 0.5$  does lift become positive and continue to increase as spin ratio

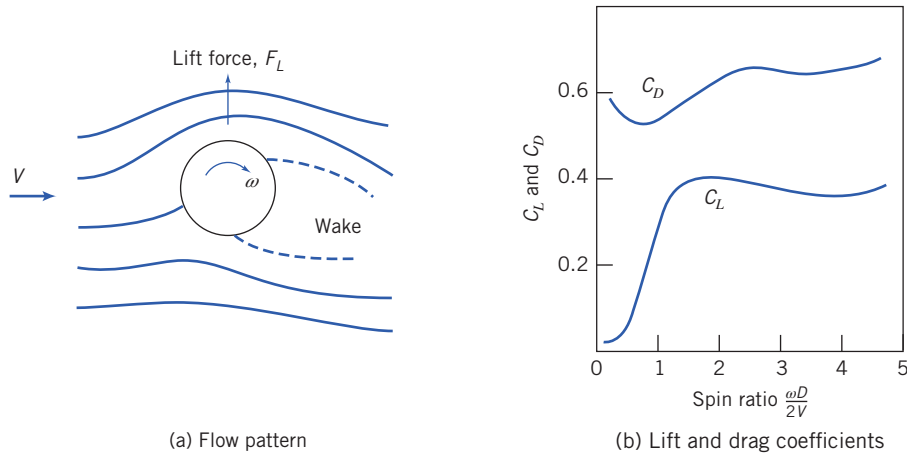


**Fig. 9.27** Flow pattern, lift, and drag coefficients for a smooth spinning sphere in uniform flow. (Data from Reference [19].)

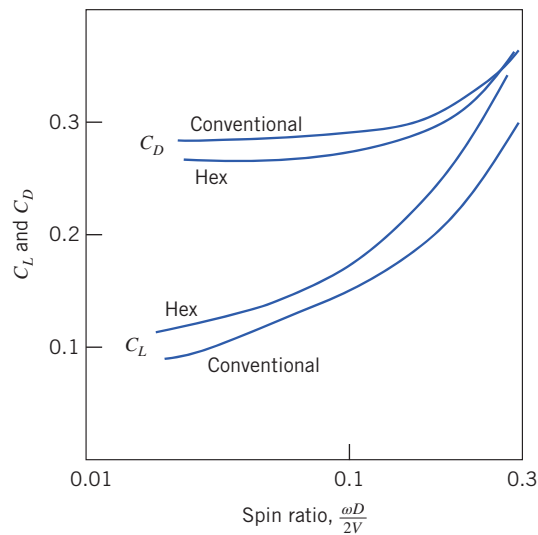


**Fig. 9.28** Comparison of conventional and hex-dimpled golf balls (based on data from Reference [30]).

increases. Lift coefficient levels out at about 0.35. Spin has little effect on sphere drag coefficient, which varies from about 0.5 to about 0.65 over the range of spin ratio shown.

Earlier we mentioned the effect of dimples on the drag of a golf ball. Experimental data for lift and drag coefficients for spinning golf balls are presented in Fig. 9.28 for subcritical Reynolds numbers between 126,000 and 238,000. Again the independent variable is spin ratio; a much smaller range of spin ratio, typical of golf balls, is presented in Fig. 9.28.

A clear trend is evident: The lift coefficient increases consistently with spin ratio for both hexagonal and “conventional” (round) dimples. The lift coefficient on a golf ball with hexagonal dimples is significantly—as much as 15 percent—higher than on a ball with round dimples. The advantage for hexagonal dimples continues to the largest spin ratios that were measured. The drag coefficient for a ball with hexagonal dimples is consistently 5 to 7 percent lower than the drag coefficient for a ball with round dimples at low spin ratios, but the difference becomes less pronounced as spin ratio increases.

The combination of higher lift and lower drag increases the carry of a golf shot. A recent design—the Callaway HX—has improved performance further by using a “tubular lattice network” using ridges of hexagons and pentagons (at a precise height of 0.21 mm) instead of dimples, so that there are no flat spots at all on the surface [34]. Callaway claims the HX flies farther than any ball they ever tested. Example 9.8 illustrates the effect of spin on the lift of a spinning ball.



**Example 9.8** LIFT OF A SPINNING BALL

A smooth tennis ball, with 57 g mass and 64 mm diameter, is hit at 25 m/s with topspin of 7500 rpm. Calculate the aerodynamic lift acting on the ball. Evaluate the radius of curvature of its path at maximum elevation in a vertical plane. Compare with the radius for no spin.

**Given:** Tennis ball in flight, with  $m = 57$  g and  $D = 64$  mm, hit with  $V = 25$  m/s and topspin of 7500 rpm.

**Find:** (a) Aerodynamic lift acting on ball.  
(b) Radius of curvature of path in vertical plane.  
(c) Comparison with radius for no spin.

**Solution:** Assume ball is smooth.  
Use data from Fig. 9.27 to find lift:

$$C_L = f\left(\frac{\omega D}{2V}, Re_D\right).$$

From given data (for standard air,  $\nu = 1.46 \times 10^{-5} \text{ m}^2/\text{s}$ ),

$$\begin{aligned}\frac{\omega D}{2V} &= \frac{1}{2} \times 7500 \frac{\text{rev}}{\text{min}} \times 0.064 \text{ m} \times \frac{\text{s}}{25 \text{ m}} \times 2\pi \frac{\text{rad}}{\text{rev}} \times \frac{\text{min}}{60 \text{ s}} = 1.01 \\ Re_D &= \frac{VD}{\nu} = 25 \frac{\text{m}}{\text{s}} \times 0.064 \text{ m} \times \frac{\text{s}}{1.46 \times 10^{-5} \text{ m}^2} = 1.10 \times 10^5\end{aligned}$$

From Fig. 9.27,  $C_L \approx 0.3$ , so

$$\begin{aligned}F_L &= C_L A \frac{1}{2} \rho V^2 \\ &= C_L \frac{\pi D^2}{4} \frac{1}{2} \rho V^2 = \frac{\pi}{8} C_L D^2 \rho V^2 \\ F_L &= \frac{\pi}{8} \times 0.3 \times (0.064)^2 \text{ m}^2 \times 1.23 \frac{\text{kg}}{\text{m}^3} \times (25)^2 \frac{\text{m}^2}{\text{s}^2} \times \frac{\text{N} \cdot \text{s}^2}{\text{kg} \cdot \text{m}} = 0.371 \text{ N} \leftarrow F_L\end{aligned}$$

Because the ball is hit with topspin, this force acts downward.

Use Newton's second law to evaluate the curvature of the path. In the vertical plane,

$$\begin{aligned}\sum F_z &= -F_L - mg = ma_z = -m \frac{V^2}{R} \quad \text{or} \quad R = \frac{V^2}{g + F_L/m} \\ R &= (25)^2 \frac{\text{m}^2}{\text{s}^2} \left[ \frac{1}{9.81 \frac{\text{m}}{\text{s}^2} + 0.371 \text{ N} \times \frac{1}{0.057 \text{ kg}} \times \frac{\text{kg} \cdot \text{m}}{\text{N} \cdot \text{s}^2}} \right] \\ R &= 38.3 \text{ m (with spin)} \leftarrow R \\ R &= (25)^2 \frac{\text{m}^2}{\text{s}^2} \times \frac{\text{s}^2}{9.81 \text{ m}} = 63.7 \text{ m (without spin)} \leftarrow R\end{aligned}$$

Thus topspin has a significant effect on trajectory of the shot!

It has long been known that a spinning projectile in flight is affected by a force perpendicular to the direction of motion and to the spin axis. This effect, known as the *Magnus effect*, is responsible for the systematic drift of artillery shells.

Cross flow about a rotating circular cylinder is qualitatively similar to flow about the spinning sphere shown schematically in Fig. 9.27a. If the velocity of the upper surface of a cylinder is in the same direction as the freestream velocity, separation is delayed on the upper surface; it occurs earlier on the lower surface. Thus the wake is deflected and the pressure distribution on the cylinder surface is altered

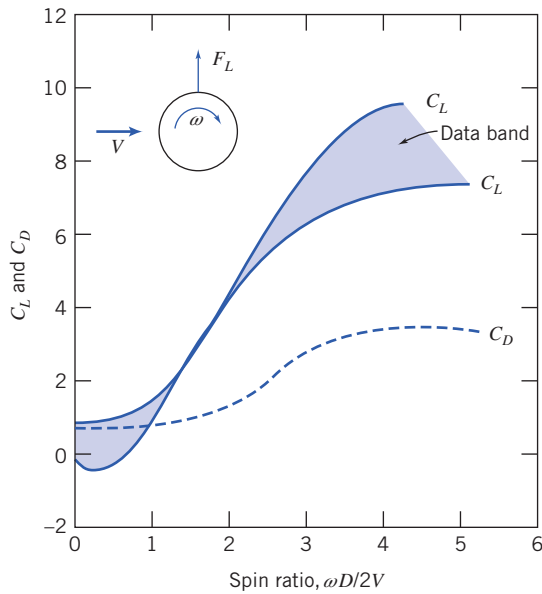


**Fig. 9.29** Lift and drag of a rotating cylinder as a function of relative rotational speed; Magnus force. (Data from Reference [35].)

when rotation is present. Pressure is reduced on the upper surface and increased on the lower surface, causing a net lift force acting upward. Spin in the opposite direction reverses these effects and causes a downward lift force.

Lift and drag coefficients for the rotating cylinder are based on projected area,  $LD$ . Experimentally measured lift and drag coefficients for subcritical Reynolds numbers between 40,000 and 660,000 are shown as functions of spin ratio in Fig. 9.29. When surface speed exceeds flow speed, the lift coefficient increases to surprisingly high values, while in two-dimensional flow, drag is affected only moderately. Induced drag, which must be considered for finite cylinders, can be reduced by using end disks larger in diameter than the body of the cylinder.

The power required to rotate a cylinder may be estimated from the skin friction drag of the cylinder surface. Hoerner [35] suggests basing the skin friction drag estimate on the tangential surface speed and surface area. Goldstein [19] suggests that the power required to spin the cylinder, when expressed as an equivalent drag coefficient, may represent 20 percent or more of the aerodynamic  $C_D$  of a stationary cylinder.

## 9.8 Summary and Useful Equations

In this chapter we have:

- ✓ Defined and discussed various terms commonly used in aerodynamics, such as boundary-layer disturbance, displacement, and momentum thicknesses; flow separation; streamlining; skin friction and pressure drag and drag coefficient; lift and lift coefficient; wing chord, span, and aspect ratio; and induced drag.
- ✓ Derived expressions for the boundary-layer thickness on a flat plate (zero pressure gradient) using exact and approximate methods (using the momentum integral equation).
- ✓ Learned how to estimate the lift and drag from published data for a variety of objects.

While investigating the above phenomena, we developed insight into some of the basic concepts of aerodynamic design, such as how to minimize drag, how to determine the optimum cruising speed of an airplane, and how to determine the lift required for flight.

**Note:** Most of the equations in the table below have a number of constraints or limitations—*be sure to refer to their page numbers for details!*

### Useful Equations

Definition of displacement thickness:	$\delta^* = \int_0^\infty \left(1 - \frac{u}{U}\right) dy \approx \int_0^\delta \left(1 - \frac{u}{U}\right) dy$	(9.1)	Page 355
Definition of momentum thickness:	$\theta = \int_0^\infty \frac{u}{U} \left(1 - \frac{u}{U}\right) dy \approx \int_0^\delta \frac{u}{U} \left(1 - \frac{u}{U}\right) dy$	(9.2)	Page 356
Boundary-layer thickness (laminar, exact—Blasius):	$\delta \approx \frac{5.0}{\sqrt{U/\nu x}} = \frac{5.0x}{\sqrt{Re_x}}$	(9.13)	Table 9-2, Page W9-2
Wall stress (laminar, exact—Blasius):	$\tau_w = 0.332U\sqrt{\rho\mu U/x} = \frac{0.332\rho U^2}{\sqrt{Re_x}}$	(9.14)	Page W9-3
Skin friction coefficient (laminar, exact—Blasius):	$C_f = \frac{\tau_w}{\frac{1}{2}\rho U^2} = \frac{0.664}{\sqrt{Re_x}}$	(9.15)	Table 9-2, Page W9-3
Momentum integral equation:	$\frac{\tau_w}{\rho} = \frac{d}{dx}(U^2\theta) + \delta^* U \frac{dU}{dx}$	(9.17)	Page 362
Boundary-layer thickness for flat plate (laminar, approximate—polynomial velocity profile):	$\frac{\delta}{x} = \sqrt{\frac{30\mu}{\rho U x}} = \frac{5.48}{\sqrt{Re_x}}$	(9.21)	Page 364
Definition of skin friction coefficient:	$C_f \equiv \frac{\tau_w}{\frac{1}{2}\rho U^2}$	(9.22)	Page 364
Skin friction coefficient for flat plate (laminar, approximate—polynomial velocity profile):	$C_f = \frac{0.730}{\sqrt{Re_x}}$	(9.23)	Page 365
Boundary-layer thickness for flat plate (turbulent, approximate— $\frac{1}{7}$ -power-law velocity profile):	$\frac{\delta}{x} = 0.382 \left(\frac{\nu}{Ux}\right)^{1/5} = \frac{0.382}{Re_x^{1/5}}$	(9.26)	Page 368
Skin friction coefficient for flat plate (turbulent, approximate— $\frac{1}{7}$ -power-law velocity profile):	$C_f = \frac{\tau_w}{\frac{1}{2}\rho U^2} = \frac{0.0594}{Re_x^{1/5}}$	(9.27)	Page 368
Definition of drag coefficient:	$C_D \equiv \frac{F_D}{\frac{1}{2}\rho V^2 A}$	(9.30)	Page 374
Drag coefficient for flat plate (entirely laminar, based on Blasius solution):	$C_D = \frac{1.33}{\sqrt{Re_L}}$	(9.33)	Page 375
Drag coefficient for flat plate (entirely turbulent, based on $\frac{1}{7}$ -power-law velocity profile):	$C_D = \frac{0.0742}{Re_L^{1/5}}$	(9.34)	Page 375
Drag coefficient for flat plate (empirical, $Re_L < 10^9$ ):	$C_D = \frac{0.455}{(\log Re_L)^{2.58}}$	(9.35)	Page 375
Drag coefficient for flat plate (based on $\frac{1}{7}$ -th power-law velocity profile, $5 \times 10^5 \leq Re_L \leq 10^7$ ):	$C_D = \frac{0.0742}{Re_L^{1/5}} - \frac{1740}{Re_L}$	(9.37a)	Page 375
Drag coefficient for flat plate (empirical, $5 \times 10^5 \leq Re_L \leq 10^9$ ):	$C_D = \frac{0.455}{(\log Re_L)^{2.58}} - \frac{1610}{Re_L}$	(9.37b)	Page 375

Table (Continued)

Definition of lift coefficient:	$C_L \equiv \frac{F_L}{\frac{1}{2} \rho V^2 A_p}$	(9.38)	Page 385
Definition of aspect ratio:	$AR \equiv \frac{b^2}{A_p}$	(9.39)	Page 390
Drag coefficient of a wing (finite span airfoil, using $C_{D,\infty}$ ):	$C_D = C_{D,\infty} + C_{D,i} = C_{D,\infty} + \frac{C_L^2}{\pi AR}$	(9.42)	Page 391
Drag coefficient of a wing (finite span airfoil, using $C_{D,0}$ ):	$C_D = C_{D,0} + C_{D,i} = C_{D,0} + \frac{C_L^2}{\pi AR}$	(9.43)	Page 391

## REFERENCES

- Prandtl, L., "Fluid Motion with Very Small Friction (in German)," *Proceedings of the Third International Congress on Mathematics*, Heidelberg, 1904; English translation available as NACA TM 452, March 1928.
- Blasius, H., "The Boundary Layers in Fluids with Little Friction (in German)," *Zeitschrift für Mathematik und Physik*, 56, 1, 1908, pp. 1–37; English translation available as NACA TM 1256, February 1950.
- Schlichting, H., *Boundary-Layer Theory*, 7th ed. New York: McGraw-Hill, 1979.
- Stokes, G. G., "On the Effect of the Internal Friction of Fluids on the Motion of Pendulums," *Cambridge Philosophical Transactions*, IX, 8, 1851.
- Howarth, L., "On the Solution of the Laminar Boundary-Layer Equations," *Proceedings of the Royal Society of London*, A164, 1938, pp. 547–579.
- Hess, J. L., and A. M. O. Smith, "Calculation of Potential Flow About Arbitrary Bodies," in *Progress in Aeronautical Sciences*, Vol. 8, D. Kuchemann et al., eds. Elmsford, NY: Pergamon Press, 1966.
- Kraus, W., "Panel Methods in Aerodynamics," in *Numerical Methods in Fluid Dynamics*, H. J. Wirz and J. J. Smolderen, eds. Washington, DC: Hemisphere, 1978.
- Rosenhead, L., ed., *Laminar Boundary Layers*. London: Oxford University Press, 1963.
- Rotta, J. C., "Turbulent Boundary Layers in Incompressible Flow," in *Progress in Aeronautical Sciences*, A. Ferri, et al., eds. New York: Pergamon Press, 1960, pp. 1–220.
- Kline, S. J., et al., eds., *Proceedings, Computation of Turbulent Boundary Layers—1968 AFOSR-IFP-Stanford Conference*, Vol. I: Methods, Predictions, Evaluation, and Flow Structure, and Vol. II: Compiled Data. Stanford, CA: Thermosciences Division, Department of Mechanical Engineering, Stanford University, 1969.
- Kline, S. J., et al., eds., *Proceedings, 1980–81 AFOSR-HTTM-Stanford Conference on Complex Turbulent Flows: Comparison of Computation and Experiment*, three volumes. Stanford, CA: Thermosciences Division, Department of Mechanical Engineering, Stanford University, 1982.
- Cebeci, T., and P. Bradshaw, *Momentum Transfer in Boundary Layers*. Washington, DC: Hemisphere, 1977.
- Bradshaw, P., T. Cebeci, and J. H. Whitelaw, *Engineering Calculation Methods for Turbulent Flow*. New York: Academic Press, 1981.
- Fluent. Fluent Incorporated, Centerra Resources Park, 10 Cavendish Court, Lebanon, NH 03766 (www.fluent.com).
- STAR-CD. Adapco, 60 Broadhollow Road, Melville, NY 11747 (www.cd-adapco.com).
- Hoerner, S. F., *Fluid-Dynamic Drag*, 2nd ed. Midland Park, NJ: Published by the author, 1965.
- Shapiro, A. H., *Shape and Flow, the Fluid Dynamics of Drag*. New York: Anchor, 1961 (paperback).
- Fage, A., "Experiments on a Sphere at Critical Reynolds Numbers," Great Britain, *Aeronautical Research Council, Reports and Memoranda*, No. 1766, 1937.
- Goldstein, S., ed., *Modern Developments in Fluid Dynamics*, Vols. I and II. Oxford: Clarendon Press, 1938. (Reprinted in paperback by Dover, New York, 1967.)
- Morel, T., and M. Bohn, "Flow over Two Circular Disks in Tandem," *Transactions of the ASME, Journal of Fluids Engineering*, 102, 1, March 1980, pp. 104–111.
- Abbott, I. H., and A. E. von Doenhoff, *Theory of Wing Sections, Including a Summary of Airfoil Data*. New York: Dover, 1959 (paperback).
- Stratford, B. S., "An Experimental Flow with Zero Skin Friction," *Journal of Fluid Mechanics*, 5, Pt. 1, January 1959, pp. 17–35.
- Liebeck, R. H., "Design of Subsonic Airfoils for High Lift," *AIAA Journal of Aircraft*, 15, 9, September 1978, pp. 547–561.
- Smith, A. M. O., "Aerodynamics of High-Lift Airfoil Systems," in *Fluid Dynamics of Aircraft Stalling*, AGARD CP-102, 1973, pp. 10–1 through 10–26.
- Morel, T., "Effect of Base Slant on Flow in the Near Wake of an Axisymmetric Cylinder," *Aeronautical Quarterly*, XXXI, Pt. 2, May 1980, pp. 132–147.
- Hucho, W. H., "The Aerodynamic Drag of Cars—Current Understanding, Unresolved Problems, and Future Prospects," in *Aerodynamic Drag Mechanisms of Bluff Bodies and Road*

Vehicles, G. Sovran, T. Morel, and W. T. Mason, eds. New York: Plenum, 1978.

27. McDonald, A. T., and G. M. Palmer, "Aerodynamic Drag Reduction of Intercity Buses," *Transactions, Society of Automotive Engineers*, 89, Section 4, 1980, pp. 4469–4484 (SAE Paper No. 801404).

28. Grosser, M., *Gossamer Odyssey*. Boston: Houghton Mifflin, 1981.

29. Carr, G. W., "The Aerodynamics of Basic Shapes for Road Vehicles. Part 3: Streamlined Bodies," The Motor Industry Research Association, Warwickshire, England, Report No. 107/4, 1969.

30. Goetz, H., "The Influence of Wind Tunnel Tests on Body Design, Ventilation, and Surface Deposits of Sedans and Sports Cars," SAE Paper No. 710212, 1971.

31. Hall, J., "What's Jim Hall Really Like?" *Automobile Quarterly*, VIII, 3, Spring 1970, pp. 282–293.

32. Mokhtarian, F., and V. J. Modi, "Fluid Dynamics of Airfoils with Moving Surface Boundary-Layer Control," *AIAA Journal of Aircraft*, 25, 2, February 1988, pp. 163–169.

33. Mehta, R. D., "Aerodynamics of Sports Balls," in *Annual Review of Fluid Mechanics*, Vol. 17, M. van Dyke, et al., ed. Palo Alto, CA: Annual Reviews, 1985, pp. 151–189.

34. "The Year in Ideas," *New York Times Magazine*, December 9, 2001, pp. 58–60.

35. Hoerner, S. F., and H. V. Borst, *Fluid-Dynamic Lift*. Bricktown, NJ: Hoerner Fluid Dynamics, 1975.

36. Chow, C.-Y., *An Introduction to Computational Fluid Mechanics*. New York: Wiley, 1980.

37. Carr, G. W., "The Aerodynamics of Basic Shapes for Road Vehicles, Part 1: Simple Rectangular Bodies," The Motor Industry Research Association, Warwickshire, England, Report No. 1968/2, 1967.

38. L. Prandtl, *Ergebnisse der aerodynamischen, Veersuchsanstalt su Gottingen*. Vol II, 1923.

39. H. Brauer, D. Sucker, "Umstromung von Platten, Zylindern und Kugeln," *Chemie Ingenieur Technik*, 48. Jahrgang, No. 8, 1976, p 665–671. Copyright Wiley-VCH Verlag GmbH & Co. KGaA. Reproduced with permission.

## PROBLEMS

### The Boundary-Layer Concept

9.1 The roof of a minivan is approximated as a horizontal flat plate. Plot the length of the laminar boundary layer as a function of minivan speed,  $V$ , as the minivan accelerates from 16 km/h to 144 km/h.

9.2 A model of a river towboat is to be tested at 1:16 scale. The boat is designed to travel at 5.5 m/s in fresh water at 15°C. Estimate the distance from the bow where transition occurs. Where should transition be stimulated on the model towboat?

9.3 The takeoff speed of a Boeing 757 is 260 km/h. At approximately what distance will the boundary layer on the wings become turbulent? If it cruises at 850 km/h at 10,000 m, at approximately what distance will the boundary layer on the wings become turbulent?

9.4 For flow around a sphere the boundary layer becomes turbulent around  $Re_D \approx 2.5 \times 10^5$ . Find the speeds at which (a) an American golf ball ( $D = 43$  mm), (b) a British golf ball ( $D = 41.1$  mm), and (c) a soccer ball ( $D = 222$  mm) develop turbulent boundary layers. Assume standard atmospheric conditions.

9.5 1 m  $\times$  2 m sheet of plywood is attached to the roof of your vehicle after being purchased at the hardware store. At what speed (in kilometers per hour, in 20°C air) will the boundary layer first start becoming turbulent? At what speed is about 90 percent of the boundary layer turbulent?

9.6 Plot on one graph the length of the laminar boundary layer on a flat plate, as a function of freestream velocity, for (a) water and standard air at (b) sea level and (c) 10 km altitude. Use log-log axes, and compute data for the boundary-layer length ranging from 0.01 m to 10 m.

### Boundary-Layer Thickness

9.7 The most general sinusoidal velocity profile for laminar boundary-layer flow on a flat plate is  $u = A \sin(By) + C$ . State three

boundary conditions applicable to the laminar boundary-layer velocity profile. Evaluate constants  $A$ ,  $B$ , and  $C$ .

9.8 Velocity profiles in laminar boundary layers often are approximated by the equations

$$\text{Linear: } \frac{u}{U} = \frac{y}{\delta}$$

$$\text{Sinusoidal: } \frac{u}{U} = \sin\left(\frac{\pi}{2} \frac{y}{\delta}\right)$$

$$\text{Parabolic: } \frac{u}{U} = 2\left(\frac{y}{\delta}\right) - \left(\frac{y}{\delta}\right)^2$$

Compare the shapes of these velocity profiles by plotting  $y/\delta$  (on the ordinate) versus  $u/U$  (on the abscissa).

9.9 An approximation for the velocity profile in a laminar boundary layer is

$$\frac{u}{U} = \frac{3y}{2\delta} - \frac{1}{2}\left(\frac{y}{\delta}\right)^3$$

Does this expression satisfy boundary conditions applicable to the laminar boundary-layer velocity profile? Evaluate  $\delta^*/\delta$  and  $\theta/\delta$ .

9.10 A simplistic laminar boundary-layer model is

$$\frac{u}{U} = \sqrt{2} \frac{y}{\delta} \quad 0 < y \leq \frac{\delta}{2}$$

$$\frac{u}{U} = (2 - \sqrt{2}) \frac{y}{\delta} + (\sqrt{2} - 1) \quad \frac{\delta}{2} < y \leq \delta$$

Does this expression satisfy boundary conditions applicable to the laminar boundary-layer velocity profile? Evaluate  $\delta^*/\delta$  and  $\theta/\delta$ .

9.11 The velocity profile in a turbulent boundary layer often is approximated by the  $\frac{1}{7}$ -power-law equation

$$\frac{u}{U} = \left(\frac{y}{\delta}\right)^{1/7}$$

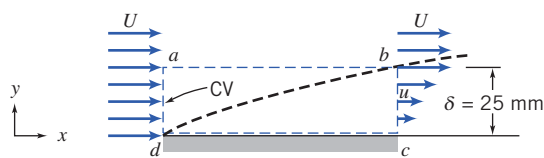


Compare the shape of this profile with the parabolic laminar boundary-layer velocity profile (Problem 9.8) by plotting  $y/\delta$  (on the ordinate) versus  $u/U$  (on the abscissa) for both profiles.

**9.12** Evaluate  $\delta^*/\delta$  for each of the laminar boundary-layer velocity profiles given in Problem 9.8.

**9.13** Evaluate  $\delta^*/\delta$  and  $\theta/\delta$  for the turbulent  $\frac{1}{7}$ -power-law velocity profile given in Problem 9.11. Compare with ratios for the parabolic laminar boundary-layer velocity profile given in Problem 9.8.

**9.14** A fluid, with density  $\rho = 800 \text{ kg/m}^3$ , flows at  $U = 3 \text{ m/s}$  over a flat plate 3 m long and 1 m wide. At the trailing edge, the boundary-layer thickness is  $\delta = 25 \text{ mm}$ . Assume that the velocity profile is linear, as shown, and that the flow is two-dimensional (flow conditions are independent of  $z$ ). Using control volume  $abcd$ , shown by the dashed lines, compute the mass flow rate across surface  $ab$ . Determine the drag force on the upper surface of the plate. Explain how this (viscous) drag can be computed from the given data even though we do not know the fluid viscosity (see Problem 9.31).



P9.14

**9.15** The flat plate of Problem 9.14 is turned so that the 1 m side is parallel to the flow (the width becomes 3 m). Should we expect that the drag increases or decreases? Why? The trailing edge boundary-layer thickness is now  $\delta = 14 \text{ mm}$ . Assume again that the velocity profile is linear and that the flow is two-dimensional (flow conditions are independent of  $z$ ). Repeat the analysis of Problem 9.14.

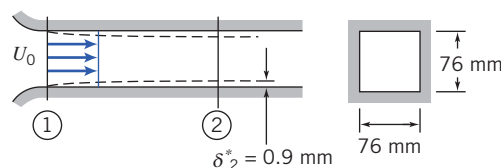
**9.16** The test section of a low-speed wind tunnel is 1.5 m long, preceded by a nozzle with a diffuser at the outlet. The tunnel cross section is  $20 \text{ cm} \times 20 \text{ cm}$ . The wind tunnel is to operate with  $40^\circ\text{C}$  air and have a design velocity of  $50 \text{ m/s}$  in the test section. A potential problem with such a wind tunnel is boundary-layer blockage. The boundary-layer displacement thickness reduces the effective cross-sectional area (the test area, in which we have uniform flow); in addition, the uniform flow will be accelerated. If these effects are pronounced, we end up with a smaller useful test cross section with a velocity somewhat higher than anticipated. If the boundary layer thickness is  $10 \text{ mm}$  at the entrance and  $25 \text{ mm}$  at the exit, and the boundary layer velocity profile is given by  $u/U = (y/\delta)^{1/7}$ , estimate the displacement thickness at the end of the test section and the percentage change in the uniform velocity between the inlet and outlet.

**9.17** Air flows in a horizontal cylindrical duct of diameter  $D = 100 \text{ mm}$ . At a section a few meters from the entrance, the turbulent boundary layer is of thickness  $\delta_1 = 5.25 \text{ mm}$ , and the velocity in the inviscid central core is  $U_1 = 12.5 \text{ m/s}$ . Farther downstream the boundary layer is of thickness  $\delta_2 = 24 \text{ mm}$ . The velocity profile in the boundary layer is approximated well by the  $\frac{1}{7}$ -power expression. Find the velocity,  $U_2$ , in the inviscid central core at the second section, and the pressure drop between the two sections.

**9.18** The square test section of a small laboratory wind tunnel has sides of width  $W = 40 \text{ cm}$ . At one measurement location, the turbulent boundary layers on the tunnel walls are  $\delta_1 = 1 \text{ cm}$  thick. The velocity profile is approximated well by the  $\frac{1}{7}$ -power expression.

At this location, the freestream air speed is  $U_1 = 20 \text{ m/s}$ , and the static pressure is  $p_1 = -250 \text{ Pa}$  (gage). At a second measurement location downstream, the boundary layer thickness is  $\delta_2 = 1.3 \text{ cm}$ . Evaluate the air speed in the freestream in the second section. Calculate the difference in static pressure from section ① to section ②.

**9.19** Air flows in the entrance region of a square duct, as shown. The velocity is uniform,  $U_0 = 30 \text{ m/s}$ , and the duct is  $76 \text{ mm}$  square. At a section  $0.3 \text{ m}$  downstream from the entrance, the displacement thickness,  $\delta^*$ , on each wall measures  $0.9 \text{ mm}$ . Determine the pressure change between sections ① and ②.



P9.19


**9.20** Flow of  $20^\circ\text{C}$  air develops in a flat horizontal duct following a well-rounded entrance section. The duct height is  $H = 300 \text{ mm}$ . Turbulent boundary layers grow on the duct walls, but the flow is not yet fully developed. Assume that the velocity profile in each boundary layer is  $u/U = (y/\delta)^{1/7}$ . The inlet flow is uniform at  $V = 10 \text{ m/s}$  at section ①. At section ②, the boundary-layer thickness on each wall of the channel is  $\delta_2 = 100 \text{ mm}$ . Show that, for this flow,  $\delta^* = \delta/8$ . Evaluate the static gage pressure at section ①. Find the average wall shear stress between the entrance and section ②, located at  $L = 5 \text{ m}$ .


**9.21** A laboratory wind tunnel has a square test section with sides of width  $W = 305 \text{ mm}$  and length  $L = 610 \text{ mm}$ . When the freestream air speed at the test section entrance is  $U_1 = 24.4 \text{ m/s}$ , the head loss from the atmosphere is  $6.5 \text{ mm H}_2\text{O}$ . Turbulent boundary layers form on the top, bottom, and side walls of the test section. Measurements show that the boundary-layer thicknesses are  $\delta_1 = 20.3 \text{ mm}$  at the entrance and  $\delta_2 = 25.4 \text{ mm}$  at the outlet of the test section. The velocity profiles are of  $\frac{1}{7}$ -power form. Evaluate the freestream air speed at the outlet from the test section. Determine the static pressures at the test section inlet and outlet.


**9.22** Flow of air develops in a horizontal cylindrical duct, of diameter  $D = 400 \text{ mm}$ , following a well-rounded entrance. A turbulent boundary layer grows on the duct wall, but the flow is not yet fully developed. Assume that the velocity profile in the boundary layer is  $u/U = (y/\delta)^{1/7}$ . The inlet flow is  $U = 15 \text{ m/s}$  at section ①. At section ②, the boundary-layer thickness is  $\delta_2 = 100 \text{ mm}$ . Evaluate the static gage pressure at section ②, located at  $L = 6 \text{ m}$ . Find the average wall shear stress.

**9.23** Air flows into the inlet contraction section of a wind tunnel in an undergraduate laboratory. From the inlet the air enters the test section, which is square in cross-section with side dimensions of  $305 \text{ mm}$ . The test section is  $609 \text{ mm}$  long. At one operating condition air leaves the contraction at  $50.2 \text{ m/s}$  with negligible boundary-layer thickness. Measurements show that boundary layers at the downstream end of the test section are  $20.3 \text{ mm}$  thick. Evaluate the displacement thickness of the boundary layers at the downstream end of the wind tunnel test section. Calculate the change in static pressure along the wind tunnel test section. Estimate the approximate total drag force caused by skin friction on each wall of the wind tunnel.


### Laminar Flat-Plate Boundary Layer: Exact Solution


 **\*9.24** Using numerical results obtained by Blasius (Table 9.1), evaluate the distribution of shear stress in a laminar boundary layer on a flat plate. Plot  $\tau/\tau_w$  versus  $y/\delta$ . Compare with results derived from the approximate sinusoidal velocity profile given in Problem 9.8.

 **\*9.25** Using numerical results obtained by Blasius (Table 9.1), evaluate the distribution of shear stress in a laminar boundary layer on a flat plate. Plot  $\tau/\tau_w$  versus  $y/\delta$ . Compare with results derived from the approximate parabolic velocity profile given in Problem 9.8.

 **\*9.26** Verify that the  $y$  component of velocity for the Blasius solution to the Prandtl boundary-layer equations is given by Eq. 9.10. Obtain an algebraic expression for the  $x$  component of the acceleration of a fluid particle in the laminar boundary layer. Plot  $a_x$  versus  $\eta$  to determine the maximum  $x$  component of acceleration at a given  $x$ .

**\*9.27** Numerical results of the Blasius solution to the Prandtl boundary-layer equations are presented in Table 9.1. Consider steady, incompressible flow of standard air over a flat plate at free-stream speed  $U = 5$  m/s. At  $x = 20$  cm, estimate the distance from the surface at which  $u = 0.95 U$ . Evaluate the slope of the streamline through this point. Obtain an algebraic expression for the local skin friction,  $\tau_w(x)$ . Obtain an algebraic expression for the total skin friction drag force on the plate. Evaluate the momentum thickness at  $L = 1$  m.

 **\*9.28** The Blasius exact solution involves solving a nonlinear equation, Eq. 9.11, with initial and boundary conditions given by Eq. 9.12. Set up an *Excel* workbook to obtain a numerical solution of this system. The workbook should consist of columns for  $\eta$ ,  $f$ ,  $f'$ , and  $f''$ . The rows should consist of values of these, with a suitable step size for  $\eta$  (e.g., for 1000 rows the step size for  $\eta$  would be 0.01 to generate data through  $\eta = 10$ , to go a little beyond the data in Table 9.1). The values of  $f$  and  $f'$  for the first row are zero (from the initial conditions, Eq. 9.12); a guess value is needed for  $f''$  (try 0.5). Subsequent row values for  $f$ ,  $f'$ , and  $f''$  can be obtained from previous row values using the Euler method of Section 5.5 for approximating first derivatives (and Eq. 9.11). Finally, a solution can be found by using *Excel's* *Goal Seek* or *Solver* functions to vary the initial value of  $f''$  until  $f' = 1$  for large  $\eta$  (e.g.,  $\eta = 10$ , boundary condition of Eq. 9.12). Plot the results. Note: Because the Euler method is relatively crude, the results will agree with Blasius' only to within about 1%.

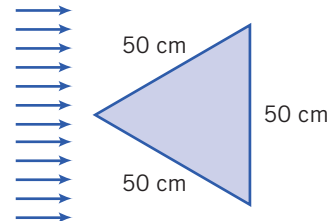
 **\*9.29** A thin flat plate,  $L = 0.25$  m. long and  $b = 1$  m wide, is installed in a water tunnel as a splitter. The freestream speed is  $U = 1.75$  m/s, and the velocity profile in the boundary layer is approximated as parabolic. Plot  $\delta$ ,  $\delta^*$ , and  $\tau_w$  versus  $x/L$  for the plate.

**9.30** Consider flow over the splitter plate of Problem 9.29. Show algebraically that the total drag force on one side of the splitter plate may be written  $F_D = \rho U^2 \theta_L b$ . Evaluate  $\theta_L$  and the total drag for the given conditions.

**9.31** In Problems 9.14 and 9.15 the drag on the upper surface of a flat plate, with flow (fluid density  $\rho = 800$  kg/m<sup>3</sup>) at freestream speed  $U = 3$  m/s, was determined from momentum flux calculations. The drag was determined for the plate with its long edge (3 m) and its short edge (1 m) parallel to the flow. If the fluid viscosity

$\mu = 0.02$  N·s/m<sup>2</sup>, compute the drag using boundary-layer calculations.

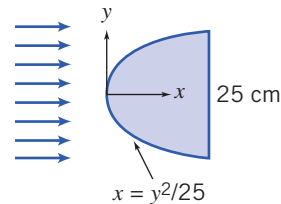
**9.32** Assume laminar boundary-layer flow to estimate the drag on the plate shown when it is placed parallel to a 5 m/s air flow. The air is 20°C and 101.3 kPa.



**P9.32, P9.33**

**9.33** Assume laminar boundary-layer flow to estimate the drag on the plate shown when it is placed parallel to a 5 m/s air flow, except that the base rather than the tip faces the flow. Would you expect this to be larger than, the same as, or lower than the drag for Problem 9.32?

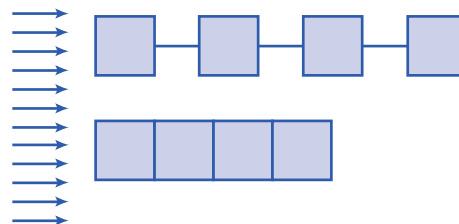
**9.34** Assume laminar boundary-layer flow to estimate the drag on the plate shown when it is placed parallel to a 7.5 m/s air flow. The air is at 20°C and 101.3 kPa. (Note that the shape is given by  $x = y^2/25$ , where  $x$  and  $y$  are in centimeters.)



**P9.34, P9.35**

**9.35** Assume laminar boundary-layer flow to estimate the drag on the plate shown when it is placed parallel to a 7.5 m/s flow, except that the base rather than the tip faces the flow. Would you expect this to be large than, the same as, or lower than the drag for Problem 9.34?

**9.36** Assume laminar boundary-layer flow to estimate the drag on four square plates (each 7.5 cm × 7.5 cm) placed parallel to a 1 m/s water flow, for the two configurations shown. Before calculating, which configuration do you expect to experience the lower drag? Assume that the plates attached with string are far enough apart for wake effects to be negligible and that the water is at 20°C.




**P9.36**

### Momentum Integral Equation


**9.37** The velocity profile in a laminar boundary-layer flow at zero pressure gradient is approximated by the linear expression given in Problem 9.8. Use the momentum integral equation with this profile to obtain expressions for  $\delta/x$  and  $C_f$ .

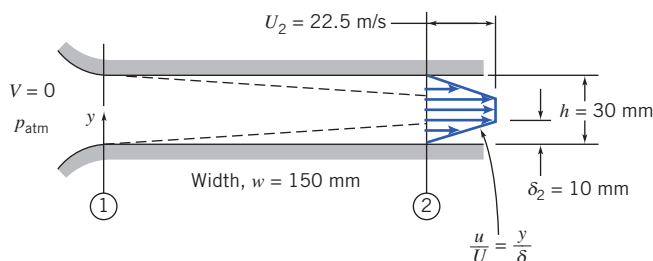
\*These problems require material from sections that may be omitted without loss of continuity in the text material.



 **9.38** A horizontal surface, with length  $L = 1.8$  m and width  $b = 0.9$  m, is immersed in a stream of standard air flowing at  $U = 3.2$  m/s. Assume a laminar boundary layer forms and approximate the velocity profile as sinusoidal. Plot  $\delta$ ,  $\delta^*$ , and  $\tau_w$  versus  $x/L$  for the plate.


**9.39** Water at  $20^\circ\text{C}$  flows over a flat plate at a speed of 2 m/s. The plate is 0.6 m long and 2 m wide. The boundary layer on each surface of the plate is laminar. Assume that the velocity profile may be approximated as linear. Determine the drag force on the plate.

 **9.40** Standard air flows from the atmosphere into the wide, flat channel shown. Laminar boundary layers form on the top and bottom walls of the channel (ignore boundary-layer effects on the side walls). Assume that the boundary layers behave as on a flat plate, with linear velocity profiles. At any axial distance from the inlet, the static pressure is uniform across the channel. Assume uniform flow at section ①. Indicate where the Bernoulli equation can be applied in this flow field. Find the static pressure (gage) and the displacement thickness at section ②. Plot the stagnation pressure (gage) across the channel at section ② and explain the result. Find the static pressure (gage) at section ① and compare to the static pressure (gage) at section ②.



P9.40

**9.41** For the flow conditions of Example 9.4, develop an algebraic expression for the variation of wall shear stress with distance along the surface. Integrate to obtain an algebraic expression for the total skin friction drag on the surface. Evaluate the drag for the given conditions.

 **9.42** Consider flow of air over a flat plate of length 5 m. On one graph, plot the boundary-layer thickness as a function of distance along the plate for freestream speed  $U = 10$  m/s assuming (a) a completely laminar boundary layer, (b) a completely turbulent boundary layer, and (c) a laminar boundary layer that becomes turbulent at  $Re_x = 5 \times 10^5$ . Use Excel's Goal Seek or Solver to find the speeds  $U$  for which transition occurs at the trailing edge, and at  $x = 4$  m, 3 m, 2 m, and 1 m.

**9.43** Repeat Problem 9.32, except that the air flow is now at 25 m/s (assume turbulent boundary-layer flow).

**9.44** Repeat Problem 9.34, except that the air flow is now at 25 m/s (assume turbulent boundary-layer flow).

**9.45** Repeat Problem 9.36, except that the air flow is now at 10 m/s (assume turbulent boundary-layer flow).

**9.46** The velocity profile in a turbulent boundary-layer flow at zero pressure gradient is approximated by the  $\frac{1}{6}$ -power profile expression,

$$\frac{u}{U} = \eta^{1/6}, \quad \text{where} \quad \eta = \frac{y}{\delta}$$

Use the momentum integral equation with this profile to obtain expressions for  $\delta/x$  and  $C_f$ . Compare with results obtained in Section 9.5 for the  $\frac{1}{7}$ -power profile.

**9.47** Air at standard conditions flows over a flat plate. The free-stream speed is 10 m/s. Find  $\delta$  and  $\tau_w$  at  $x = 1$  m from the leading edge assuming (a) completely laminar flow (assume a parabolic velocity profile) and (b) completely turbulent flow (assume a  $\frac{1}{7}$ -power velocity profile).

### Use of the Momentum Integral Equation for Flow with Zero Pressure Gradient

**9.48** A laboratory wind tunnel has a flexible upper wall that can be adjusted to compensate for boundary-layer growth, giving zero pressure gradient along the test section. The wall boundary layers are well represented by the  $\frac{1}{7}$ -power-velocity profile. At the inlet the tunnel cross section is square, with height  $H_1$  and width  $W_1$ , each equal to 305 mm. With freestream speed  $U_1 = 26.5$  m/s, measurements show that  $\delta_1 = 12.2$  mm and downstream  $\delta_6 = 16.6$  mm. Calculate the height of the tunnel walls at ⑥. Determine the equivalent length of a flat plate that would produce the inlet boundary layer thickness. Estimate the streamwise distance between sections ① and ⑥ in the tunnel. Assume standard air.

### Pressure Gradients in Boundary-Layer Flow

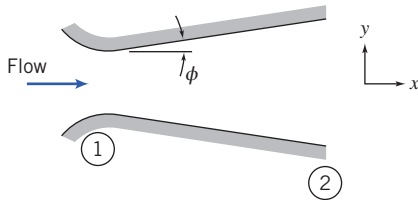
**9.49** Small wind tunnels in an undergraduate laboratory have 305-mm square test sections. Measurements show the boundary layers on the tunnel walls are fully turbulent and well represented by  $\frac{1}{7}$ -power profiles. At cross section ① with freestream speed  $U_1 = 26.1$  m/s, data show that  $\delta_1 = 12.2$  mm; at section ②, located downstream,  $\delta_2 = 16.6$  mm. Evaluate the change in static pressure between sections ① and ②. Estimate the distance between the two sections.

**9.50** Air flows in a cylindrical duct of diameter  $D = 150$  mm. At section ①, the turbulent boundary layer is of thickness  $\delta_1 = 10$  mm, and the velocity in the inviscid central core is  $U_1 = 25$  m/s. Further downstream, at section ②, the boundary layer is of thickness  $\delta_2 = 30$  mm. The velocity profile in the boundary layer is approximated well by the  $\frac{1}{7}$ -power expression. Find the velocity,  $U_2$ , in the inviscid central core at the second section, and the pressure drop between the two sections. Does the magnitude of the pressure drop indicate that we are justified in approximating the flow between sections ① and ② as one with zero pressure gradient? Estimate the length of duct between sections ① and ②. Estimate the distance downstream from section ① at which the boundary layer thickness is  $\delta = 20$  mm. Assume standard air.

**9.51** Consider the linear, sinusoidal, and parabolic laminar boundary-layer approximations of Problem 9.8. Compare the momentum fluxes of these profiles. Which is most likely to separate first when encountering an adverse pressure gradient?

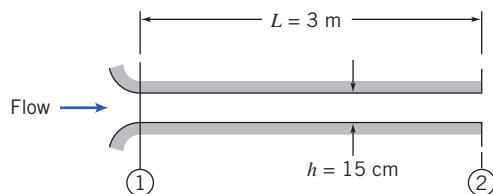
**9.52** Perform a cost-effectiveness analysis on a typical large tanker used for transporting petroleum. Determine, as a percentage of the petroleum cargo, the amount of petroleum that is consumed in traveling a distance of 3200 km. Use data from Example 9.5, and the following: Assume the petroleum cargo constitutes 75% of the total weight, the propeller efficiency is 70%, the wave drag and power to run auxiliary equipment constitute losses equivalent to an additional 20%, the engines have a thermal efficiency of 40%, and the petroleum energy is 46,520 kJ/kg. Also compare the performance of this tanker to that of the Alaskan Pipeline, which requires about 79 kJ of energy for each ton-mile of petroleum delivery.

**9.53** Consider the plane-wall diffuser shown in Fig. P9.53. First, assume that the fluid is inviscid. Describe the flow pattern, including the pressure distribution, as the diffuser angle  $\phi$  is increased from zero degrees (parallel walls). Second, modify your description to allow for boundary layer effects. Which fluid (inviscid or viscous) will generally have the highest exit pressure?



P9.53

**9.54** Cooling air is supplied through the wide, flat channel shown. For minimum noise and disturbance of the outlet flow, laminar boundary layers must be maintained on the channel walls. Estimate the maximum inlet flow speed at which the outlet flow will be laminar. Assuming parabolic velocity profiles in the laminar boundary layers, evaluate the pressure drop,  $p_1 - p_2$ . Express your answer in inches of water.



P9.54

**9.55** A laboratory wind tunnel has a test section that is square in cross section, with inlet width  $W_1$  and height  $H_1$ , each equal to 305 mm. At freestream speed  $U_1 = 24.5$  m/s, measurements show the boundary-layer thickness is  $\delta_1 = 9.75$  mm with a  $1/7$ -power turbulent velocity profile. The pressure gradient in this region is given approximately by  $dp/dx = -0.035$  mm.  $H_2O$ /mm. Evaluate the reduction in effective flow area caused by the boundary layers on the tunnel bottom, top, and walls at section ①. Calculate the rate of change of boundary-layer momentum thickness,  $d\theta/dx$ , at section ①. Estimate the momentum thickness at the end of the test section, located at  $L = 254$  mm downstream.



**9.56** The variable-wall concept is proposed to maintain constant boundary-layer thickness in the wind tunnel of Problem 9.55. Beginning with the initial conditions of Problem 9.55, evaluate the freestream velocity distribution needed to maintain constant boundary-layer thickness. Assume constant width,  $W_1$ . Estimate and plot the top-height settings along the test section from  $x = 0$  at section ① to  $x = 254$  mm at section ② downstream.

### Drag



**9.57** A flat-bottomed barge, 24 m long and 10.7 m wide, submerged to a depth of 1.5 m, is to be pushed up a river (the river water is at  $15.5^\circ\text{C}$ ). Estimate and plot the power required to overcome skin friction for speeds ranging up to 24 km/h.

**9.58** Repeat Problem 9.36, except that the water flow is now at 10 m/s. (Use formulas for  $C_D$  from Section 9.7.)

**9.59** A towboat for river barges is tested in a towing tank. The towboat model is built at a scale ratio of 1:13.5. Dimensions of the model are overall length 3.5 m, beam 1 m, and draft 0.2 m. (The model displacement in fresh water is 5500 N.) Estimate the average length of wetted surface on the hull. Calculate the skin friction drag force of the prototype at a speed of 3.601 m/s relative to the water.

**9.60** A jet transport aircraft cruises at 12 km in steady level flight at 800 km/h. Model the aircraft fuselage as a circular cylinder with diameter  $D = 4$  m and length  $L = 38$  m. Neglecting compressibility effects, estimate the skin friction drag force on the fuselage. Evaluate the power needed to overcome this force.

**9.61** Resistance of a barge is to be determined from model test data. The model is constructed to a scale ratio of 1:13.5 and has length, beam, and draft of 7.00 m, 1.4 m, and 0.2 m, respectively. The test is to simulate performance of the prototype at 18.5 km/h. What must the model speed be for the model and prototype to exhibit similar wave drag behavior? Is the boundary layer on the prototype predominantly laminar or turbulent? Does the model boundary layer become turbulent at the comparable point? If not, the model boundary layer could be artificially triggered to turbulent by placing a tripwire across the hull. Where could this be placed? Estimate the skin-friction drag on model and prototype.

**9.62** A vertical stabilizing fin on a land-speed-record car is  $L = 1.65$  m long and  $H = 0.785$  m tall. The automobile is to be driven at the Bonneville Salt Flats in Utah, where the elevation is 1340 m and the summer temperature reaches  $50^\circ\text{C}$ . The car speed is 560 km/h. Evaluate the length Reynolds number of the fin. Estimate the location of transition from laminar to turbulent flow in the boundary layers. Calculate the power required to overcome skin friction drag on the fin.

**9.63** A nuclear submarine cruises fully submerged at 13.9 m/s. The hull is approximately a circular cylinder with diameter  $D = 11.0$  m and length  $L = 107$  m. Estimate the percentage of the hull length for which the boundary layer is laminar. Calculate the skin friction drag on the hull and the power consumed.

**9.64** A sheet of plastic material 10 mm thick, with specific gravity  $SG = 1.5$ , is dropped into a large tank containing water. The sheet is  $0.5 \text{ m} \times 1 \text{ m}$ . Estimate the terminal speed of the sheet as it falls with (a) the short side vertical and (b) the long side vertical. Assume that the drag is due only to skin friction and that the boundary layers are turbulent from the leading edge.

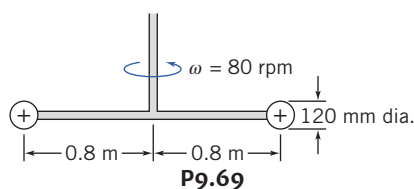
**9.65** The 600-seat jet transport aircraft proposed by Airbus Industrie has a fuselage that is 70 m long and 7.5 m in diameter. The aircraft is to operate 14 h per day, 6 days per week; it will cruise at 257 m/s ( $M = 0.87$ ) at 12-km altitude. The engines consume fuel at the rate of 0.06 kg/h for each N of thrust produced. Estimate the skin friction drag force on the aircraft fuselage at cruise. Calculate the annual fuel savings for the aircraft if friction drag on the fuselage could be reduced by 1 percent by modifying the surface coating.

**9.66** A supertanker displacement is approximately 600,000 metric tons. The ship has length  $L = 300$  m, beam (width)  $b = 80$  m, and draft (depth)  $D = 25$  m. The ship steams at 7.20 m/s through seawater at  $4^\circ\text{C}$ . For these conditions, estimate (a) the thickness of the boundary layer at the stern of the ship, (b) the total skin friction drag acting on the ship, and (c) the power required to overcome the drag force.

**9.67** As part of the 1976 bicentennial celebration, an enterprising group hung a giant American flag (59 m high and 112 m wide) from the suspension cables of the Verrazano Narrows Bridge. They apparently were reluctant to make holes in the flag to alleviate the wind force, and hence they effectively had a flat plate normal to the flow. The flag tore loose from its mountings when the wind speed reached 16 km/h. Estimate the wind force acting on the flag at this wind speed. Should they have been surprised that the flag blew down?

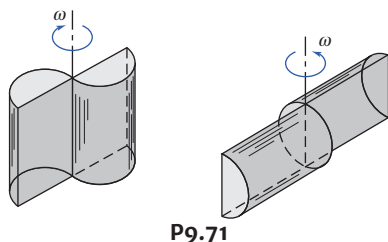
**9.68** A fishing net is made of 0.75 mm diameter nylon thread assembled in a rectangular pattern. The horizontal and vertical distances between adjacent thread centerlines are 1 cm. Estimate the drag on a 2 m  $\times$  12 m section of this net when it is dragged (perpendicular to the flow) through 15°C water at 6 knots. What is the power required to maintain this motion?

**9.69** A rotary mixer is constructed from two circular disks as shown. The mixer is rotated at 80 rpm in a large vessel containing a brine solution (SG = 1.1). Neglect the drag on the rods and the motion induced in the liquid. Estimate the minimum torque and power required to drive the mixer.



**9.70** The vertical component of the landing speed of a parachute is to be less than 6 m/s. The total weight of the jumper and the chute is 120 kg. Determine the minimum diameter of the open parachute.

**9.71** It has been proposed to use surplus 208 L oil drums to make simple windmills for underdeveloped countries. (It is a simple Savonius turbine.) Two possible configurations are shown. Estimate which would be better, why, and by how much. The diameter and length of a 208 drum are  $D = 610$  mm and  $H = 737$  mm.



**9.72** The resistance to motion of a good bicycle on smooth pavement is nearly all due to aerodynamic drag. Assume that the total weight of rider and bike is  $M = 100$  kg. The frontal area measured from a photograph is  $A = 0.46$  m<sup>2</sup>. Experiments on a hill, where the road grade is 8 percent, show that terminal speed is  $V_t = 15$  m/s. From these data, the drag coefficient is estimated as  $C_D = 1.2$ . Verify this calculation of drag coefficient. Estimate the distance needed for the bike and rider to decelerate from 15 m/s to 10 m/s while coasting after reaching level road.

**9.73** A cyclist is able to attain a maximum speed of 30 km/h on a calm day. The total mass of rider and bike is 65 kg. The rolling resistance of the tires is  $F_R = 7.5$  N, and the drag coefficient and frontal area are  $C_D = 1.2$  and  $A = 0.25$  m<sup>2</sup>. The cyclist bets that today, even though there is a headwind of 10 km/h, she can maintain a speed of

24 km/h. She also bets that, cycling with wind support, she can attain a top speed of 40 km/h. Which, if any, bets does she win?

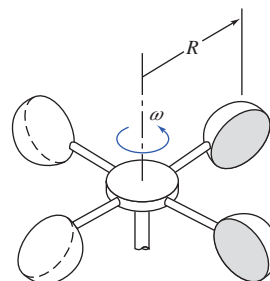
**9.74** Consider the cyclist in Problem 9.73. She is having a bad day, because she has to climb a hill with a 5° slope. What is the speed she is able to attain? What is the maximum speed if there is also a headwind of 10 km/h? She reaches the top of the hill and turns around and heads down the hill. If she still pedals as hard as possible, what will be her top speed (when it is calm, and when the wind is present)? What will be her maximum speed if she decides to coast down the hill (with and without the aid of the wind)?

**9.75** Consider the cyclist in Problem 9.73. Determine the maximum speeds she is actually able to attain today (with the 10 km/h wind) cycling into the wind, and cycling with the wind. If she were to replace the tires with high-tech ones that had a rolling resistance of only 3.5 N, determine her maximum speed on a calm day, cycling into the wind, and cycling with the wind. If she in addition attaches an aerodynamic fairing that reduces the drag coefficient to  $C_D = 0.9$ , what will be her new maximum speeds?

**9.76** At a surprise party for a friend you've tied a series of 20 cm diameter helium balloons to a flagpole, each tied with a short string. The first one is tied 1 m above the ground, and the other eight are tied at 1 m spacings, so that the last is tied at a height of 9 m. Being quite a nerdy engineer, you notice that in the steady wind, each balloon is blown by the wind so it looks like the angles that the strings make with the vertical are about 10°, 20°, 30°, 35°, 40°, 45°, 50°, 60°, and 65°. Estimate and plot the wind velocity profile for the 9-m range. Assume that the helium is at 20°C and 10 kPa gage and that each balloon is made of 3 g of latex.

**9.77** A simple but effective anemometer to measure wind speed can be made from a thin plate hinged to deflect in the wind. Consider a thin plate made from brass that is 20 mm high and 10 mm wide. Derive a relationship for wind speed as a function of deflection angle,  $\theta$ . What thickness of brass should be used to give  $\theta = 30^\circ$  at 10 m/s?

**9.78** An anemometer to measure wind speed is made from four hemispherical cups of 50 mm diameter, as shown. The center of each cup is placed at  $R = 80$  mm from the pivot. Find the theoretical calibration constant,  $k$ , in the calibration equation  $V = k\omega$ , where  $V$  (km/h) is the wind speed and  $\omega$  (rpm) is the rotation speed. In your analysis, base the torque calculations on the drag generated at the instant when two of the cups are orthogonal and the other two cups are parallel and ignore friction in the bearings. Explain why, in the absence of friction, at any given wind speed, the anemometer runs at constant speed rather than accelerating without limit. If the actual anemometer bearing has (constant) friction such that the anemometer needs a minimum wind speed of 1 km/h to begin rotating, compare the rotation speeds with and without friction for  $V = 10$  km/h.



P9.78


**9.79** Experimental data [16] suggest that the maximum and minimum drag area ( $C_D A$ ) for a skydiver varies from about  $0.85 \text{ m}^2$  for a prone, spread-eagle position to about  $0.11 \text{ m}^2$  for vertical fall. Estimate the terminal speeds for a  $75 \text{ kg}$  skydiver in each position. Calculate the time and distance needed for the skydiver to reach 90 percent of terminal speed at an altitude of  $3000 \text{ m}$  on a standard day.

**9.80** A vehicle is built to try for the land-speed record at the Bonneville Salt Flats, elevation  $1340 \text{ m}$ . The engine delivers  $373 \text{ kW}$  to the rear wheels, and careful streamlining has resulted in a drag coefficient of  $0.15$ , based on a  $1.4 \text{ m}^2$  frontal area. Compute the theoretical maximum ground speed of the car (a) in still air and (b) with a  $32 \text{ km/h}$  headwind.

**9.81** An F-4 aircraft is slowed after landing by dual parachutes deployed from the rear. Each parachute is  $3.7 \text{ m}$  in diameter. The F-4 weighs  $142,400 \text{ N}$  and lands at  $160 \text{ m/s}$ . Estimate the time and distance required to decelerate the aircraft to  $100 \text{ m/s}$ , assuming that the brakes are not used and the drag of the aircraft is negligible.


**9.82** A tractor-trailer rig has frontal area  $A = 9.5 \text{ m}^2$  and drag coefficient  $C_D = 0.9$ . Rolling resistance is  $6 \text{ N}$  per  $1000 \text{ N}$  of vehicle weight. The specific fuel consumption of the diesel engine is  $0.206 \text{ kg}$  of fuel per  $\text{kW}$  hour, and drivetrain efficiency is  $92$  percent. The density of diesel fuel is  $812 \text{ kg/m}^3$ . Estimate the fuel economy of the rig at  $88 \text{ km/h}$  if its gross weight is  $320,400 \text{ N}$ . An air fairing system reduces aerodynamic drag  $15$  percent. The truck travels  $192,000 \text{ km}$  per year. Calculate the fuel saved per year by the roof fairing.

**9.83** A bus travels at  $80 \text{ km/h}$  in standard air. The frontal area of the vehicle is  $7.5 \text{ m}^2$ , and the drag coefficient is  $0.92$ . How much power is required to overcome aerodynamic drag? Estimate the maximum speed of the bus if the engine is rated at  $346.75 \text{ kW}$ . A young engineer proposes adding fairings on the front and rear of the bus to reduce the drag coefficient. Tests indicate that this would reduce the drag coefficient to  $0.86$  without changing the frontal area. What would the required power be at  $80 \text{ km/h}$  and the new top speed? If the fuel cost for the bus is currently  $\$300/\text{day}$ , how long would the modification take to pay for itself if it costs  $\$4800$  to install?

 **9.84** Compare and plot the power ( $\text{kW}$ ) required by a typical large American sedan of the 1970s and a current midsize sedan to overcome aerodynamic drag versus road speed in standard air, for a speed range of  $32 \text{ km/h}$  to  $160 \text{ km/h}$ . Use the following as representative values:

	Weight (N)	Drag Coefficient	Frontal Area ( $\text{m}^2$ )
1970s Sedan	20,025	0.5	2.23
Current Sedan	15,575	0.3	1.86

If rolling resistance is  $1.5$  percent of curb weight, determine for each vehicle the speed at which the aerodynamic force exceeds frictional resistance.

 **9.85** A  $134.23 \text{ kW}$  sports car of frontal area  $1.72 \text{ m}^2$ , with a drag coefficient of  $0.31$ , requires  $12.677 \text{ kW}$  to cruise at  $100 \text{ km/h}$ . At what speed does aerodynamic drag first exceed rolling resistance? (The rolling resistance is  $1.2$  percent of the car weight, and the car mass is  $1250 \text{ kg}$ .) Find the drivetrain efficiency. What is the maximum acceleration at  $100 \text{ km/h}$ ? What is the maximum speed? Which redesign will lead to a higher maximum speed: improving the drive train efficiency by  $6$  percent from its current value, reducing the drag

coefficient to  $0.29$ , or reducing the rolling resistance to  $0.91$  percent of the car weight?

**9.86** Consider a negatively charged spherical particle of radius  $a$  bearing a charge,  $Q_s$ , suspended in a pure dielectric fluid (containing no ions). When subject to a uniform electric field,  $\vec{E}_\infty$ , the particle will translate under the influence of the electric force acting on it. The induced particle motion refers to electrophoresis, which has been widely used to characterize and purify molecules and colloidal particles. The net electrical force on the charged particle will simply be  $\vec{F}_E = Q_s \vec{E}_\infty$ . As soon as the particle starts to move under the influence of this electric force, it encounters an oppositely directed fluid drag force.

- Under the Stokes flow regime and neglecting the gravitational force and the buoyancy force acting on the microparticle, derive an expression to calculate the particle's steady-state translational velocity.
- Based on the above results, explain why electrophoresis can be used to separate biological samples.
- Calculate the translational velocities of two particles of radius  $a = 1 \text{ }\mu\text{m}$  and  $10 \text{ }\mu\text{m}$  using  $Q_s = -10^{-2} \text{ C}$ ,  $E_\infty = 1000 \text{ V/m}$ , and  $\mu = 10^{-3} \text{ Pa}\cdot\text{s}$ .

**9.87** A round thin disk of radius  $R$  is oriented perpendicular to a fluid stream. The pressure distributions on the front and back surfaces are measured and presented in the form of pressure coefficients. The data are modeled with the following expressions for the front and back surfaces, respectively:

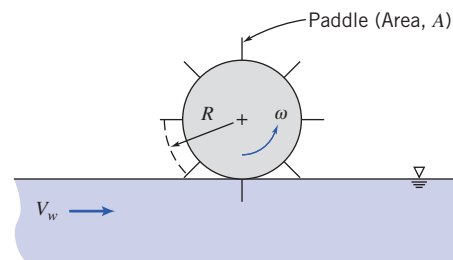
$$\text{Front surface } C_p = 1 - \left(\frac{r}{R}\right)^6$$

$$\text{Rear surface } C_p = -0.42$$

Calculate the drag coefficient for the disk.

**9.88** A light plane tows an advertising banner over a football stadium on a Saturday afternoon. The banner is  $1.2 \text{ m}$  tall and  $13.7 \text{ m}$  long. According to Hoerner [16], the drag coefficient based on area ( $Lh$ ) for such a banner is approximated by  $C_D = 0.05 L/h$ , where  $L$  is the banner length and  $h$  is the banner height. Estimate the power required to tow the banner at  $V = 88 \text{ km/h}$ . Compare with the drag of a rigid flat plate. Why is the drag larger for the banner?

**9.89** A large paddle wheel is immersed in the current of a river to generate power. Each paddle has area  $A$  and drag coefficient  $C_D$ ; the center of each paddle is located at radius  $R$  from the centerline of the paddle wheel. Assume the equivalent of one paddle is submerged continuously in the flowing stream. Obtain an expression for the drag force on a single paddle in terms of geometric variables, current speed,  $V$ , and linear speed of the paddle center,  $U = R\omega$ . Develop expressions for the torque and power produced by the paddle wheel. Find the speed at which the paddle wheel should rotate to obtain maximum power output from the wheel in a given current.



P9.89



**9.90** A large three-blade horizontal axis wind turbine (HAWT) can be damaged if the wind speed is too high. To avoid this, the blades of the turbine can be oriented so that they are parallel to the flow. Find the bending moment at the base of each blade when the wind speed is 45 m/s. Model each blade as a flat plate 35 m wide  $\times$  0.45 m long.

**9.91** The HAWT of Problem 9.90 is not self-starting. The generator is used as an electric motor to get the turbine up to the operating speed of 20 units. To make this easier, the blades are aligned so that they lie in the plane of rotation. Assuming an overall efficiency of motor and drive train of 65 percent, find the power required to maintain the turbine at the operating speed. As an approximation, model each blade as a series of flat plates (the outer region of each blade moves at a significantly higher speed than the inner region).


**9.92** A runner maintains a speed of 12 km/h during a 6.4 km run. The runner's route consists of running straight down a road for 3.22 km, then turning around and returning the 3.22 km straight home. The  $C_D A$  for the runner is  $0.84 \text{ m}^2$ . On a windless day, how many calories (kcal) will the runner burn overcoming drag? On a day in which the wind is blowing 8 km/h directly along the runner's route how many calories (kcal) will the runner burn overcoming drag?

**9.93** Standard air is drawn into a low-speed wind tunnel. A 30-mm diameter sphere is mounted on a force balance to measure lift and drag. An oil-filled manometer is used to measure static pressure inside the tunnel; the reading is  $-40 \text{ mm}$  of oil ( $\text{SG} = 0.85$ ). Calculate the freestream air speed in the tunnel, the Reynolds number of flow over the sphere, and the drag force on the sphere. Are the boundary layers on the sphere laminar or turbulent? Explain.

**9.94** A spherical helium-filled balloon, 0.6 m in diameter, exerts an upward force of 1.3 N on a restraining string when held stationary in standard air with no wind. With a wind speed of 3 m/s, the string holding the balloon makes an angle of  $60^\circ$  with the horizontal. Calculate the drag coefficient of the balloon under these conditions, neglecting the weight of the string.

**9.95** A field hockey ball has diameter  $D = 73 \text{ mm}$  and mass  $m = 160 \text{ g}$ . When struck well, it leaves the stick with initial speed  $U_0 = 50 \text{ m/s}$ . The ball is essentially smooth. Estimate the distance traveled in horizontal flight before the speed of the ball is reduced 10 percent by aerodynamic drag.

**9.96** Compute the terminal speed of a 3-mm diameter raindrop (assume spherical) in standard air.

 **9.97** The following curve-fit for the drag coefficient of a smooth sphere as a function of Reynolds number has been proposed by Chow [36]:

$C_D = 24/Re$	$Re \leq 1$
$C_D = 24/Re^{0.646}$	$1 < Re \leq 400$
$C_D = 0.5$	$400 < Re \leq 3 \times 10^5$
$C_D = 0.000366 Re^{0.4275}$	$3 \times 10^5 < Re \leq 2 \times 10^6$
$C_D = 0.18$	$Re > 2 \times 10^6$

Use data from Fig. 9.11 to estimate the magnitude and location of the maximum error between the curve fit and data.


**9.98** A tennis ball with a mass of 57 g and diameter of 64 mm is dropped in standard sea level air. Calculate the terminal velocity of the ball. Assuming as an approximation that the drag coefficient

remains constant at its terminal-velocity value, estimate the time and distance required for the ball to reach 95% of its terminal speed.

**9.99** Consider a cylindrical flag pole of height  $H$ . For constant drag coefficient, evaluate the drag force and bending moment on the pole if wind speed varies as  $u/U = (y/H)^{1/7}$ , where  $y$  is distance measured from the ground. Compare with drag and moment for a uniform wind profile with constant speed  $U$ .

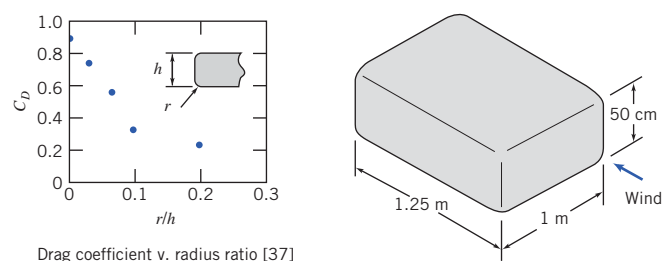
**9.100** A model airfoil of chord 15 cm and span 60 cm is placed in a wind tunnel with an air flow of 30 m/s (the air is at  $20^\circ\text{C}$ ). It is mounted on a cylindrical support rod 2 cm in diameter and 25 cm tall. Instruments at the base of the rod indicate a vertical force of 50 N and a horizontal force of 6 N. Calculate the lift and drag coefficients of the airfoil.

**9.101** The Stokes drag law for smooth spheres is to be verified experimentally by dropping steel ball bearings in glycerin. Evaluate the largest diameter steel ball for which  $Re < 1$  at terminal speed. Calculate the height of glycerin column needed for a bearing to reach 95 percent of terminal speed.

**9.102** The air bubble of Problem 3.8 expands as it rises in water.  Find the time it takes for the bubble to reach the surface. Repeat for bubbles of diameter 5 mm and 15 mm. Compute and plot the depth of the bubbles as a function of time.

**9.103** Why is it possible to kick a football farther in a spiral motion than in an end-over-end tumbling motion?

**9.104** Approximate dimensions of a rented rooftop carrier are shown. Estimate the drag force on the carrier ( $r = 10 \text{ cm}$ ) at 100 km/h. If the drivetrain efficiency of the vehicle is 0.85 and the brake specific fuel consumption of its engine is  $0.3 \text{ kg}/(\text{kW}\cdot\text{h})$ , estimate the additional rate of fuel consumption due to the carrier. Compute the effect on fuel economy if the auto achieves 12.75 km/L without the carrier. The rental company offers you a cheaper, square-edged carrier at a price \$5 less than the current carrier. Estimate the extra cost of using this carrier instead of the rounded one for a 750 km trip, assuming fuel is \$0.92 per liter. Is the cheaper carrier really cheaper?



**P9.104**

**9.105** A cylinder of diameter 90 mm and of length 220 mm is placed in a stream of fluid which is flowing at speed of 0.8 m/s. The flow of direction is normal to the axis of the cylinder. The density of the fluid is  $900 \text{ kg}/\text{m}^3$ . The drag force is measured and found to be 40 N. Calculate the drag coefficient. The pressure at a point on the surface is measured as 105 Pa above the ambient level. Calculate the velocity at this point.


**9.106** Coastdown tests, performed on a level road on a calm day, can be used to measure aerodynamic drag and rolling resistance coefficients for a full-scale vehicle. Rolling resistance is estimated from

$dV/dt$  measured at low speed, where aerodynamic drag is small. Rolling resistance then is deducted from  $dV/dt$  measured at high speed to determine the aerodynamic drag. The following data were obtained during a test with a vehicle, of weight  $W = 111,250$  N and frontal area  $A = 7.34$  m<sup>2</sup>:

$V(\text{km/h})$	8	88
$\frac{dV}{dt} \left( \frac{\text{km/h}}{\text{s}} \right)$	0.24	0.76

Estimate the aerodynamic drag coefficient for this vehicle. At what speed does the aerodynamic drag first exceed rolling resistance?


**9.107** A spherical sonar transducer with 0.375 m diameter is to be towed in seawater. The transducer must be fully submerged at 16 m/s. To avoid cavitation, the minimum pressure on the surface of the transducer must be greater than 30 kPa (abs). Calculate the hydrodynamic drag force acting on the transducer at the required towing speed. Estimate the minimum depth to which the transducer must be submerged to avoid cavitation.

 **9.108** Motion of a small rocket was analyzed in Example 4.12 assuming negligible aerodynamic drag. This was not realistic at the final calculated speed of 369 m/s. Use the Euler method of Section 5.5 for approximating the first derivatives, in an *Excel* workbook, to solve the equation of motion for the rocket. Plot the rocket speed as a function of time, assuming  $C_D = 0.3$  and a rocket diameter of 700 mm. Compare with the results for  $C_D = 0$ .

**9.109** A baseball is popped straight up with an initial velocity of 25 m/s. The baseball has a diameter of 0.073 m and a mass of 0.143 kg. The drag coefficient for the baseball can be estimated as 0.47 for  $Re < 10^4$  and 0.10 for  $Re > 10^4$ . Determine how long the ball will be in the air and how high it will go.

**9.110** Wiffle™ balls made from light plastic with numerous holes are used to practice baseball and golf. Explain the purpose of the holes and why they work. Explain how you could test your hypothesis experimentally.

**9.111** Towers for television transmitters may be up to 500 m in height. In the winter, ice forms on structural members. When the ice thaws, chunks break off and fall to the ground. How far from the base of a tower would you recommend placing a fence to limit danger to pedestrians from falling ice chunks?

 **9.112** Design a wind anemometer that uses aerodynamic drag to move or deflect a member or linkage, producing an output that can be related to wind speed, for the range from 1 to 10 m/s in standard air. Consider three alternative design concepts. Select the best concept and prepare a detailed design. Specify the shape, size, and material for each component. Quantify the relation between wind speed and anemometer output. Present results as a theoretical “calibration curve” of anemometer output versus wind speed. Discuss reasons why you rejected the alternative designs and chose your final design concept.

**9.113** A model airfoil of chord 150 mm and span 750 mm is placed in a wind tunnel with an air flow of 30 m/s (the air is at 20°C). It is mounted on a cylindrical support rod 25 mm in diameter and 250 mm tall. Instruments at the base of the rod indicate a vertical force of 44.5 N and a horizontal force of 6.7 N. Calculate the lift and drag coefficients of the airfoil.

**9.114** Why do modern guns have rifled barrels?

**9.115** How do cab-mounted wind deflectors for tractor-trailer trucks work? Explain using diagrams of the flow pattern around the truck and pressure distribution on the surface of the truck.

**9.116** An aircraft is in level flight at 225 km/h through air at standard conditions. The lift coefficient at this speed is 0.45 and the drag coefficient is 0.065. The mass of the aircraft is 900 kg. Calculate the effective lift area for the craft, and the required engine thrust and power.

**9.117** The foils of a surface-piercing hydrofoil watercraft have a total effective area of 0.7 m<sup>2</sup>. Their coefficients of lift and drag are 1.6 and 0.5, respectively. The total mass of the craft in running trim is 1800 kg. Determine the minimum speed at which the craft is supported by the hydrofoils. At this speed, find the power required to overcome water resistance. If the craft is fitted with a 110 kW engine, estimate its top speed.

**9.118** A high school project involves building a model ultralight airplane. Some of the students propose making an airfoil from a sheet of plastic 1.5 m long  $\times$  2 m wide at an angle of attack of 12°. At this airfoil’s aspect ratio and angle of attack, the lift and drag coefficients are  $C_L = 0.72$  and  $C_D = 0.17$ . If the airplane is designed to fly at 12 m/s, what is the maximum total payload? What will be the required power to maintain flight? Does this proposal seem feasible?

**9.119** The U.S. Air Force F-16 fighter aircraft has wing planform area  $A = 27.9$  m<sup>2</sup>; it can achieve a maximum lift coefficient of  $C_L = 1.6$ . When fully loaded, its mass is  $M = 11,600$  kg. The airframe is capable of maneuvers that produce 9 g vertical accelerations. However, student pilots are restricted to 5 g maneuvers during training. Consider a turn flown in level flight with the aircraft banked. Find the minimum speed in standard air at which the pilot can produce a 5 g total acceleration. Calculate the corresponding flight radius. Discuss the effect of altitude on these results.

**9.120** The teacher of the students designing the airplane of Problem 9.118 is not happy with the idea of using a sheet of plastic for the airfoil. He asks the students to evaluate the expected maximum total payload and required power to maintain flight, if the sheet of plastic is replaced with a conventional section (NACA 23015) airfoil with the same aspect ratio and angle of attack. What are the results of the analysis?

**9.121** A light airplane has 10 m effective wingspan and 1.8 m chord. It was originally designed to use a conventional (NACA 23015) airfoil section. With this airfoil, its cruising speed on a standard day near sea level is 225 km/h. A conversion to a laminar-flow (NACA 662–215) section airfoil is proposed. Determine the cruising speed that could be achieved with the new airfoil section for the same power.

**9.122** Assume that the Boeing 727 aircraft has wings with NACA 23012 section, planform area of 150 m<sup>2</sup>, double-slotted flaps, and effective aspect ratio of 6.5. If the aircraft flies at 77.2 m/s in standard air at 778,750 N gross weight, estimate the thrust required to maintain level flight.

**9.123** An airplane with mass of 4500 kg is flown at constant elevation and speed on a circular path at 240 km/h. The flight circle has a radius of 990 m. The plane has lifting area of 23 m<sup>2</sup> and is fitted with NACA 23015 section airfoils with effective aspect ratio of 7. Estimate the drag on the aircraft and the power required.

**9.124** Find the minimum and maximum speeds at which the airplane of Problem 9.123 can fly on a 990-m radius circular flight path and estimate the drag on the aircraft and power required at these extremes.

**9.125** Jim Hall's Chaparral 2F sports-racing cars in the 1960s pioneered use of airfoils mounted above the rear suspension to enhance stability and improve braking performance. The airfoil was effectively 1.8 wide (span) and had a 0.3 m chord. Its angle of attack was variable between 0 and minus  $12^\circ$ . Assume lift and drag coefficient data are given by curves (for conventional section) in Fig. 9.17. Consider a car speed of 192 km/h on a calm day. For an airfoil deflection of  $12^\circ$  down, calculate (a) the maximum downward force and (b) the maximum increase in deceleration force produced by the airfoil.

**9.126** The glide angle for unpowered flight is such that lift, drag, and weight are in equilibrium. Show that the glide slope angle,  $\theta$ , is such that  $\tan \theta = C_D/C_L$ . The minimum glide slope occurs at the speed where  $C_L/C_D$  is a maximum. For the conditions of Example 9.8, evaluate the minimum glide slope angle for a Boeing 727-200. How far could this aircraft glide from an initial altitude of 10 km on a standard day?

**9.127** The wing loading of the Gossamer Condor is  $19 \text{ N/m}^2$  of wing area. Crude measurements showed drag was approximately 27 N at 19.2 km/h. The total weight of the Condor was 890 N. The effective aspect ratio of the Condor is 17. Estimate the minimum power required to fly the aircraft. Compare to the 290 W that pilot Brian Allen could sustain for 2 h.

**9.128** Some cars come with a "spoiler," a wing section mounted on the rear of the vehicle that salespeople sometimes claim significantly increases traction of the tires at highway speeds. Investigate the validity of this claim. Are these devices really just cosmetic?

**9.129** How does a Frisbee<sup>TM</sup> fly? What causes it to curve left or right? What is the effect of spin on its flight?

**9.130** An automobile travels down the road with a bicycle attached to a carrier across the rear of the trunk. The bicycle wheels rotate slowly. Explain why and in what direction the rotation occurs.

**9.131** A golf ball (diameter  $D = 43 \text{ mm}$ ) with circular dimples is hit from a sand trap at 20 m/s with backspin of 2000 rpm. The mass of the ball is 48 g. Evaluate the lift and drag forces acting on the ball. Express your results as fractions of the weight of the ball.

**9.132** Rotating cylinders were proposed as a means of ship propulsion in 1924 by the German engineer, Flettner. The original Flettner rotor ship had two rotors, each about 3 m in diameter and 15 m high, rotating at up to 750 rpm. Calculate the maximum lift and drag forces that act on each rotor in a 50 km/h wind. Compare the total force to that produced at the optimum  $L/D$  at the same wind speed. Estimate the power needed to spin the rotor at 750 rpm.

**9.133** A baseball pitcher throws a ball at 128 km/h. Home plate is 18.3 m away from the pitcher's mound. What spin should be placed on the ball for maximum horizontal deviation from a straight path? (A baseball has a mass of 142 g and a circumference of 230 mm.) How far will the ball deviate from a straight line?

**9.134** American and British golf balls have slightly different diameters but the same mass (see Problems 1.101 and 1.102). Assume a professional golfer hits each type of ball from a tee at 85 m/s with backspin of 9000 rpm. Evaluate the lift and drag forces on each ball. Express your answers as fractions of the weight of each ball. Estimate the radius of curvature of the trajectory of each ball. Which ball should have the longer range for these conditions?

**9.135** A soccer player takes a free kick. Over a distance of 10 m, the ball veers to the right by about 1 m. Estimate the spin the player's kick put on the ball if its speed is 30 m/s. The ball has a mass of 420 g and has a circumference of 70 cm.